Preparation and properties of conductive polymer nanocomposites

by

JEREMIA SHALE SEFADI (M.Sc.)

Submitted in accordance with the requirements for the degree of

Doctor of Philosophy (Ph.D.) in Polymer Science

Department of Chemistry

Faculty of Natural and Agricultural Sciences

at the

UNIVERSITY OF THE FREE STATE (QWAQWA CAMPUS)

SUPERVISOR: PROF A.S. LUYT

CO-SUPERVISOR: DR J. PIONTECK

JANUARY 2015

DECLARATION

I hereby declare that the research work in this thesis is my own original piece of work and has not previously, in its entirety or in part, been submitted to any other university in order to obtain a degree. I therefore relinquish all the copyrights of this dissertation in good deed of the University of the Free State.

_____

J.S. Sefadi

DEDICATIONS

This research work is dedicated to my late father Mahlaku Paul Sefadi for raising me well. Daddy where ever you are, you deserve a standing ovation and may your soul rest in peace.

To my beloved wife Ntebaleng Eva Sefadi for her invariable patience, unconditional love and priceless support. Honey you are my ever shining golden diamond of my heart and I love you.

To my two hilarious boys Kananelo Samuel Sefadi and Karabelo Joseph Sefadi, for their endless love, you boys make me enjoy my fatherhood. Morena wa kgotso a le apese ka mohau.

To my mother Mapalesa Sefadi for the ever lasting love and the patience to bring me on this world.

To my uncle (Pule Sefadi) and his great spouse (Limakatso Mokoena), I would not have achieved this feet without you. You are like father and mother to me and thank you for your help, moral support and kindness.

“Life exists in the universe only because the carbon chains in the expanded graphite possess certain exceptional properties” - Sir James Jeans

ACKNOWLEDGEMENTS

- First and foremost I would like to offer my unreserved gratitude and praises to **Almighty God** for His kind blessings and the undying strength bestowed upon me during the course of this study.

- I would like to express my most sincere and deepest gratitude and appreciation to my supervisor, **Prof. Adriaan Stephanus Luyt,** for his great efforts, immeasurable patience, constant guidance and dedication to my intellectual and personal growth throughout the course of my study. Throughout the entire study he showed unwavering support, gave sound advices and emphasized on a high-quality research work coupled with critical thinking. My special thanks to him for being so inspirational and he sacrificed his family time for this project to become a massive success.

- I am also grateful to my co-supervisor **Dr. J. Pionteck**, at Leibnitz Institute for Polymer research (IPF), Germany (Dresden), for his outstanding contributions, scientific suggestions throughout the research work, critical reading of my writings, robust discussions and his hospitality during my stay in Germany was unforgettable. Thanks for introducing me to your family and for the gifts you brought specifically for my son. May the grace of the Lord continue to sprinkle unto you and your entire family.

- I would like to sincerely thank **Dr. Francesco Piana** from Italy for his exceptional interaction, talk on *electrical conductivity of polyurethane/poplypyrrole/expanded graphite in Polymer Composites* that inspired the bulk of my PhD work. His hospitality and friendly induction around corners and streets of Dresden was amazing, not forgetting the great exchange of ideas and knowledge we had.

- I am also grateful to **Dr. U Gohs, Dresden,** for his shared experience on electron beam irradiation processing of the material composites.

- To all members of **polymer blends and reaction division** in IPF, Dresden in particular those expert in the electrical conductivity room and preparation laboratory, for the

training provided in order to carry out the experimental work. Thank you **Marco** for your inputs in my research work.

- I would like to express my deepest appreciation and acknowledgement for the financial support from the **NRF, the University of the Free State and International Bureau of the BMBF Germany.**

- I am grateful to Dr. Thabang Hendrica Mokhothu, CSIR, who has been a good friend and source of inspiration in my life. For his ever presence, support, encouragement and most for being there in times of troubles through the course of this project. *"A friend in need is a friend in deed".*

- From CSIR in Pretoria and Port-Elizabeth, special thanks to Mr Tladi Gideon Mofokeng and Mokhena Teboho for doing the hardness, electrical conductivity and rheology measurements on my behalf in Germany, Dresden.

- All special thanks to the entire Chemistry department and entire polymer research crew (Mr RG Moji (HOD), Dr. Nomampondomise Molefe, Mrs Moipone Malimabe, Mr. Tsietsi Tsotetsi, Mr Jonas Mochane, Mr Mosoabisane Mafereka, Mr Mpitso Kgotso, Dr Dusko Dudic, Ms Mamohanoe Molaba, Ms Thandi Gumede, and Ms Thollwana Makhetha), for their invaluable discussions on various research topics, experimental insights, unwavering support and valuable inputs) for the collective efforts, maximum co-operation, and help displayed during the whole research project.

- I would also like to appreciate the sensational work done by Ms Julia Puseletso Mofokeng, Ms Motshabi Sibeko and Mrs König (Clarke) for the comprehensive operation of various analytical techniques in the research lab.

- I am grateful to the Faculty programme secretary and programme officer, Mrs Marlize Jackson and Mpho Leripa for their unself-centred service rendered and moral support.

- My earnest gratitude goes to Dr Tshwafo Motaung and Mr Mngomezulu Mfiso from CSIR in PE for their robust discussions and shared knowledge of research in many different aspects.

- I would like to gratefully acknowledge the inspiration and motivation drawn from Dr LF Koao, Mr SV Motloung, Mr SJ Motloung and Mr Kamohelo George Tshabalala from Physics department.

- I am greatly appreciative to Boitumelo Tsotetsi, Langa Ncubuka, Joseph Mbule, Kamohelo Mokhatla, Kauwane Motaung, Elias Monareng and other host of friends for their support, love, and encouragement.

- My genuine thanks to all my brothers and sisters Tshidiso Sefadi, Sello Sefadi, Tanki Eric Sefadi, Telang Eric Nkosi, Tshepo Isaac Mokoena, Lebohang Ernest Mokoena, Mr. Enock Themba Ngwenya Mokoena, Palesa Sefadi, Pontsho Gloria Mokoena, Malefa Alice Sefadi, Ausi Jwana, Katlego Mokoena, and others who are not included here.

- My utmost gratitude to my parents and sisters in laws ntate Moleleki Simon Molise, Mme Mantebaleng Martha Molise, Matieho Roselina Molise, Mosela Francina Molise for everything you have done for me during the tough times including the horrific car accident and you stood by my side at all times.

- The following are the most important families with their maximum contribution in my studies: Moloi's family, Motaung's family, Mabe's family, Thateng's family, Mlangeni's family and Mahlakolisane's family

- To all the structures such as prayer warriors, men's ministry and church council of the Uniting Reformed Church in South Africa Phuthaditjhaba, thanks for your continuous prayers, support and understanding during trying times. May the great Lord be with you all and your entire families.

ABSTRACT

In this study, composites based on polyolefin matrices (EVA, PP and MAPE) filled with nano-structured expanded graphite (EG) were prepared through melt mixing. Functionalized EG was prepared using a non-covalent surfactant functionalization method. Anionic sodium dodecyl sulphate (SDS) surfactant in water was used for surface modification of EG through sonication processing, and composites containing EG with and without surfactant treatment were compared. Electron beam (EB) irradiation treatment was performed on the samples, and its influence on the overall properties of the composites was investigated.

For the EG containing samples, the results showed big agglomerations and poor particle dispersion, while SDS treatment reduced the interparticle attraction resulting in better particle dispersion and interaction between the graphite platelets and the polymer matrix. EB irradiation had no influence on the morphology of the samples, since there was no polymer melting at macroscopic level when the electron beam penetrated the polymer, and the particles could not re-disperse. The gel contents of the irradiated EVA samples without and with SDS treatment increased with an increase in EG loading. The irradiated EVA/SDS-EG composites had significantly higher gel content values than the irradiated EVA/EG samples due to the improved interaction and dispersion of the EG platelets in the EVA, which enhanced the energy transfer to the EVA chains and thus the crosslinking efficiency. In the case of the PP samples, there was no gel after soxhlet extraction, indicating that the formation of crosslinked material was a minor process during EB irradiation. For the MAPE samples, three different EB irradiation doses were applied, and their gel contents increased with increasing filler content and EB irradiation dose up to maxima at 4 wt% filler and 100 kGy dose respectively. The number average and weight average molar masses of PP increased with increasing EG and SDS-EG contents, but decreased after EB irradiation due to radiation induced degradation.

For the EVA/graphite system, the stress and elongation at break values decreased and the tensile modulus values increased with increasing EG content, and SDS-EG containing samples showed slightly higher values due to better dispersion. This was because of the inherent stiffness of the graphite platelets, and the better dispersion of the SDS modified EG nanosheets because of better interaction between the EG and EVA. EB irradiation gave rise to significantly better tensile properties due to the radiation induced formation of a crosslinking network. For PP reinforced with EG particles, the tensile stress and elongation at break values of the composites generally

decreased with increasing EG content due to poor wettability of EG by the PP and poor interfacial adhesion. The tensile modulus of the composites increased with increasing filler content, because of the higher modulus of the EG filler. EB irradiation did not significantly influence the maximum stress values due to the crosslinking and degradation effects which balanced out. For the MAPE/graphite composites all the mechanical properties increased up to a maximum of 4 wt% filler, and the SDS-EG containing samples gave better mechanical properties than the EG containing composites. EB irradiation increased both tensile stress at break and tensile modulus values, while the elongation at break values decreased with increasing EB irradiation dose.

The composites exhibited a transition from insulator to conductor with an electrical percolation threshold of 5-8 wt%. The EG containing samples generally showed lower percolation thresholds than the SDS-EG containing samples because SDS formed an electrical isolation layer around the EG particles. The EB irradiation increased the electrical percolation threshold due to radiation induced crosslinking which disturbed the formation of electrical percolation networks.

The thermal stability of polymer matrices increased with increasing filler content, but the SDS-EG containing samples were more stable because of the better interaction between the graphite platelets and the polymer matrix. EB irradiation increased the thermal stability when crosslinking dominated, and decreased the thermal stability when chain scission dominated. The presence of EG particles did not influence the melting temperature of the matrix, but shifted crystallization towards higher temperatures, indicating that EG acted as a nucleating agent, but SDS-EG showed slightly lower nucleation efficiency. EB irradiation did not have any influence on the melting and crystallization temperatures of the polymers.

Both the storage modulus and complex viscosity of the molten polymer observably increased with increasing filler content, but the storage modulus values increased and complex viscosity values decreased with increasing frequency. The SDS-EG containing samples had a more significant effect on both properties at low EG contents, while at high EG loadings the effect was similar. The presence of EB irradiation significantly increased the storage modulus and complex viscosity values of MAPE samples due to radiation induced crosslinking of the polymer chains.

TABLE OF CONTENTS

LIST OF TABLES

LIST OF FIGURES

LIST OF SYMBOLS AND ABBREVIATIONS

0-D	zero dimensional
1-D	one dimensional
2-D	two dimensional
AC	alternating current
ASTM	American Society of Testing methods
CMNCs	ceramic matrix nanocomposites
C_p	specific heat capacity
$–CH_2^–$	methylene group
C-H	carbon-hydrogen
DAA	dicarboxylic acid anhydride
$\Delta H_{m,EVA}$	experimentally observed melting enthalpy for the pure EVA
ΔH_m^{Norm}	normalised enthalpy of melting
ΔH_m^o	specific enthalpy of melting for 100% crystalline PE
ΔH_m	measured melting enthalpy
$\Delta H_{m,PP}$	experimentally observed melting enthalpy for the pure PP
DI	dispersity index
DMA	dynamic mechanical analysis
DMF	dimethyl formamide
DSC	differential scanning calorimetry
E	tensile modulus
E′	storage modulus
EB	electron beam
ε_b	elongation at break
EG	expanded graphite
EPDM	ethylene propylene diene monomer
EVA	ethylene vinyl acetate
F	fraction of filler insoluble in xylene in the composites
G′	complex shear modulus
GO	graphite oxide

GOS	surfactant intercalated graphite oxide
GPC	gel permeation chromatography
HDPE	high-density polyethylene
Hz	Hertz
iPP	isotactic polypropylene
I_α	diffraction peak intensities of the α-crystals
I_β	diffraction peak intensities of the β-crystals
JCPDS	Joint Committee on Powder Diffraction Standards
k_β	relative β-crystal content
MA	maleic anhydride
m_{AE}	sample mass after extraction
m_{BE}	sample mass before extraction
MAPE	maleic anhydride-grafted polyethylene
MAPP	maleic anhydride-grafted polypropylene
MFI	melt flow index
MMNCs	metal matrix nanocomposites
MWCNT	multi-wall carbon nanotubes
M_n	number average molar mass
M_w	weight average molar mass
ODA	octadecylamine
PA6	polyamide 6
PE	polyethylene
PET	poly(ethylene terephthalate)
PGNs	polymer-graphite nanocomposites
PMNCs	polymer matrix nanocomposites
PNCs	polymer nanocomposites
PP	polypropylene
PS	polystyrene
PVA	poly(vinyl alcohol)
PVC	poly(vinyl chloride)
ρ_{th}	material density

ρ_{EVA}, ρ_{EG}	density of EVA, that of expanded graphite
SEM	scanning electron microscopy
SDS	sodium dodecyl sulphate
SDBS	sodium dodecyl benzene sulfonate
s	standard deviation
tan δ	damping coefficient
T_c	crystallization temperature
T_g	glass transition temperature
T_m	melting temperature
T_{max}	temperature at maximum or chain scission loss
$T_{10\%}$	degradation temperatures at 10 % mass loss
T_{-40}, T_{40}	temperature at -40 °C and 40 °C
$T_{50\%}$	temperature at 50 % mass loss rate
TGA	thermogravimetric analysis
THF	tetrahydrofuran
$T_{p,m}$	peak temperature of melting
TPU	thermoplastic polyurethane
VA	vinyl acetate
vol%	volume percentage
UV	ultra-violet
w_{EVA}	weight fraction of EVA
wt%	weight percentage
xGnP	exfoliated graphite nanoplatelets
XRD	X-ray diffraction
χ_c	degree of crystallinity
Ω	resistance
λ	thermal conductivity
α	thermal diffusivity
φ	filler volume fraction
φ_c	percolation threshold
σ_m	maximum stress

η	complex viscosity
ω	angular frequency

Chapter 1

Introduction and literature review

1.1 Introduction

The incorporation of conducting nano-structured fillers in a polymer matrix gives rise to a very interesting class of materials called polymer nanocomposites (PNCs) [1-4]. These polymeric materials are expected to display desired properties emerging from the combination of different constituents. According to their matrix material, nanocomposites can be categorized as ceramic matrix nanocomposites (CMNCs), metal matrix nanocomposites (MMNCs) and polymer matrix nanocomposites (PMNCs), the latter of which is the focus of the work in this thesis. PMNCs are commonly defined as multiphase materials, where one of the constituent phases has nanoscale with at least one dimension less than 100 nm [5-7]. They are mixed at the macroscopic level. With the decrease in the size of the reinforcement particles, the contact area of the reinforcement with the matrix is increased, which means that the efficiency of the reinforcement can be extensively improved. However, to mix different components on microscopic or nanoscopic levels is far more difficult than on a macroscopic level due to the significant increase in the surface energy derived from the increase in interfacial areas [8].

Polymers are currently the most used class of materials in the field of technical textiles, packaging and the cable industry [9,10]. Various organic polymers such as nylons, polyesters, polyurethane and polyolefins have been used for key features like lightweight, easy fabrication, exceptional processability, durability, availability and relatively low cost [11,12]. The major challenge in polymer or materials science is to broaden the application period of such materials by retaining their features, while improving certain characteristics such as modulus, strength, fire performance and heat resistance [13]. However, polymers have relatively poor mechanical, electrical and thermal properties compared to metals and ceramics. Various types of polymers such as copolymers, homopolymers, blended polymers and modified polymers are not satisfactory enough to compensate for the many properties required, but reinforcement with fibres, whiskers, platelets or particles may change the situation. The choice of the polymers used

in this study and presented in Figure 1.1 was mainly motivated by their mechanical, thermal, electrical and rheological properties. However, other properties such as hydrophobic or hydrophilic character, chemical stability, compatibility and chemical functionalities (functional groups, wettability, etc.) have to be considered when choosing the required polymer.

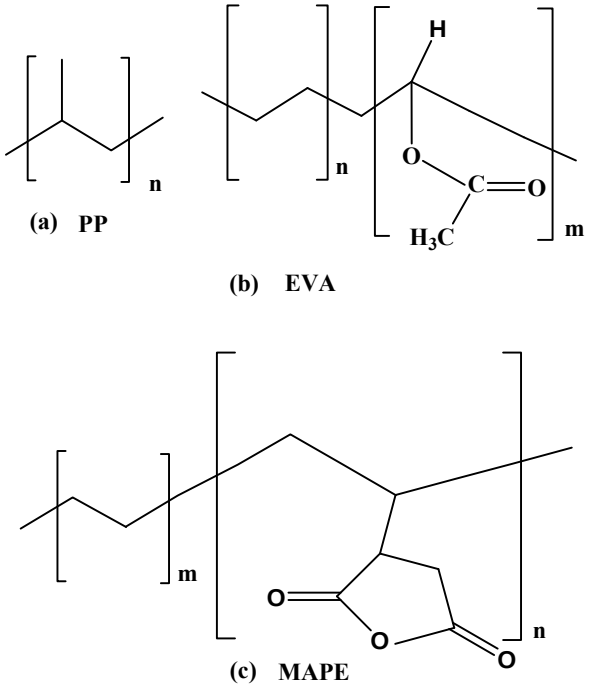

Figure 1.1 Chemical structures of the polyolefins used in this study (a) polypropylene (PP), (b) ethylene vinyl acetate (EVA), and (c) maleic anhydride-grafted polyethylene (MAPE)

Polymers can be easily shaped and processed, and nanoplatelets or nanoparticles may provide mechanical and thermal stability, and/or new functionalities that depend on the chemical nature, structure, size and crystallinity of the nanoparticles. Nanoparticles may also remarkably improve the mechanical, thermal, density, electro-optical, and barrier properties of the polymers [14]. Nanoparticles have much higher aspect ratios, surface areas, and strengths than conventional micro-sized particles. As the particle size decreases, the percentage of matrix molecules in contact with the nanoparticle surfaces is significantly higher [15-17], and as a result the interparticle forces such as van der Waals and electrostatic forces become stronger. Without proper chemical treatment to reduce the surface energy, it is a common behaviour for nanoparticles to form clusters or agglomerates that are difficult to uniformly disperse in the polymer matrix, so that they act in the same way as fillers in conventional composites [14,16-

18]. Nanoparticles can be classified according to their shapes and dimensions as 0-D (spherical), 1-D (rod- or tube-like), and 2-D (plate-like particles) [19-22]. They can also be classified depending on the material: nanoclays, carbon nanotubes, metals and metal oxides, cellulose, and graphite platelets. The extent of property enhancement depends on many factors such as the aspect ratio (length-to-diameter) of the filler, its degree of dispersion and orientation in the matrix, and the adhesion at the filler-matrix interface [14,22].

Conductive polymer-matrix composites based on polymers containing graphite nanoparticles or carbon derivatives attracted significant interest because of their unique properties emerging from the combination of organic polymer and conducting filler particles. Generally, the resulting nanocomposites exhibit many improved properties such as optical, mechanical, thermal, electrical and rheological properties. These types of composites have therefore been widely used in various fields like military equipment, safety, protective garments, automotive, aerospace, electronics and optical devices. These application areas, however, consistently and constantly demand additional properties and functions like good mechanical properties, flame retardancy, chemical resistance, UV resistance, electrical conductivity, environmental stability, and water-resistance. The effective properties of the composites are solely dependent upon the individual constituents, the morphology of the system, the volume fraction of components, the shapes and arrangement of fillers, and the interfacial interaction between the matrix and the filler [14,15].

1.2 Expanded graphite (EG)

Graphite is a naturally abundant allotrope of carbon with very strong anisotropic properties, and it consists of graphene layers stacked along the c-axis in a staggered array of two-dimensional hexagons (sp^2-hybridized graphene layers) [19-25]. It is regarded as a layered material where carbon atoms are held together by covalent bonds or other carbons in the same plane (Figure 1.2), with only relatively weak van der Waals forces between the layers that make the intercalation of atoms, molecules and ions possible [16,17]. Graphite is classified into natural and synthetic graphite. Natural graphite is considered as a mineral with three common classes based on the different geological environments in which they occur. The three classes are as follows: (i) amorphous, (ii) vein/plumbago, and (iii) natural flake. Natural flake graphite is

commonly divided into microcrystalline and macrocrystalline graphite, and synthetic graphite into primary and secondary synthetic graphite. Microcrystalline graphite (amorphous) has a low crystallinity, purity and thus an extremely low conductivity, while macrocrystalline graphite has large oriented crystals in a lamellar shape with acceptable conductivity [26-28]. Synthetic or artificial graphites are manufactured through heating a carbonaceous precursor in an inert atmosphere to temperatures above 2400 ºC. EG is the result of a structural treatment of graphite obtained from intercalated [26,27,29,30] or oxidized [22] graphite through thermal reduction. This treatment of the graphite leads to a light worm-like structure comprising of graphene nanoplatelets (GNPs).

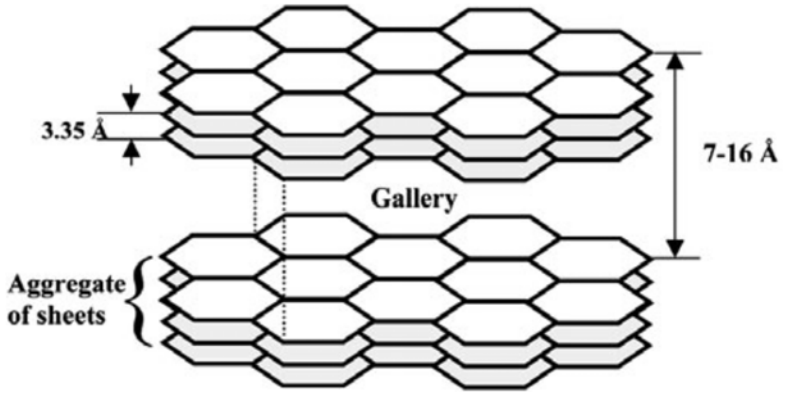

Figure 1.2 Schematic representation of the crystal structure of graphite [30]

1.3 Dispersion of expanded graphite in polymers

Dispersion is a key issue in polymer-EG composites processing since their properties depend strongly on how well dispersed they are. The EG particles tend to aggregate to form bundles or sheets due to the van der Waals interaction, and further agglomerate when dispersed in a polymer matrix. The high aspect ratio and surface area of the EG sheets also result in high viscosities of the polymer/graphite composites, particularly when preparing nanocomposites with high filler concentrations. The dispersion of EG sheets in a polymer can be improved through several techniques such as sonication, ball milling and shear mixing, as well as extrusion and calendaring after functionalization of the EG particles.

1.3.1 Sonication

Sonication is a processing technique widely used in the laboratory to disperse solid particles in solution. This process uses ultrasound energy to agitate the nanoparticles in the polymer in solution, and is carried out by an ultrasonic bath or a horn/probe called the sonicator. During the sonication process, the ultrasound propagates through a series of compressions. When it passes through the polymer medium, attenuated waves are induced, promoting the 'peeling off' of the EG sheets situated at the surface of the nanoparticle bundles or agglomerates. As a result, single layers are separated and high quality dispersion can be accomplished [31]. However, this process is only appropriate to disperse the nanoplatelets in solutions that have a very low viscosity such as water, acetone, ethanol, chloroform, tetrahydrofuran (THF), dimethyl formamide (DMF) and toluene [32]. However, most polymers are viscous and therefore it is vital to dissolve the polymer prior to the dispersion process. When the duration of the process is longer, the intensity of the input energy is higher, and better dispersion quality can then be achieved. However, greater care must be taken when such processes are carried out, since severe treatment can lead to serious damage of the CNT structure, in particular when a probe sonicator is used. For instance, the graphene layers of carbon nanotubes can be completely destroyed and the particles become amorphous carbon graphite [33]. Ultimately, such induced damages would deteriorate the electrical, thermal and mechanical properties of the nanocomposites.

1.3.2 Ball milling

Ball milling is a grinding method that grinds EG into extremely fine powders. During this process, the collision between the tiny rigid balls in a masked container will generate localized high pressure. Usually, ceramic, flint pebbles and stainless steel are used. In order to further improve the quality of dispersion and introduce functional groups onto the EG surface, preferred chemicals can be included in the container during the process. The factors that affect the quality of dispersion are the milling time, rotational speed, size of the balls, and EG aspect ratio. Under certain processing conditions, the particles can be ground to as small as 100 nm. This process has been used to transform EG into smaller nanoparticles to generate highly closed sheets or stacked layers from graphite to enhance the modification. Despite the fact that ball milling is easy to

operate and suitable for powder polymers or monomers, the process can induce some damage to EG particles [34].

1.3.3 Shear mixing, extrusion and calendaring

The sonication and ball milling processes may seldomly induce damage to the CNT structure, but there are alternatives to disperse the CNT without damage. These are shear mixing, extrusion and calendaring which is also known as three-roll milling. Shear mixing is widely used in the laboratory to disperse CNT into a polymer matrix. The size and shape of the propeller and its rotational speed determine the dispersion quality. However, for some thermosetting polymers the re-agglomeration of the CNT becomes spontaneous under static conditions [18,33], and a much higher mixing speed is then required. The extrusion process is usually carried out by a twin screw available in industry for large-scale production. This process is only suitable to blend the CNT particles with thermoplastics, and the dispersion is influenced by factors such as environmental temperature, configuration and rotational speed of the screw. Calendaring utilizes shear force created by the rollers to mix, disperse or homogenize the nanotubes in viscous polymers, oligomers, and/or monomers. Factors such as the rotational speed of the rollers and the distance between adjacent rollers significantly affect the quality of dispersion.

1.3.4 Functionalization of EG

An efficient stress transfer from the polymer matrix to the graphite sheets is required to take advantage of the very high Young's modulus and strength of graphite platelets in the nanocomposite. In contrast to conventional fibre-reinforced polymer composites, large interfacial areas are available for stress transfer in polymer-EG based composites due to the high aspect ratio of the nanoparticles. On the other hand, the lack of strong interfacial bonding between the EG and the polymer matrix causes EG to agglomerate, creating some voids or cracks under stress and resulting into inefficiency of stress transfer. For this reason, there are common dispersing methods used in nanocomposites like the modification of EG surfaces by covalent functionalization [22,35-38] or non-covalent treatments [39-41] to unbundle the EG sheets and increase the interfacial bonding between the EG and the matrix.

1.3.4.1 Covalent functionalization of EG

Covalent functionalization of EG has been used to significantly improve the platelets' solubility in solvents and chemical compatibility with the matrix to reinforce various composite materials. For example, strong acids or other strong oxidizing agents are used to treat graphite to create open sites (break bonds in the graphitic structure) and to subsequently attach various functional groups to the open-ended and/or defect sites [22]. Typical methods for covalent functionalization include fluorination, ozonolysis, organic functionalization, osmylation, and azomethineylation [35,36,37]. Covalent functionalization has been shown to greatly improve EG dispersion in polymer matrices, and to play a critical role in the thermal and electrical properties of EG/polymer composites [39,40]. Chemical or covalent functionalization increases the interparticle contacts (i.e. useful for building up a conductive network) and provides more possibilities to bond the graphite to a matrix due to reactive chemical groups, while covalent surface treatments can destroy the graphite structure, resulting in shortening of the platelets, the creation of defects in the graphitic structure of the EG chains and, in some cases, unzipping of the chain structure. Consequently, chemical functionalization will reduce the mechanical properties of EG [39-41].

1.3.4.2 Non-covalent functionalization of EG

Non-covalent dispersing methods also exfoliate graphite bundles into individual particles in different solvents using various anionic, cationic or nonionic surfactants [35,37] (see Figure 1.3) or polymers [14,17]. The adhesion of chemical moieties or polymer molecular wrapping on the EG surface occurs as a result of non-covalent supramolecular interactions, including hydrophobic–hydrophobic interactions, van der Waals forces, π–π interactions, hydrogen bond linkages, and electrostatic attraction [16-18]. These non-covalent interactions eliminate the chemical modification of the graphitic structure (thus preserving mechanical, electrical, and optical characteristics of the nanoplatelets), and enable the EG to have improved interactions with and/or solubility in more solvents (see Figure 1.3).

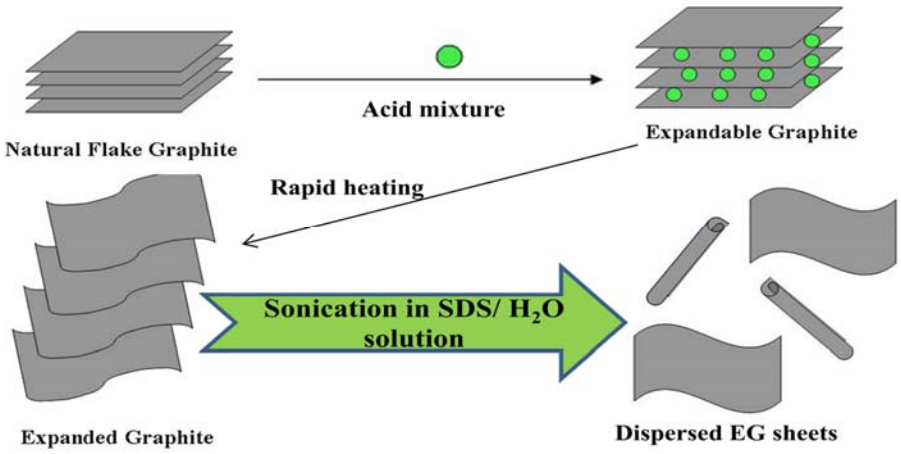

Figure 1.3 Schematic representation of expanded graphite dispersion

1.4 Preparation methods of graphite (nano)composites

Graphite has a layered nanostructure similar to that of clay nanoparticles; hence the preparation methods used for polymer-graphite nanocomposites (PGNs) are similar to those used for polymer-clay nanocomposites (PCNs). Many methods, such as exfoliation-adsorption (solution) intercalation, melt intercalation and *in situ* intercalation polymerization, are widely used for the preparation of PCNs and can also be used to produce PGNs. However, natural graphite is chemically different from clay; the relatively simple exchange reactions used to modify clay cannot be used with graphite. Furthermore, due to the non-dispersibility of graphite in aqueous or organic media, it is very difficult for a monomer or polymer to attach to its surface. Graphite is also insoluble in most common solvents, and therefore modified graphite platelets are used for the preparation of PGNs. There are three main methods for the preparation of polymer-graphite containing composites.

1.4.1 Solution intercalation

Solution intercalation is considered as a solvent system in which the polymer or pre-polymer is dissolved and graphite layers are allowed to expand or swell. The graphite or expanded graphite can be readily dispersed in a suitable solvent such as water, acetone, chloroform, tetrahydrofuran (THF), dimethyl formamide (DMF) and toluene owing to the weak forces that hold the layers

together. The polymer then adsorbs onto the sheets' surfaces and when the solvent is evaporated *via* the vaccum drying and mixing, the sheets reassembled, sandwiching the polymer to form the nanocomposites. This method can be easily employed to fabricate polymer-based nanocomposites, but equally important is the removal of the solvent. The solvent molecules need to be desorbed from the graphite to accommodate the polymer segments. The prime advantage of this method is to allow the synthesis of intercalated nanocomposites based on polymers that possess extremely low or no polarity. Several polymers like MAPE, PP, poly(vinyl alcohol) (PVA) and poly(vinyl chloride) (PVC) [42-44] have been used in this method to prepare nanocomposites.

1.4.2 Melt intercalation

Melt mixing deals with insoluble polymers and is useful in preparing nanocomposites based on thermoplastic polymers such as polypropylene (PP), high-density polyethylene (HDPE), polyamide 6 (PA6), thermoplastic polyurethane (TPU), ethylene vinyl acetate (EVA) and polystyrene (PS). This method is mostly preferred for thermoplastic polymers that become soft when subjected to heat, while their properties remain the same after cooling. Polymers that are not suitable for solution mixing or *in situ* polymerization can be processed by this technique. A thermoplastic polymer in pellet form is normally mechanically mixed with a large volume of EG particles at elevated temperatures to form a viscous liquid. The EG particles are then blended into the viscous polymer by a high shear mixer or in an extruder. The addition of nanoparticles into a molten polymer will affect its viscosity and lead to unexpected polymer degradation under high shear conditions. During the melt-mixing process the polymer molecules penetrate into the interlayer space between the EG sheets and the diffusion process peels the layers away. Depending on the compatibility between the components and the processing conditions, either an intercalated or exfoliated structure can be achieved [45,46].

1.4.3 *In situ* intercalation polymerization

During an *in situ* polymerization process, nanoparticles like EG are first dispersed in a liquid monomer. The polymerization reaction is then initiated either by heat or radiation, by diffusion

of a suitable initiator, or by an organic initiator or catalyst attached on the surface of EG [21,22]. After completion of the polymerization, the polymer molecules are either wrapped around or covalently bonded to the nanoparticles, depending on the surface functionality of the filler particles and the polymer being formed [22]. *In situ* polymerization can be used to prepare a nanocomposite containing an insoluble or thermally unstable polymer, which cannot be processed by solution or melt intercalation processes. Ring-opening, radical, anionic and chain transfer metathesis polymerizations were used, depending on the required molecular weight and molecular weight distribution of the polymers [47]. The advantages of this process include the enabling of grafting of the polymer chains onto the surfaces of the nanoparticles, and allowing the preparation of nanocomposites with good compatibility between the components. The polymerization reactions can lead to two competing processes crosslinking and chain scission (polymer degradation).

1.5 Crosslinking

Crosslinking is the intermolecular bond formation between polymer chains and leads to the formation of network structures. Crosslinking restricts chains from sliding past one another and produces elasticity in an amorphous polymer. Crosslinking is generally irreversible [48-50]. Crosslinked polymers subjected to heat will not undergo any melting or flowing. When semi-crystalline polymers are crosslinked, they exhibit thermoplastic mechanical properties below their melting temperatures (T_m), and rubbery mechanical properties above their T_m. Crosslinking leads to an increase in the viscosity of the polymer melt, increased tensile strength, improvement in creep properties and an increase in the resistance to environmental stress cracking [51,52]. The effects of crosslinking on the physical properties of polymers are primarily influenced by the degree of crosslinking, the regularity of the network formed, and the absence or presence of crystallinity in the polymer. A molten polymer undergoing a chemical crosslinking process is transformed from a viscoelastic liquid into a viscoelastic solid.

Chemical modification in reactive polymer processing may cause important changes in the rheological behaviour, leading to critical consequences in the flow behaviour [53]. Mixing and film processing for instance require sufficient segmental or molecular mobility, which disappears when the chain motion slows down in the vicinity of the gel point [54]. The latter process

enables a thermoplastic polymer like PE to show viscoelastic behaviour, similar to the characteristics of an elastomer, at temperatures above the crystalline melting temperature of the thermoplastic. This property is broadly utilized commercially in the preparation of heat-shrinkable materials, wire and cable coatings, hot-water tubing and food packaging [55-57]. Sulphur crosslinking is normally used for polymers with unsaturated double bonds. If the polymer does not have double bonds in its structure, other methods such as peroxide initiated curing [58], silane-water crosslinking [59], and electron beam irradiation [48,60] can be used. The latter method is the focus of this study.

Radiation crosslinking of polyolefins has a number of advantages over thermal curing, such as the absence of various noxious chemical additives, high speed of the curing process, effective penetration depth of radiation into the sample, uniformity and ease of curing [61]. Radiation crosslinking is a well-established industrial process which is usually applied to the final products at ambient temperatures [48-50,55-60]. The most commonly used industrial irradiation processing techniques are gamma (γ) and electron beam (EB) irradiation. In the work reported in this thesis EB irradiation has been selected because it is very energy-efficient, and all the energy is deposited into the material. EB irradiation has no radioactive isotope, which makes it a safer technique to use [48,60].

The degree of crosslinking is directly proportional to the radiation dose, and does not require unsaturated or reactive groups. Gel content is commonly determined in radiation polymer chemistry, and is accepted as a measure of the crosslinking degree after exposure to EB irradiation in the presence of either air or nitrogen. Several papers reported on irradiated polyolefin/graphite composites [2,18,50,51,53,60,61]. Generally the gel content of these composites was significantly higher than that of the polymer irradiated in the absence of graphite, which was ascribed to the graphite sheets conducting energy from the electron beam irradiation and improving the efficiency of free radical formation and crosslinking.

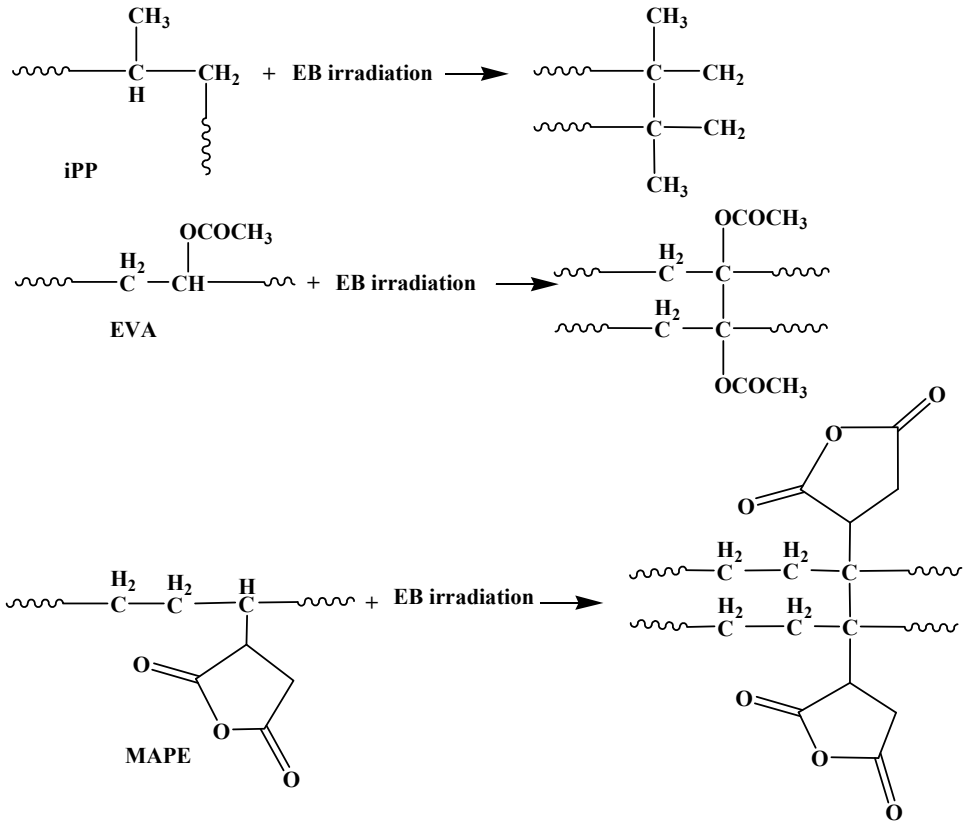

Figure 1.4 Typical radiation induced crosslinking reactions of polymers used in this study

Generally the gel content values were found to significantly increase with increasing graphite content for polymer/graphite composites [14,15]. The increase in the crosslinking degree was ascribed to the increased formation of insoluble macromolecular networks called crosslinks in the polymer. The presence of conducting filler like graphite conducts radiation energy, and therefore could enhance the efficiency of free radical formation and crosslinking. The universally accepted crosslinking mechanism involves the cleavage of a C-H bond on the polymer chain to release a hydrogen free radical, followed by the abstraction of a second hydrogen free radical from a neighboring chain to produce molecular hydrogen. The two adjacent polymeric radicals then combine to form a crosslink (Figure 1.4), leading the formation of a three-dimensional polymer network. Electron beam radiation provides the energy needed to cleave the C-H bonds [58].

1.6 Chain scission and degradation

Polymer degradation is a well-known natural and/or accelerated process which occurs in oxygen atmosphere during synthesis, processing and/or service life, or under the action of ageing factors like temperature, UV/gamma/electron beam irradiation, or pollutants in the atmosphere. The chemical structure, morphology, physical and/or mechanical properties of the polymer can change because of degradation. Although degradation should be inhibited for some applications, it can also be used to tailor the polymer chemical structure in order to obtain goods with desired properties [58-61].

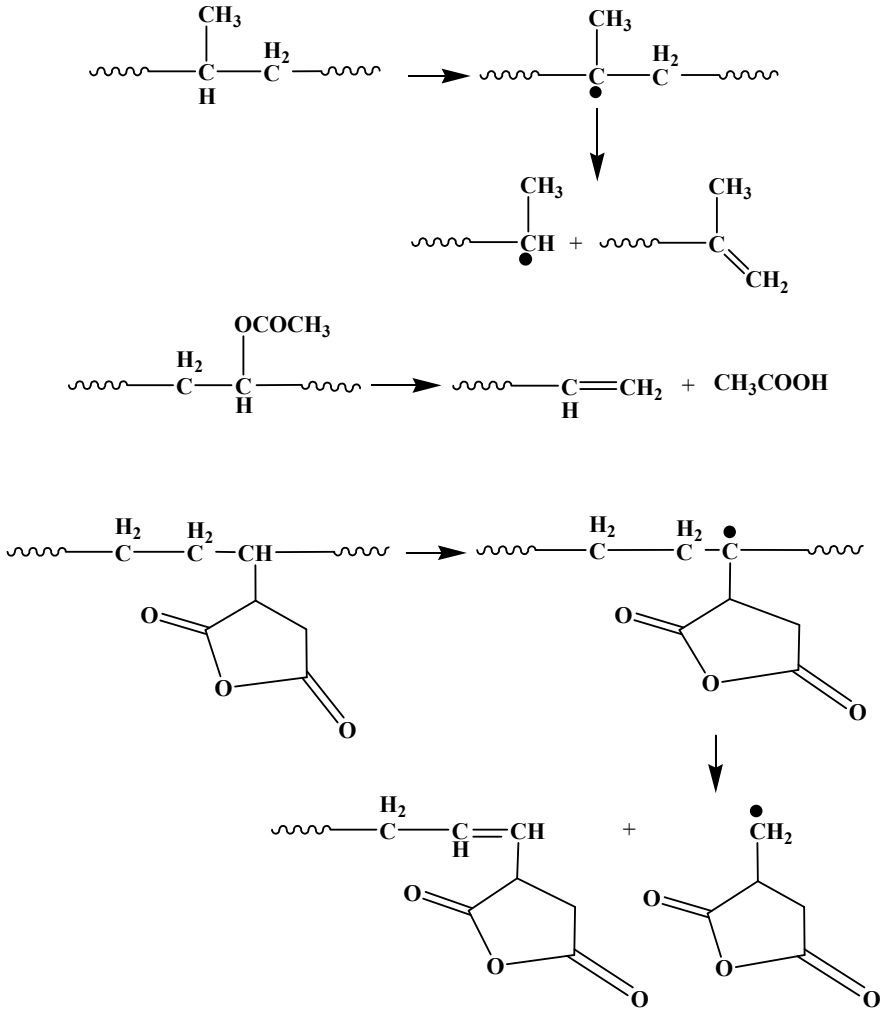

Figure 1.5 Possible chain scission reaction-mechanisms in iPP, EVA and MAPE polymers

1.7 Properties of polymer nanocomposites

Polymer-based nanocomposites were prepared using various processes, and they showed some changes in morphology, as well as improved thermal, electrical, rheological and mechanical properties. However, these properties were not consistently improved because of a number of contributing factors such as the aspect ratio of the filler, their dispersion and orientation in the matrix, and the adhesion at the filler-matrix interface. It was often found that one property improved at the expense of another property. During the preparation of polymer nanocomposites, one needs to take into account this behaviour and tries to find the optimum properties for specific applications.

1.7.1 Morphology

A study of the morphology of non-irradiated and irradiated polymers reinforced with graphite nanoparticles is of great importance, because the filler content, particle size and dispersion of the expanded graphite particles significantly influence the properties of the polymer composites. In most cases scanning electron microscopy (SEM) and polarized optical microscopy (POM) were used to characterize the morphology of these composites. Several studies were conducted on melt-compounded non-irradiated and irradiated polyolefins reinforced with graphite platelets in the absence and presence of ionic surfactants (sodium dodecyl sulphate (SDS) and sodium dodecyl benzene sulfonate (SDBS)) under different preparation conditions [36-38]. The main observation from these studies was that both SDS and SDBS gave rise to a uniform dispersion of EG, but SDBS contributed to better long-term stability of EG dispersion. This was attributed to the steric hindrance effect of the additional benzene ring of SDBS. In a study where polyolefin matrices were filled with expanded graphite particles, a significant amount of particle agglomerations were observed with increasing filler content, while in the presence of detergent or surfactant the filler particles were homogeneously dispersed [62-65]. The particle agglomerations were attributed to the high degree of particle-particle attraction and insufficient shear force during mixing. The presence of surfactant treatment restricted the graphite agglomeration, which resulted in a much better dispersed system.

1.7.2 Thermal properties

The thermal properties of polyolefin/graphite composites were studied by a number of researchers using thermal conductivity measurements, thermogravimetric analysis (TGA), and differential scanning calorimetry (DSC) [29,30,66]. The thermal conductivity of these materials is important because of the use of these materials in heat sink applications such as computers, laptop cases, and transformer housings [26,27], and it normally increased with increasing filler content. This was due to the fact that the filler had a much higher thermal conductivity (6.0 W m^{-1} K^{-1}) [67] than the polymers (0.11-0.35 W m^{-1} K^{-1}). Non-irradiated polyolefin/graphite composites were found to have higher thermal conductivities than the irradiated composites [26,61]. This was related to the degree of crosslinking in the irradiated composites inducing restricted chain mobility and reduced vibration of phonons, hampering the heat transfer and leading to lower conductivities.

The melting temperature of neat PP and its graphite composites was pretty much the same within experimental error, but the melting enthalpy significantly increased up to 5% of graphite content [30]. The crystallization temperature of PP increased in the presence of graphite, and maleic anhydride grafted PP (MAPP) modified PP/graphite composites had higher crystallinity values than the non-modified PP composites. This behaviour confirmed that the graphite particles acted as nucleating agents for the crystallization of PP, and that they were better dispersed as a result of the chemical interaction between the maleic anhydride groups of MAPP and the graphite layers. Another study on maleated PP filled with graphite oxide (GO) or octadecylamine (ODA) surfactant intercalated graphite oxide (GOS) [65] showed the same behaviour. It also showed that the crystallization of maleated PP was faster in the presence of GOS. In a non-isothermal crystallization study of poly(ethylene terephthalate) (PET) and PET/EG composites it was found that the addition of EG improved the crystallization, but only at low EG contents [68]. This implied that EG nucleated the polymer but also immobilized the polymer chains.

The presence of graphite particles enhanced the thermal stability of PP [30], which further improved after surfactant treatment of the graphite [37,38]. In some studies the thermal stability of polyolefin-based graphite composites was found to be significantly higher than that of the polymer matrix [70,71]. Reasons given for this are: (i) numerous defect sites on reduced

graphene oxide (RGO) that effectively caught the free radicals, and also retarded the release of the volatile degradation products; (ii) the strong interaction between poly(vinyl alcohol) (PVA) and graphene oxide (GO) nanoplatelets [71] at the interface, leading to a reduced mobility of the polymer chains near the interface. Poly(ethylene-co-vinyl acetate) (EVA) with about 31 wt% vinyl acetate content and filled with dispersed clay platelets showed a lower thermal stability at an early stage of degradation [72]. This was due to the fact that the layered silicates accelerated the degradation of acetic acid in the composites. However, the thermal stability of the nanocomposites increased with increasing EB irradiation dose up to 200 kGy because of the formation of crosslinking networks.

1.7.3 Electrical properties

The electrical conductivities of all the investigated polyolefin based samples as a function of graphite content prepared by melt mixing showed an improvement in electrical conductivity. This improvement was attributed to the graphite platelets forming a conductive network for the transfer of electrons within the system. Graphite is well-known for its excellent thermal and electrical conductivity, which are absent in clay materials [1,4,12,16]. Grafted PP/EG composites prepared by melt and solution mixing changed from electrical insulators to conductors [44]. Samples prepared through solution mixing had higher electrical conductivity values than those prepared through melt-mixing. Similar changes in electrical conductivity were observed for TPU/EG [66] and HDPE/EG composites [69]. These changes were explained in terms of the formation of conducting networks and the percolation theory. In a study on the EPDM rubber/HDPE/carbon black composites [73] it was found that electron beam radiation had no effect on the electrical conductivities of the polymer composites at 20 wt% carbon black. This was attributed to the high level of crosslinking which restricted the polymer chain mobility, and as a result influenced the electron movement in the composites. The electrical conductivity increased with increasing EB radiation doses at 60 and 80 wt% filler contents. This confirmed that at higher quasi-graphite carbon black loadings there were smaller distances between the particles, allowing easier transfer of electrons from one particle to the other.

1.7.4 Rheological and viscoelastic properties

Rheological studies provide further information on the structure-property relationships in polymer/graphite composites. Rheological analyses showed an increase in both the storage and loss moduli as a function of filler content, especially at lower frequencies [4,16,53]. Their storage moduli showed the development of a Newtonian plateau at low frequencies and a non-linear region at high frequencies. The plateau modulus of the samples increased with increasing organoclay content due to the reinforcement effect of the filler platelets. A rheological percolation or the formation of a network-like arrangement of the filler in the polymer melt was observed as plateau formation in the low frequency region, or as a positive deviation of the complex viscosity from the plateau level in the complex viscosity versus frequency plot. It was also found that after EB irradiation, the slope of the storage modulus decreased at low frequencies with an increase in the radiation dose, and the Newtonian plateau disappeared because of radiation induced crosslinking [53]. A rheological study on polypropylene/carbon nanotube composites [74] to investigate the influence of rheological percolation on the phase angle as a function of complex modulus showed that a significantly increased complex modulus gave rise to a lower value of rheological percolation because of the stronger adhesion between carboxylically functionalized carbon nanotube and polymer matrix. The presence of filler gave rise to a maximum phase angle at a certain level of the complex modulus because of the formation of a pseudo-solid like filler network.

Dynamic mechanical analysis (DMA) was mostly used to get information on the viscoelastic properties of graphite-filled polymer nanocomposites [49,65,68]. The presence of the nano-structured graphite particles in the polyolefin matrices generally gave rise to a significant increase in the storage modulus, loss modulus and tan δ. The storage moduli at high temperatures increased with increasing graphite content, and the glass transition shifted to higher temperatures. This was attributed to the higher stiffness of the expanded graphite and the interaction between the polymer and the filler, which resulted in a restriction of the polymer chain mobility in the composite.

1.7.5 Mechanical properties

The main reason for adding inorganic particles into polymers is generally to improve their mechanical properties such as the tensile strength and modulus *via* reinforcement mechanisms [2,11,12,26]. However, the main challenge has always been the poor compatibility between the polymers and the inorganic particles in the composites prepared by melt-mixing. Melt-mixing normally creates inherent defects that result in a reduction in the mechanical properties of the composites, as reported by a number of authors [35,52,58]. The tensile properties such as the stress and elongation at break normally decrease, while the tensile modulus normally significantly increases. However, some reports showed reduced mechanical properties, especially at high graphite loadings [23,35,56]. The differences in the influence of these nanoparticles on the mechanical properties were mainly attributed to the filler agglomeration in the polymers. The presence of aggregates in the composite results in poor compatibility and de-wetting or crazing, in which the adhesion between the filler and matrix phase is destroyed, and this result in a decline in the mechanical properties.

1.8 Objectives

The prime objectives of this study were as follows:

- The preparation of polymer nanocomposites, based on polyolefin matrices filled with nano-structured expanded graphite (EG). The incorporation of EG into a polymer matrix should increase the modulus and strength, as well as electrical and thermal conductivities compared to those of the neat polymers.
- The improvement of the interfacial interactions between the polymer matrix and the expanded graphite by chemical modification of the EG platelets and/or the functionalization of polymers.
- Obtaining good dispersion of EG in polyolefins without agglomeration in order to obtain low electrical and thermal conductivity percolation thresholds.
- Determination of the effect of an anionic surfactant, used to improve EG particle dispersion, on the electrical and thermal conductivities of the systems.

- ❖ Study the influence of electron beam irradiation in nitrogen atmosphere on all the investigated properties.

1.9 References

1. K. Prashantha, M.F. Lacrampe, P. Krawczak. Processing and characterization of halloysite nanotubes filled polypropylene nanocomposites based on a masterbatch route: Effect of halloysite treatment on structural and mechanical properties. eXPRESS Polymer Letters 2011; 5:295-307.
   DOI: 10.3144/expresspolymlett.2011.30
2. I. Krupa, V. Cecen, A. Boudenne, Z. Križanová, I. Vávra, R. Srnánek, G. Radnóczi. Mechanical properties and morphology of composites based on the EVA copolymer filled with expanded graphite. Polymer-Plastics Technology and Engineering 2012; 51:1388-1393.
   DOI: 10.1080/03602559.2012.704114
3. G. Schmidt, M.M. Malwitz. Properties of polymer-nanoparticle composites. Current Opinion in Colloid and Interface Science 2003; 8:103-108.
   DOI: 10.1016/S1359-0294(03)00008-6
4. A. Kasgoz, D. Akin, A. Durmus. Rheological and mechanical properties of cycloolefin copolymer/organoclay nanocomposites. Journal of Reinforced Plastics and Composites 2012; 31:1329-1341.
   DOI: 10.1177/0731684412461190
5. Y.-Q. Zhang, J.-H. Lee, J.M. Rhee, K.Y. Rhee. Polypropylene-clay nanocomposites prepared by in situ grafting-intercalating in melt. Composites Science and Technology 2004; 64:1383-1389.
   DOI: 10.1016/j.compscitech.2003.10.014
6. J. Ma, H. Deng, T. Peijs. Processing of poly(propylene)/carbon nanotubes composites using $scCO_2$-assisted mixing. Macromolecular Materials and Engineering 2010; 295:566-574.
   DOI: 10.1002/mame.200900405

7. T. Ramanathan, S. Stankovich, D.A. Dikin, H. Liu, H. Shen, S.T. Nguyen, L.C. Brinson. Graphitic nanofillers in PMMA nanocomposites – An investigation of particle size and dispersion and their influence on nanocomposite properties. Journal of Polymer Science Part B: Polymer Physics 2007; 45:2097-2112.
DOI: 10.1002/polb.21187
8. W. Zheng, S.-C. Wong, H.-J. Sue. Transport behaviour of PMMA/expanded graphite nanocomposites. Polymer 2002; 73:6767-6773.
DOI: S0032-3861(02)00599-2
9. S. Dadbin, M. Frounchi, M.H. Saeid, F. Gangi. Molecular structure and physical properties of e-beam crosslinked low-density polyethylene for wire and cable insulation applications. Journal of Applied Polymer Science 2002; 86:1959-1969.
DOI: 10.1002/app.11111
10. Effect of vinyl acetate content and electron beam irradiation on the flame retardancy, mechanical and thermal properties of intumescent flame retardant ethylene-vinyl acetate copolymer. Radiation Physics and Chemistry 2012; 81:308-315.
DOI: 10.1016/j.radphyschem.2011.10.021
11. K. Kalaitzidou, H. Fukushima, L.T. Drzal. Mechanical properties and morphological characterization of exfoliated graphite-polypropylene nanocomposites. Composites: Part A 2007; 38:1675-1682.
DOI: 10.1016/j.compositesa.2007.02.003
12. D.P.N. Vlasveld, M. de Jong, H.E.N. Bersee, A.D. Gotsis, S.J. Picken. The relation between rheological and mechanical properties of PA6 nano- and micro-composites. Polymer 2005; 46:10279-10289.
DOI: 10.1016/j.polymer.2005.08.002
13. J.-J. Su, G.-H. Yang, T.-N. Zhou, X. Gao, K. Wang, Q. Fu. Enhanced crystallization behaviours of poly(ethylene terephthalate) via adding expanded graphite and poly(ethylene glycol). Colloid Polymer Science 2012; 291:911-917.
DOI: 10.1007/s00396-012-2809-5
14. P. Steurer, R. Wissert, R. Thomann, R. Mülhaupt. Functionalized graphenes and thermoplastic nanocomposites based upon expanded graphite oxide. Macromolecular Rapid Communications 2009; 30:316-327.

DOI: 10.1002/marc.200800754

15. A. Yasmin, J.-J. Luo, I.M. Daniel. Processing of expanded graphite reinforced polymer nanocomposites. Composites Science and Technology 2006; 66:1179-1186.
DOI: 10.1016/j.compscitech.2005.10.014
16. I.S. Suh, S.H. Ryu, J.H. Bae, Y.W. Chang. Effects of compatibilizer on the layered silicate/ethylene vinyl acetate nanocomposite. Journal of Applied Polymer Science 2004; 94:1057-1061.
DOI: 10.1002/app.20962
17. L. Hua, W. Kai, J. Yang, Y. Inoue. A new poly(L-lactide)-grafted graphite oxide composite: Facile synthesis, electrical properties and crystallization behaviours. Polymer Degradation and Stability 2010; 95:2619-2627.
DOI: 10.1016/j.polymdegradstab.2010.07.023
18. J. Li, J.-K. Kim, M.L. Sham. Conductive graphite nanoplatelets/epoxy nanocomposites: Effects of exfoliation and UV/ozone treatment of graphite. Scripta Materialia 2005; 53:235-240.
DOI: 10.1016/j.scriptamat.2005.03.034
19. J.C. Wang, P. Chen, L. Chen, K. Wang, H. Deng, Q. Zhang, Q. Fu. Preparation and properties of poly(vinylidene fluoride) nanocomposites blended with graphene oxide coated silica hybrids. eXPRESS Polymer Letters 2012; 6:299-307.
DOI: 10.3144/expresspolymlett.2012.33
20. D. Dixon, P. Lemonine, J. Hamilton, G. Lubarsky, E. Archer. Graphene oxide-polyamide 6 nanocomposites produced via in situ polymerization. Journal of Thermoplastic Composite Materials 2013:1-18.
DOI: 10.1177/0892705713484749
21. S. Stankovich, D.A. Dikin, R.D. Piner, K.A. Kohlhaas, A. Kleinhammes, Y. Jia, Y. Wu, S.T. Nguyen, R.S. Ruoff. Synthesis of graphene-based nanosheets via chemical reduction of exfoliated graphite oxide. Carbon 2007; 45:1558-1565.
DOI: 10.1016/j.carbon.2007.02.034
22. H. Kim, A.A. Abdala, C.W. Macosko. Graphene/polymer nanocomposites. Macromolecules 2010; 43:6515-6530.
DOI: 10.1021/ma100572e

23. G. Carotenuto, S.D. Nicola, M. Palomba, D. Pullini, A. Horsewell. T.W. Hansen, L. Nicolais. Mechanical properties of low-density polyethylene filled by graphite nanoplatelets. Nanotechnology 2012; 23:485-705.
DOI: 10.1088/0957-4484/23/48/485705
24. L.M. Viculis, J.J. Mack, O.M. Mayer, H.T. Hahn, R.B. Kaner. Intercalation and exfoliation routes to graphite nanoplatelets. Journal of Materials Chemistry 2005; 15:974-978.
DOI: 10.1039/b413029d
25. J.J. George, A.K. Bhowmick. Ethylene vinyl acetate/expanded graphite nanocomposites by solution intercalation: Preparation, characterization and properties. Journal of Materials Science 2008; 43:702-708.
DOI: 10.1007/s10853-007-2193-6
26. I.M. Afanasov, D.V. Savchenko, S.G. Ionov, D.A. Rusakov, A.N. Seleznev, V.V. Avdeev. Thermal conductivity and mechanical properties of expanded graphite. Inorganic Materials 2009; 45:540-544.
DOI: 10.1134/S0020168509050057
27. S.R. Kim, M. Poostforush, J.H. Kim, S.G. Lee. Thermal diffusivity of in-situ exfoliated graphite intercalated compound/polyamide and graphite/polyamide composites. eXPRESS Polymer Letters 2012; 6:476-484.
DOI: 10.3144/expresspolymlett.2012.50
28. R.K. Goyal, S.D. Samant, A.K. Thakar, A. Kadam. Electrical properties of polymer/expanded graphite nanocomposites with low percolation. Journal of Physics D: Applied Physics 2010; 43:365-404.
DOI: 10.1088/0022-3727/43/36/365404
29. V. Causin, C. Marega, A. Marigo, G. Ferrara, A. Ferraro. Morphological and structural characterization of polypropylene/conductive graphite nanocomposites. European Polymer Journal 2006; 42:3153-3161.
DOI: 10.1016/j.eurpolymj.2006.08.017
30. T.G. Gopakumar, D.J.Y.S. Page. Polypropylene/graphite nanocomposites by thermo-kinetic mixing. Polymer Engineering and Science 2004; 44:1162-1169.
DOI: 10.1002/pen.20109

31. A.A. Green and M.C. Hersam. Emerging methods for producing monodisperse graphene dispersions. The Journal of Physical Chemistry Letters 2010; 1:544-549.
DOI: 10.1021/jz900235f
32. Z.-M. Huang, Y.-Z. Zhang, M. Kotaki, S. Ramakrishna. A review on polymer nanofibers by electrospinning and their applications in nanocomposites. Composites Science and Technology 2003; 63:2223-2253.
DOI: 10.1016/S0266-3538(03)00178-7
33. P.-C. Ma, N.A. Siddiqui, G. Marom, J.-K. Kim. Dispersion and functionalization of carbon nanotubes for polymer-based nanocomposites: A review. Composites: Part A 2010; 41:1345-1369.
DOI: 10.1016/j.compositesa.2010.07.003
34. V.A. Agubra, P.S. Owuor, M.V. Hosur. Influence of nanoclay dispersion methods on the mechanical behavior of E-glass/epoxy nanocomposites. Nanomaterials 2013; 3:550-563.
DOI: 10.3390/nano3030550
35. L. Sorrentino, M. Aurilia, L. Cafiero, S. Cioffi, S. Lannace. Mechanical behaviour of solid and foamed polyester/expanded graphite nanocomposites. Journal of Cellular Plastics 2012; 48:355-368.
DOI: 10.1177/002/955X12449641
36. S. Jin, L.-S. Xie, Y.-L. Ma, J.-J. Han, Z. Xia, G.-X. Zhang, S.-M. Dong, Y.-Y. Wang. Low-temperature expanded graphite for preparation of graphite sheets by liquid-phase method. Journal of Physics: Conference Series 2009; 188:*1742-6596.*
DOI: 10.1088/1742-6596/188/1/012040
37. C. Zhang, W.W. Tjiu, W. Fan, S. Huang, T. Liu. A novel approach for transferring water-dispersible graphene nanosheets into organic media. Journal of Materials Chemistry 2012; 22:11748-11754.
DOI: 10.1039/c2jm30955f
38. J.H. Lee, D.W. Shin, V.G. Makotchenko, A.S. Nazarov, V.E. Fedorov, J.H. Yoo, S.M. Yu, J.-Y. Choi, J.M. Kim, J.-B. Yoo. The superior dispersion of easily soluble graphite. Small 2010; 6:58-62.
DOI: 10.1002/smll.200901556

39. T. Ramanathan, A.A. Abdala, S. Stankovich, D.A. Dikin, M. Herrera-Alonso, R.D. Piner, D.H. Adamson, H.C. Schniepp, X. Chen, R.S. Ruoff, S.T. Nguyen, I.A. Aksay, R.K. Prud'homme, L.C. Brinson. Functionalized graphene sheets for polymer nanocomposites. Nature Nanotechnology 2008; 3:327-331.
DOI: 10.1038/nnano.2008.96

40. L. Vaisman, H.D. Wagner, G. Marom. The role of surfactants in dispersion of carbon nanotubes. Advances in Colloid and Interface Science 2006; 128-130:37-46.
DOI: 10.1016/j.cis.2006.11.007

41. M.C. Costache, M. Heidecker, E. Manias, R. Gupta, C. Wilkie. Benzimidazolium surfactants for modification of clays for use with styrenic polymers. Polymer Degradation and Stability 2007; 92:1753-1762.
DOI: 10.1016/j.polymdegradstab.2007.08.001

42. T. Kuilla, S. Bhadra, D. Yao, N.H. Kim, S. Bose, J.H. Lee. Recent advances in graphene based polymer composites. Progress in Polymer Science 2010; 35:1350-1375.
DOI: 10.1016/j.progpolymsci.2010.07.005

43. K. Kalaitzidou, H. Fukushima, L.T. Drzal. A new compounding method for exfoliated graphite-polypropylene nanocomposites with enhanced flexural properties and lower percolation threshold. Composites Science and Technology 2007; 67:2045-2051.
DOI: 10.1016/j.compscitech.2006.11.014

44. J.-W. Shen, X.-M. Chen, W.-Y. Huang. Structure and electrical properties of grafted polypropylene/graphite nanocomposites prepared by solution intercalation. Journal of Applied Polymer Science 2003; 88:1864-1869.
DOI: 10.1002/app.11892

45. S. Ganguli, A.K. Roy, D.P. Anderson. Improved thermal conductivity for chemistry functionalized exfoliated graphite/epoxy composites. Carbon 2008; 46:806-817.
DOI: 10.1016/j.carbon.2008.02.008

46. M.L.P. Ha, B.P. Grady, G. Lolli, D.E. Resasco, W.T. Ford. Composites of single-walled carbon nanotubes and styrene-isoprene copolymer lattices. Macromolecular Chemistry and Physics 2007; 208:446-456.
DOI: 10.1002/macp.200600521

47. K. Nomura, M.M. Abdellatif. Precise synthesis of polymers containing functional end groups by living ring-opening metathesis polymerization (ROMP): Efficient tools for synthesis of block/graft copolymers. Polymer 2010; 51:1861-1881.
DOI: 10.1016/j.polymer.2010.02.028
48. H.A. Khonakdar, S.H. Jafari, U. Wagenknecht, D. Jehnichen. Effect of electron-irradiation on crosslink density and crystalline structure of low- and high-density polyethylene. Radiation Physics and Chemistry 2006; 75:78-86.
DOI: 10.1016/j.radphyschem.2005.05.014
49. Y. Hong-mei, Y. Yong-zhu, H. Xiao, Z. Qiang, Z. Hou-qiang. Linear dynamic viscoelastic response of melts for crosslinkable polyethylene insulation cable granules during crosslinking. Chemical Research in Chinese Universities 2010; 26:142-147.
DOI: 1005-9040(2010)-01-142-06
50. B. Krause, P. Pötschke, U. Gohs. Effects of high energy electrons on the properties of polyethylene/multiwalled carbon nanotubes composites: Comparison of as-grown and oxygen-functionalized MWCNT. AIP Conference Proceedings 2014;1590:290-293.
DOI: 10.1063/1.4873784
51. U. Wagenknecht, U. Gohs, A. Leuteritz, S. Volke, S. Wiessner, G. Heinrich. Modification of particle filled polymers with high energy electrons under in-stationary conditions of melt mixing. Macromolecular Symposia 2011; 301:146-150.
DOI: 10.1002/masy.201150318
52. E. Oral, A.S. Malhi, O.K. Muratoglu. Mechanisms of decrease in fatigue crack propagation resistance in irradiated and melted UHMWPE. Biomaterials 2006; 27:917-925.
DOI: 10.1016/j.biomaterials.2005.06.025
53. S.A. Mousavi, S. Dadbin, M. Frounchi, D.C. Venerus, T.G. Medina. Comparison of rheological behaviour of branched polypropylene prepared by chemical modification and electron beam irradiation under air and N_2. Radiation Physics and Chemistry 2010; 79:1088-1094.
DOI: 10.1016/j.radphyschem.2010.04.010
54. B. Krause, M. Stephan, S. Volkland, D. Voigt, L. Häußler, H. Dorschner. Long-chain branching of polypropylene by electron-beam irradiation in the molten state. Journal of Applied Polymer Science 2006; 99:260-265.

DOI: 10.1002/app.22471

55. A.A. Abiona, A.G. Osinkolu. Gamma-irradiation induced property modification of polypropylene. International Journal of Physical Sciences 2010; 5:960-967.
56. R. Nordin, H. Ismail. Electron beam treatment for enhancing the compatibility, thermal and tensile properties of LLDPE/PVA blends: Part I, Effect of irradiation doses. Journal of Engineering Research and Applications 2013; 3(6):1820-1825.
57. A.A. Basfar, Z.I. Ali. Physico-chemical properties of low density polyethylene and ethylene vinyl acetate composites crosslinked by ionizing radiation. Radiation Physics and Chemistry 2011; 80:257-263.
DOI: 10.1016/j.radphyschem.2010.07.043
58. C.P.M. Kutty, T.M. Nair, G. Unnikrishnan, M. Jahfar. Effect of crosslinking agents on morphology and mechanical properties of ethylene propylene diene monomer/polyvinyl chloride composites. Scientific Reviews & Chemical Communications 2013; 3(1):62-66
59. H. Azizi, J. Barzin, J. Morshedian. Silane crosslinking of polyethylene: the effects of EVA, ATH and Sb_2O_3 on properties of the production in continuous grafting of LDPE. eXPRESS Polymer Letters 2007; 1:378-384
DOI: 10.3144/expresspolymlett.2007.53
60. M. Porubská, I. Janigová, K. Jomová, I. Chodák. The effect of electron beam irradiation on properties of virgin and glass fibre-reinforced polyamide 6. Radiation Physics and Chemistry 2014; 102:159-166.
DOI: 10.1016/j.radphyschem.2014.04.037
61. M. Copuroğlu, M. Şen. A comparative study of thermal ageing characteristics of poly(ethylene-co-vinyl acetate) and poly(ethylene-co-vinyl acetate)/carbon black mixture. Polymers for Advanced Technologies 2004; 15:393-399.
DOI: 10.1002/pat.485
62. N.R. Tummala, B.P. Grady, A. Striolo. Lateral confinement effects on the structural properties of surfactant aggregates: SDS on graphene. Physical Chemistry Chemical Physics 2010; 12:13137-13143.
DOI: 10.1039/c0cp00600a
63. V. Schmidt, C. Giacomelli, V. Soldi. Thermal stability of films formed by soy protein isolated-sodium dodecyl sulphate. Polymer Degradation and Stability 2005; 87:25-31.

DOI: 10.1016/j.polymdegradstab.2004.07.003

64. D. Kelley, D.J. McClements. Influence of sodium dodecyl sulphate on the thermal stability of bovine serum albumin stabilized oil-in-water emulsions 2003; 17:87-93.
DOI: S0268-005X(02)00041-3

65. Y. Wang, H.-B. Tsai. Thermal, dynamic-mechanical, and dielectric properties of surfactant intercalated graphite oxide filled maleated polypropylene nanocomposites. Journal of Applied Polymer Science 2012; 123:3154-3163.
DOI: 10.1002/app.34976

66. F. Piana, J. Pionteck. Effect of the melt processing conditions on the conductive paths formation in thermoplastic polyurethane/expanded graphite (TPU/EG) composites. Composites Science and Technology 2013; 80:39-46.
DOI: 10.1016/j.compscitech.2013.03.002

67. S. Dadbin, M. Frounchi, M. Sabet. Studies on the properties and structure of electron beam crosslinked low-density polyethylene/poly(ethylene-co-(vinyl acetate)) blends. Polymer International 2005; 54:686-691.
DOI: 10.1002/pi.1750

68. M. Zhang, D.-J. Li, D.-F. Wu, C.-H. Yan, P. Lu, G.-M. Qiu. Poly(ethylene terephthalate)/expanded graphite conductive composites: structure, properties, and transport behaviour. Journal of Applied Polymer Science 2008; 108:1482-1489.
DOI: 10.1002/app.27745

69. W.-G. Weng, G.-H. Chen, D.-J. Wu, W.-L. Yan. HDPE/expanded graphite electrically conducting composite. Composite Interfaces 2004; 2:131-143.
DOI: 10.1163/156855404322971404

70. S. Cheng, X. Chen, Y. G. Hsuan, C.Y. Li. Reduced graphene oxide-induced polyethylene crystallization in solution and nanocomposites. Macromolecules 2012; 45:993-1000.
DOI: 10.1021/ma2021453

71. I. Tantis, G.C. Psarras, D. Tasis. Functionalized graphene-poly(vinyl alcohol) nanocomposites: Physical and dielectric properties. eXPRESS Polymer Letters 2012; 6:283-292.
DOI: 10.3144/expresspolymlett.2012.31

72. T.Y. Hwang, S. Lee, P.-H. Kang, K.H. Park, Y. Ahn, J.W. Lee. The effect of electron beam irradiation on the dispersion and properties of poly(ethylene-co-vinyl acetate)/clay nanocomposites. Macromolecular Research 2011; 19:1151-1156.
DOI: 10.1007/s13233-011-1104-5
73. M.A. Mohamed, M.M.A. Zeid, N.A. Shaltout, A.A.E. Miligy. Effect of energy electron beam irradiation on properties of EPDM rubber/high density polyethylene/carbon black composites. Polymer-Plastics Technology and Engineering 2012; 51:1361-1366.
DOI: 10.1080/03602559.2012.702257
74. Y. Pan, X.S. Chan, L. Li. Rheological study on the gel-like behaviour of carbon nanotube/polypropylene composites: Effect of interfacial adhesion. Journal of the Society of Rheology 2013; 41:121-128.

Chapter 2

Effect of surfactant on EG dispersion in EVA and thermal and mechanical properties of the system

This chapter has been published as:
JS Sefadi, AS Luyt, J Pionteck. Effect of surfactant on EG dispersion in EVA and thermal and mechanical properties of the system. Journal of Applied Polymer Science 2014;131:41352.
DOI: 10.1002/app.41352

ABSTRACT

The influence of expanded graphite (EG) and sodium dodecyl sulphate (SDS) modified EG on the structure, thermal stability and mechanical properties of ethylene vinyl acetate (EVA) was investigated in this study. The EVA filled with EG platelets, with and without anionic SDS modification, was prepared by melt mixing using a Brabender Plastograph mixer. The extent of dispersion and morphology of the composites were characterized using scanning electron microscopy (SEM), optical microscopy (OM), and X-ray diffraction (XRD). The optical microscopy results show better distribution of the modified EG platelets in the EVA matrix, while the SEM results show an improved interfacial adhesion between the polymer and the SDS-EG particles. Both the EVA18 copolymer and the EG platelets have monoclinic phases, and both EG and SDS do not seem to have any influence on the melting and crystallization behaviour of the EVA18. The addition of EG enhanced the thermal stability of EVA18, and this stabilizing influence was further improved when the EG was treated with SDS. All the tensile properties of EVA/EG improved after surface modification. The storage modulus of EVA generally increased with increasing both the unmodified EG and the SDS modified EG content. There was a shift in the T_g to higher temperatures with an increase in both the EG and modified EG content. The α-relaxation peak in the SDS modified EG curves was less intense than the β-relaxation peak, even for the untreated EG composites.

Keywords: Composites; degradation; mechanical properties; polyolefins; properties and characterization

2.1 Introduction

Conductive polymer nanocomposites have attracted considerable interest, which is the result of their potential application in batteries, light emitting devices, electromagnetic shields, antistatic coatings and electrode materials [1-3]. The incorporation of conducting fillers such as intercalated graphite, carbon black, or metal and ceramic oxide powders into a polymer matrix is a promising approach to prepare conductive polymer nanocomposites [4-6]. Expanded graphite (EG) was used instead of other conductive fillers in this study because of its high corrosion resistance, low density and low cost [7,8]. Furthermore, the platelet-like structures in a polymer matrix often cause remarkable improvement in the material properties compared to those of the pure polymer. The improvements include enhanced physical and mechanical properties, especially high tensile moduli, increased thermal stability, decreased gas permeability and flammability, improved solvent and UV resistance, and improved electrical properties [9,10]. The main reasons for these enhanced properties are the high aspect ratios and large surface areas of the expanded graphite (EG) particles.

Natural graphite flakes are abundantly available and highly conductive with an electrical conductivity of 10^4 S cm^{-1} at room temperature [2,11]. Graphite is an allotrope of carbon whose structure is a single planar sheet of sp^2-bonded carbon atoms that are densely packed in a unique layered crystal structure [11,12]. However, it is relatively difficult to intercalate organic polymers or molecules directly into the interlayer of the graphite to prepare conductive polymer/graphite nanocomposites, due to the incompatibility between the components. This setback can be overcome by physical or chemical modification of the graphite [13,14]. The better dispersion of EG in an EVA matrix was achieved by modifying the EG with the anionic surfactant sodium dodecyl sulphate (SDS) via sonication. This modification improved the hydrophilicity of the EG, which should improve the interaction between the EG and EVA. Several papers were published on conductive thermoplastic polymer nanocomposites reinforced with EG prepared by *in situ* polymerization or solution intercalation [13-16], but very little has been published on the preparation of these composites using melt-blending intercalation. Krupa *et al.* [17] studied the mechanical properties and morphology of composites based on an EVA copolymer mixed with EG. Their copolymer contained 14% vinyl acetate. They observed that both tensile modulus and stress at break increased with an increase in EG platelets, while the

elongation at break noticeably decreased. George *et al.* [18] investigated EVA/EG nanocomposites prepared by solution intercalation. They used an EVA with 60% vinyl acetate. In their case the tensile strength and modulus increased significantly up to 4% EG, while the elongation at break showed little change. Kim *et al.* [19] compared EVA/EG systems prepared by solution and three different melt mixing methods. Their EVA contained 18 wt% vinyl acetate, which is the same as the sample we used in our investigation. Their results show little change in thermal stability with increasing EG content and very little was reported on changes in the mechanical properties. Tavman *et al.* [20] and Tlili *et al.* [21] both compared the electrical properties of EVA (with 14 wt% vinyl acetate) containing respectively EG and unexpanded graphite. George *et al.* [22] reported a comprehensive study on reinforcement of EVA by differently treated naturally occurring graphites. The nanocomposites were prepared by a solution-mixing method. They found that the modified graphites showed better dispersion in and interfacial adhesion to the EVA matrix, containing 60% vinyl acetate, than the unmodified graphite. Similarly, significant improvements in filler dispersion and thermal stability were observed by George and Bhowmick [23] in their investigation of EVA with 40% VA content filled with modified EG nanofiller, using solution mixing and sonication.

The EVA copolymer with 18 wt% VA content used in this paper is the same as the one used in our previous work on EVA filled with empty fruit bunch fibre [24]. As far as we could establish there is no other published work where the thermal and mechanical properties of EVA blended with EG and with surfactant modified EG prepared through melt-mixing were compared. The aim of our study was to investigate the morphology and thermal stability, as well as tensile and thermomechanical properties, of EVA filled with EG, without and with anionic SDS modification. For this purpose the EVA composites were prepared *via* melt-blending.

2.2 Experimental

2.2.1 Materials

Expanded graphite, SIGRAFLEX Expandat, was provided by SGL Technologies GmbH, SGL Group. It has a conductivity of 40 S cm^{-1} (room temperature, 30 MPa, self-made 2-points conductivity tester, coupled with a DMM2000 Electrometer, Keithley Instruments), an apparent

volume of ~400 cm^3 g^{-1}, and a specific surface area of 39.4 m^2 g^{-1} (77.4 K, N_2 atmosphere, Autosorb-1, Quantachrome). Ethylene vinyl acetate (EVA-460) was manufactured and supplied in granule form by DuPont Packaging & Industrial Polymers. EVA-460 contains 18 wt% of vinyl acetate (VA) and a BHT antioxidant thermal stabilizer. It has a melt flow index (MFI) (190 °C/2.16 kg) of 2.5 g/10 min (ASTM D1238-ISO 1133), a melting temperature (T_m) of 88 °C, a Vicat softening point of 64 °C, and a density of 0.941 g cm^{-3}. The sodium lauryl sulphate known as sodium dodecyl sulphate (SDS) was supplied by SIGMA-ALDRICH. SDS is a white powder with an assay of ≥99.0% (GC), a melting temperature range of 204-207 °C and a molar mass of 288.4 g mol^{-1}.

2.2.2 Preparation of nanocomposites

4 g of SDS were dissolved in 5 L deionized water in a glass beaker, and 20 g of the expanded graphite was gradually added to the solution. 500 mL suspensions were sonicated for 30 min, filtered, followed by washing with 100 ml distilled water to remove loosely absorbed SDS and dried in a vacuum oven at 50 °C for 72 h. This modified EG, as well as the as received unmodified EG, were respectively mixed with EVA to prepare the nanocomposites. The EVA composites were prepared by melt mixing using a Brabender Plastograph 55 mL internal mixer. The mixing was done for 15 min at 60 rpm and a temperature of 100 °C. The samples were melt-pressed at 100 °C and 50 bar for 5 min into 100 mm x 100 mm x 2 mm square sheets by using a hot hydraulic press.

2.3 Characterization and analysis

The effect of surfactant on the EG dispersion of the EVA/EG and EVA/SDS-EG composites were studied by optical microscopy using a CETI-Topic B microscope, Belgium, with polarized light at 40x magnification. The thickness of the samples measured by the standard gage IP54 electronic micrometer ranges between 0.13 mm and 0.18 mm.

SEM analyses were carried out in a TESCAN VEGA3 Superscan scanning electron microscope (Brno, Czech Republic). The samples were fractured at liquid nitrogen temperature

and the fracture surfaces of the samples were coated with gold by a Cressington Sputter Coater for 30 seconds. Microscope settings of 285.5 nm probe size, 50 mA probe current, 0.1 nm lateral resolution, and 30 kV AC voltage were used.

The structures of EG, SDS-modified EG and the EVA18 composites were determined through XRD. A D8 Advance diffractometer (BRUKER AXS, Germany) with PSD Vantec-1 detectors and Cu-K_α radiation (λ = 1.5406 Å), a tube voltage of 40 kV, a current of 40 mA and a V20 variable slit was used. The samples were scanned in locked coupled mode with 2θ ranges from 0° to 120° at 2θ increments of 0.5 sec step^{-1}.

DSC analyses were carried out under nitrogen flow (20 mL min^{-1}) using a Perkin Elmer Pyris-1 differential scanning calorimeter (Waltham, Massachusetts, U.S.A). The instrument was calibrated using the onset temperatures of melting of indium and zinc standards, as well as the melting enthalpy of indium. The sample weights were in the range of 5-10 mg, and they were heated from 25 to 180 °C at a heating rate of 10 °C min^{-1}. The cooling and second heating were performed under the same conditions. For all the samples, the onset and peak temperatures of melting and crystallization, as well as the melting enthalpies, were determined from the second heating scan. The normalised enthalpies of melting in Table 2.1 were determined according to Equation 2.1.

$$\Delta H_m^{Norm} = \frac{\Delta H_{m,EVA}}{w_{EVA}} \qquad (2.1)$$

where $\Delta H_{m,EVA}$ is the experimentally observed melting enthalpy for the pure EVA, and ΔH_m^{Norm} is the calculated normalised enthalpy of melting for an EVA weight fraction w_{EVA} in the composite. The degree of crystallinity χ_c was calculated according to Equation 2.2.

$$\chi_c = (\Delta H_m^{Norm} / \Delta H_m^o) \times 100\ \% \qquad (2.2)$$

where ΔH_m^o is the specific enthalpy of melting for 100% crystalline PE. A value of 288 J g^{-1} was used in the calculations [25-27].

Thermogravimetric analysis was done under flowing nitrogen (20 mL min^{-1}) using a Perkin Elmer TGA7 thermogravimetric analyser (Waltham, Massachusetts, U.S.A). The samples, weighing ca. 20 mg each, were heated from 30 to 600 °C at a heating rate of 10 °C min^{-1}.

The tensile properties were investigated using a Hounsfield H5KS tensile tester at a cross-head speed of 10 mm min^{-1} and a gauge length of 20 mm. The tensile modulus as well as stress and elongation at break of the samples were determined from the stress-strain curves. At least five specimens were tested for each sample and the mean values and standard deviations are reported.

The viscoelastic properties of the composites were studied in the bending mode using a Perkin Elmer Diamond DMA (Waltham, Massachusetts, U.S.A) over a temperature range of -90 to +90 °C at a heating rate of 5 °C min^{-1} and a frequency of 1 Hz.

2.4 Results and discussion

2.4.1 Optical microscopy

Figure 2.1 shows the microscopic images of EVA reinforced with untreated and treated EG platelets. The EVA/EG system (Figure 2.1a) shows a poor distribution of the dispersed phase because of inhomogeneity of the sample and poor interfacial interaction between the two components. The particle size distribution of the dispersed phases in the matrix ranges between 0 and 220 μm for the untreated EG samples. In the case of the EVA/SDS-EG composites (Figure 2.1b), it seems that there is a better particle size distribution due to the sonication applied during EG treatment with SDS, and because of improved interaction between the EVA and EG as a result of SDS modification. In this case the particle size distribution ranges between 0 and 120 μm. Our optical microscopy results are comparable with those obtained by Seo *et al.* [28] who investigated polyethylene and its copolymers filled with functionalized graphene. They observed large black functionalized graphene sheet aggregates that were coarsely dispersed in the polymer and a decrease in transparency when the graphenes were stacked into multilayers or agglomerated. Improved compatibility between the functionalized graphene sheets and the PE copolymers gave rise to a finer dispersion and better transparency.

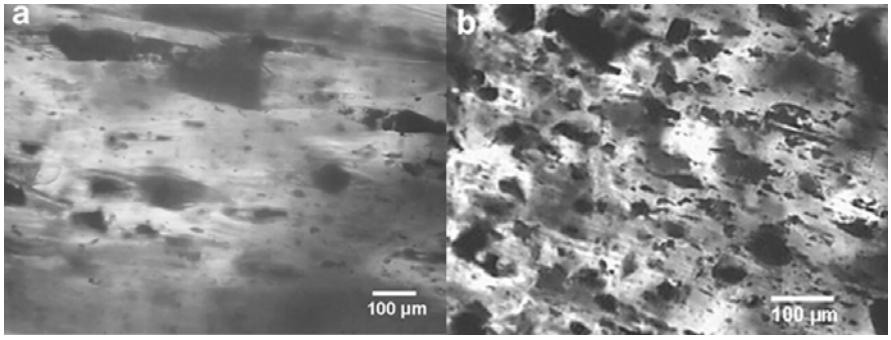

Figure 2.1 Microscopic image of the composite (a) 98/2 w/w EVA/EG and (b) 98/2 w/w EVA/SDS-EG

2.4.2 Scanning electron microscopy (SEM)

Figure 2.2 shows the SEM micrographs of EG and SDS-EG at different magnifications. Figure 2.2a shows that EG has a wormlike structure about 500 µm long and consisting of loosely packed platelets with an interparticle porous character and a low bulk density. In Figure 2.2b, the morphology of the sonicated SDS-EG seems to be similar to that of the crumpled paper. At higher magnification (Figure 2.2d), one can clearly see that the SDS has attached to the surface of EG, separating the EG layers. At higher magnification (Figure 2.2c) it is observed that EG has a structure of parallel sheets that collapse and deform randomly. This figure shows a network-like structure with many pores of different sizes, ranging from nanoscale to microscale. This observation is similar to the results reported by a number of other researchers [3,11,13,16,27-31] on the thickness of the EG sheets. Thus, the galleries between the EG sheets and the pores in the EG network provide a larger interlayer space and can readily be penetrated by the molten polymer. This finally results in a breaking up of the wormlike EG structure into dispersed platelets under melt mixing conditions.

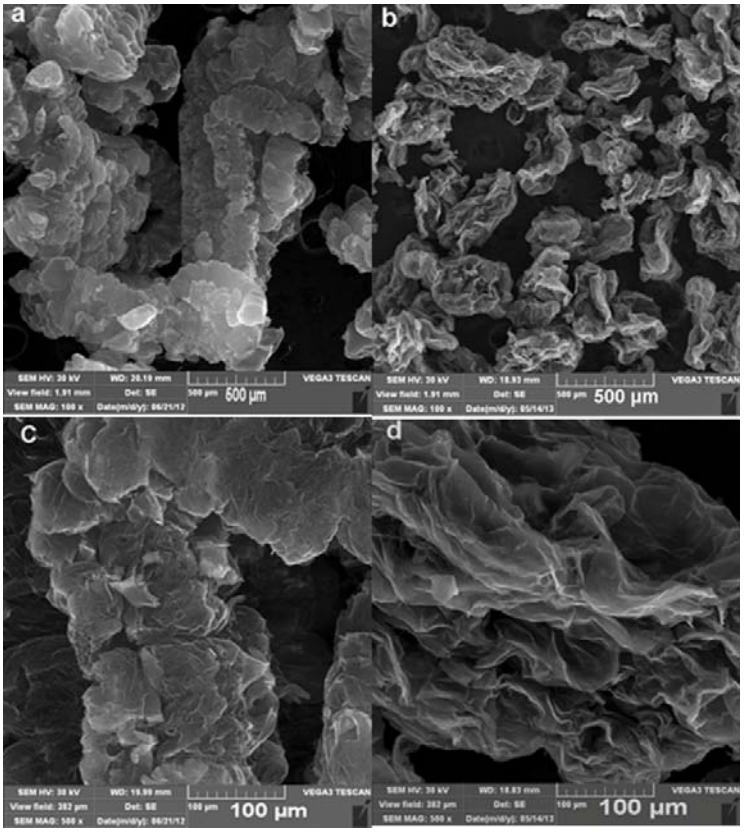

Figure 2.2 SEM micrographs of (a) EG (100 x mag); (b) SDS modified EG (100 x mag); (c) EG (500 x mag); (d) SDS modified EG (500 x mag)

The SEM micrographs of the fracture surfaces of the EVA composites filled with 2 and 6 wt% EG or SDS modified EG are shown in Figure 2.3. It can be seen, by comparing all the pictures, that the morphologies of the composites containing unmodified and modified EG are completely different. Figures 2.3a and 2.3c show that there are some particle agglomerations of EG present in the materials prepared without any dispersing agent. This is an indication that the EG sheets, like other types of nanoparticles, tend to agglomerate and are more difficult to disperse in the matrix by melt-blending than SDS-EG. During melt mixing, the shear force was insufficient to break down the EG agglomerates and to homogeneously disperse the graphite platelets in the EVA. It should be pointed out that, as the EG loading increased, the EG agglomeration observably increased for the samples prepared without SDS-modification. The presence of SDS modification seems to have restricted the graphite agglomeration, which resulted in a much better dispersed system (Figures 2.3b and 2.3d). This is due to the sonication

which was effective in dispersing the EG sheets, and the surfactant treatment, which reduced the EG particle-particle attraction. The better or finer dispersion due to the treatment of surfactant also contributed towards the improved compatibility between the EVA and SDS-EG. This has also been observed in previous literature [32,33], and was explained as the surfactant molecules serving as a link between the graphite and the polymer, providing hydrophobic interactions. They also separate the graphite sheets, as was seen in Figure 2.2 and discussed above, providing space for the polymer chains to penetrate into the expanded graphite. The structural features observed here are similar to observed on polyurethane (TPU)/graphite nanoplatelets conductive nanocomposites prepared by solution intercalation [29]. They found that there was a better shear during sonication which helped the graphite nanoplatelets to disperse better in the TPU matrix. Kim *et al.* [19] found that EG at 5 and 12 wt% was well dispersed in their EVA matrix.

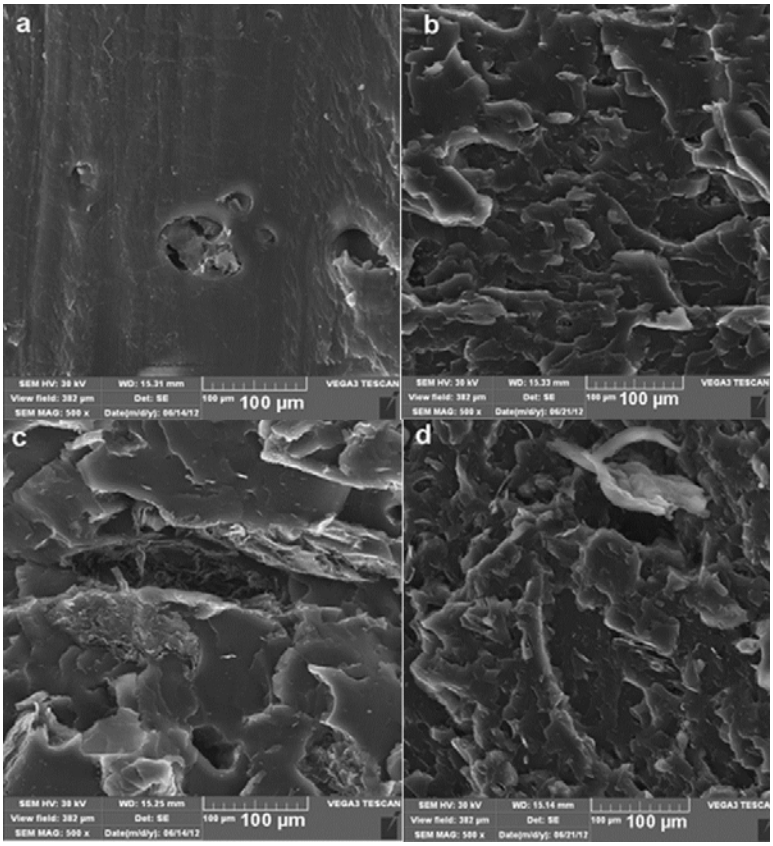

Figure 2.3 SEM micrographs of EVA18/expanded graphite nanocomposites: (a) 98/2 w/w EVA/EG; (b) 98/2 w/w EVA/SDS-EG; (c) 94/6 w/w EVA/EG; (d) 94/6 w/w EVA/SDS-EG

2.4.3 X-ray diffraction (XRD)

Figure 2.4 shows the XRD spectra of the pure EVA copolymer and EG. EG has a weak and broad peak at 2θ = 11.4º and a noticeable signal at 2θ = 26.1°, respectively matching the (001) and (002) planes. The weak and broad peak represents less crystalline segments of the expanded graphite, while the narrow peak is attributed to the diffraction of a highly crystalline phase of the EG layers at an interlamellar distance of 0.34 nm, which is similar to that observed by other authors [10,14]. The diffraction peaks of EG describes a hexagonal EG structure with a lattice constant of 0.3420 nm. The XRD perfectly matches the standard data available in the Joint Committee on Powder Diffraction Standards (JCPDS) database of the International Centre for Diffraction (JCPDS 01-0646, www.icdd.com). The EVA in Figure 2.4 shows three different diffraction peaks at 2θ = 21.3º, 23.5º and 36.3º that respectively correspond to the (110), (200) and (020) crystallographic planes. These diffraction peaks are associated with an orthorhombic crystalline phase. The broad halo below the first two diffraction peaks represents the scattering of the amorphous segments [22,25].

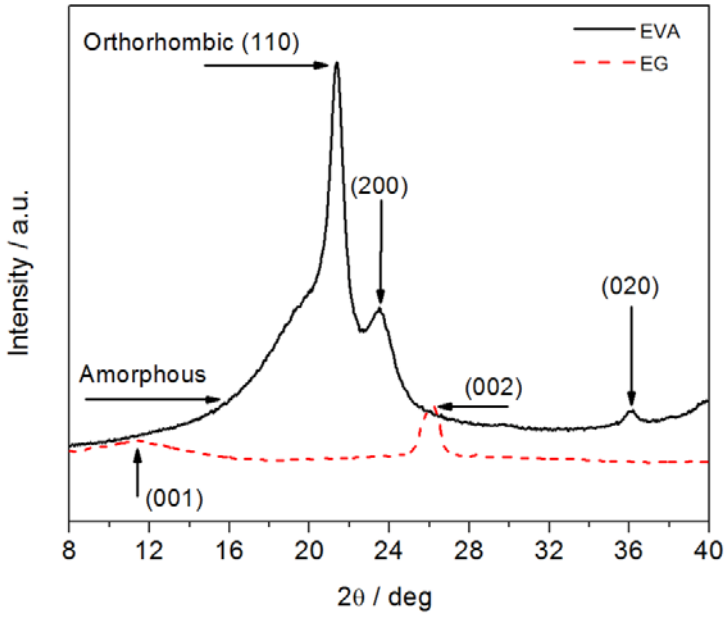

Figure 2.4 XRD diffractogram of EVA copolymer and unmodified EG

The XRD spectra of the EVA18 composites with unmodified and SDS modified EG (Figure 2.5) show no change in the position of the basal diffraction peaks (110) at 2θ = 21.3º.

This indicates that the addition of unmodified and modified EG did not significantly change the crystalline structure of the EVA18 matrix. The peak at 2θ = 26.6° is related to EG, and it shows an increased intensity with increasing EG and SDS-EG content. The peak positions were only marginally influenced and there is no trend. It is therefore clear that the presence of both EG and SDS modified EG had little influence on the crystal structure of EVA. George *et al.* [22] found that the intensity of the EG characteristic peak was reduced in the EVA/4EG composite due to an increase in amorphousness of the EVA matrix. They also found that EVA did not change the structure of EG and hence its crystal structure was retained.

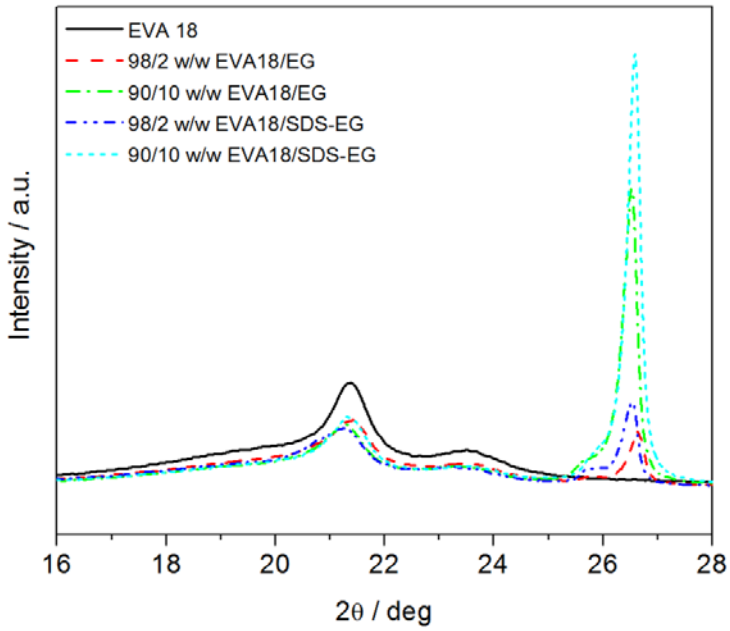

Figure 2.5 XRD spectra of the EVA 18 and its composites in the absence and presence of surfactant modification

2.4.4 Differential scanning calorimetry (DSC)

Figure 2.6 illustrates the changes in crystallinity (which was calculated from the DSC melting enthalpies) of the investigated samples as function of filler content. The enthalpy of melting of polyethylene (PE) was used to calculate the degree of crystallinity of EVA since there is no data available on the enthalpy of 100% crystalline EVA, and since only the PE segments, that form the backbone of EVA, crystallize. The crystallinity of the samples containing unmodified EG

shows a 20% decrease, while that of the samples containing SDS modified EG shows a 20% increase. This observation must be related to the extent of agglomeration and/or dispersion of the EG platelets in the polymer. The platelets can act as nucleation centres which should increase the crystallinity, or immobilize the polymer chains which should decrease the crystallinity. The nucleation effect seems to be more prevalent when the particles are smaller, as in the case of the SDS modified EG. Our previous study on the same EVA mixed with empty fruit bunch fibre [24] showed a smaller (10%) increase in EVA crystallinity, when mixed with the same amount of fibre, than the EVA mixed with SDS modified EG. The melting and crystallization temperatures as well as the melting and crystallization enthalpies of these samples are summarized in Table 2.1. The melting and crystallization temperatures are the same within experimental error for all the samples.

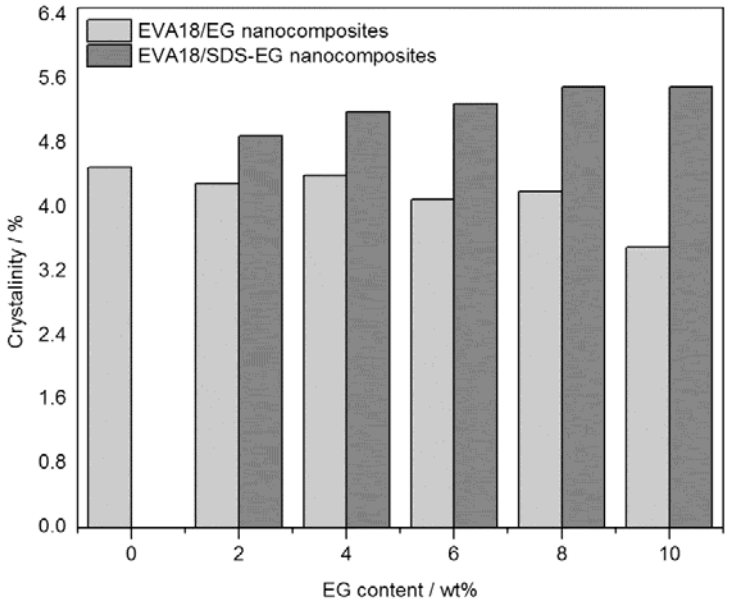

Figure 2.6 Crystallinity of the EVA18 composites with and without SDS as a function of EG content

Table 2.1 Melting and crystallization enthalpies of all the investigated samples

wt.% EG	$T_{p,m}$ / °C	T_c / °C	ΔH_m / J g^{-1}	ΔH_m^{Norm} / J g^{-1}	χ_c / %
No modification					
0	85.5 ± 0.5	64.8 ± 0.2	13.0 ± 2.9	13.0	4.5
2	85.4 ± 0.4	64.8 ± 0.2	12.1 ± 0.9	12.3	4.3
4	86.0 ± 0.4	64.5 ± 0.2	12.1 ± 0.8	12.6	4.4
6	85.3 ± 0.4	64.8 ± 0.3	11.0 ± 1.3	11.7	4.1
8	85.5 ± 0.3	64.5 ± 0.1	11.2 ± 1.5	12.2	4.2
10	85.4 ± 0.4	64.7 ± 0.3	9.1 ± 1.4	10.1	3.5
SDS modification					
2	86.2 ± 0.1	65.5 ± 0.2	13.9 ± 1.2	14.2	4.9
4	85.5 ± 0.2	65.6 ± 0.1	14.3 ± 2.0	14.9	5.2
6	85.6 ± 0.3	65.6 ± 0.1	14.3 ± 2.1	15.2	5.3
8	85.5 ± 0.3	65.7 ± 0.2	14.4 ± 2.1	15.7	5.5
10	85.6 ± 0.3	65.6 ± 0.2	14.1 ± 0.9	15.7	5.5

$T_{p,m}$ is the peak temperature of melting; T_c is the crystallization temperature; ΔH_m is the measured melting enthalpy; ΔH_m^{Norm} is the calculated melting enthalpy of EVA18 taking into account its mass fraction; χ_c is the percentage of crystallinity

2.4.5 Thermogravimetric analysis (TGA)

The TGA curves of all the investigated samples are shown in Figures 2.7 and 2.8. It can be seen that the EG does not lose mass over the investigated temperature range of 0-850 °C (Figure 2.7), confirming its thermal stability over this temperature range. The TGA plot of the SDS treated and washed EG shows a two-step degradation, which differs from that of untreated EG because of the SDS on its surface. The small mass loss of about 5% between 200 and 300 °C corresponds to the evolution of degradation products of SDS. The mass loss of about 22% above 600 °C can be ascribed to the decomposition of labile oxygen-containing functional groups present on the edges of the EG, which may be formed during sonication with SDS [34-36]. The TGA curve of SDS shows several mass loss steps in the temperature range 100-500 °C. These are attributed to the dehydration of physically adsorbed water, followed by a decomposition process, the nature of

which is not well defined. The SDS shows a residual amount of 23 % after heating to 850 °C. Assuming that there is an additive degradation behaviour of the EG-SDS sample, and taking the residuals of the EG, SDS, and EG-SDS at 550 °C (99.3 %, 95.8 % and 24.0%, respectively), one can calculate the SDS-content in EG-SDS to be 4.6 wt%.

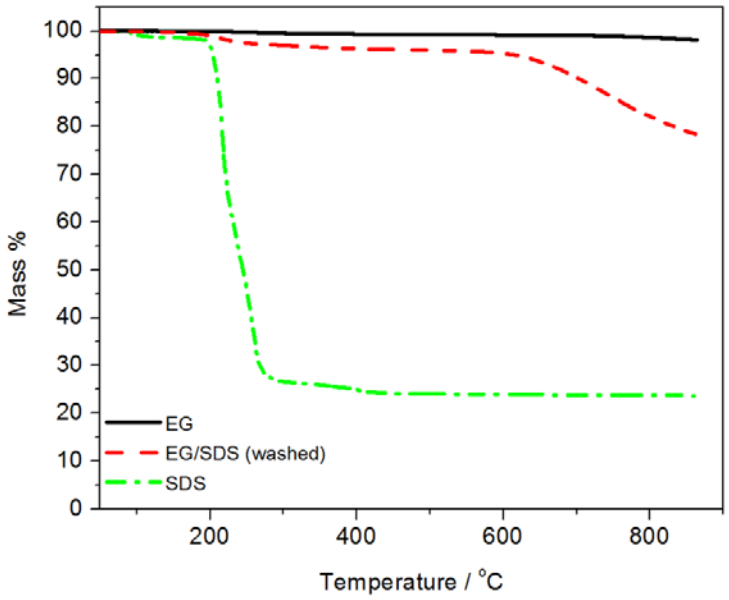

Figure 2.7 TGA curves of the EG, EG/SDS (washed) and pure SDS

The TGA curve of EVA (Figure 2.8) shows two degradation steps. The first step is attributed to deacetylation with β-elimination of the acetic acid and the formation of carbon-carbon double bonds along the polymer backbone. The second step is due to the main chain degradation and volatilization of the products formed through chain scission of the copolymer [31,34-36]. The decomposition of EVA and the volatilization of the decomposition products are completed at 500 °C.

The EVA18/EG composites also show two degradation steps (Figure 2.8). Generally the incorporation of EG improved the thermal stability of EVA. The influence is not so obvious during the first degradation step. It seems that there is no stabilizing effect of EG on acetic acid elimination, but a strong effect on the main chain scission. It can be seen (Table 2) that the T_{max} for the second degradation step of the EVA/EG samples increases with an increase in EG loading due to its strong stabilization effect, which is in line with previous observations on a similar

system [19]. This was ascribed to the hindering effect of the EG layers on the diffusion of oxygen and volatile products through the composites.

The thermal stability of EVA was more significantly enhanced in the presence of SDS-EG than in the presence of unmodified EG (Figure 2.8). This is particularly clear when comparing the temperatures at the maximum rate of main chain scission of the composites containing small amounts of filler (Table 2.2). Only small amounts of SDS-EG already significantly improve the thermal stability of EVA. At 2 wt.% SDS-EG, the T_{max} increased by 17 °C, while in the case of unmodified EG the increase was only 3 °C (Table 2.2). The value of T_{max} continuously increases with increasing filler content in the case of EG, while this value only slightly increases with filler content in the case of SDS-EG, so much so that the T_{max} values are almost the same for the samples containing 10% EG and EG-SDS respectively. Two parameters seem to play a role in determining the mass loss of EVA/EG and EVA-SDS-EG composites: strength of interaction between the polymer free radical chains and volatile degradation products and the filler, and the amount of filler that may interact with the free radical chains and volatile degradation products, and retard the degradation of the polymer and/or the diffusion of the volatile degradation products out of the polymer. It seems as if the strength of interaction is more dominant than the amount of filler, giving rise to the observed TGA results. For both EG and SDS-EG containing samples the residual amounts in Table 2.2 correlate well with the filler contents initially mixed into the polymer matrix, indicating that there is a good dispersion of the filler in EVA. This indicates the filler treatment only reduces the sizes of the filler particles, but does not have a significant influence on its dispersion in the polymer.

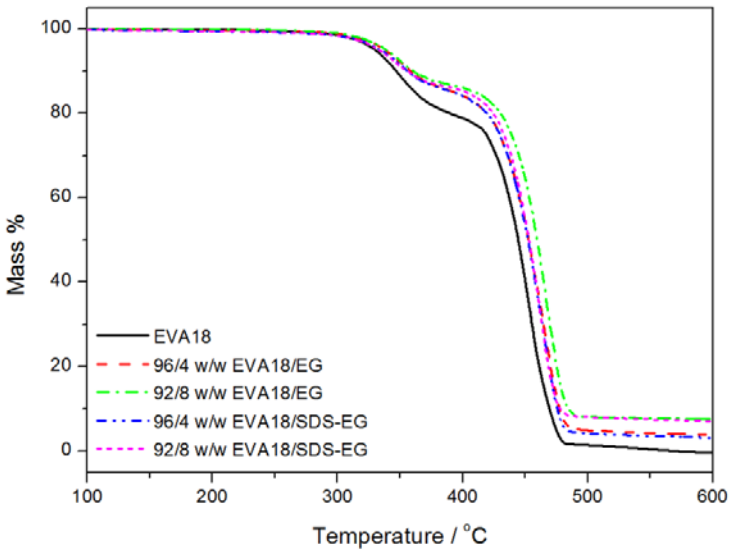

Figure 2.8 TGA curves of EVA18 and its nanocomposites: EG and SDS modified EG

Table 2.2 TGA results for all the investigated samples

wt.% EG	$T_{10\%}$ / °C	T_{max} / °C	Weight % residue
No modification			
0	359.9	466.0	0
2	361.8	469.0	2.0
4	362.5	474.6	4.4
6	363.9	482.8	6.2
8	364.1	486.9	8.5
10	365.0	487.7	10.6
SDS modification			
2	362.9	482.9	2.3
4	364.9	484.0	4.1
6	366.4	485.0	5.7
8	367.0	485.2	8.3
10	367.7	486.1	9.9

$T_{10\%}$ and T_{max} are degradation temperatures at 10 % mass loss and maximum or chain scission mass loss, respectively

2.4.6 Tensile properties

The stress and strain at break of pure EVA18 and its composites were determined from the stress-strain curves, some of which are shown in Figure 2.9. Both sets of samples exhibit considerable strain hardening, which decreases with increasing EG and SDS-EG content. There is also no clear yield point and no necking during stretching. The stress-strain curves show ductility which decreases with an increase in both EG and SDS-EG content. This suggests that the presence of EG inhibited the orientation of the chains in the amorphous regions of the polymer and the reorientation of the chains in the crystalline parts. This seems to be more prevalent in the case of the samples containing modified EG because of the finer dispersion and improved interaction with the polymer chains resulting in increased resistance against deformation.

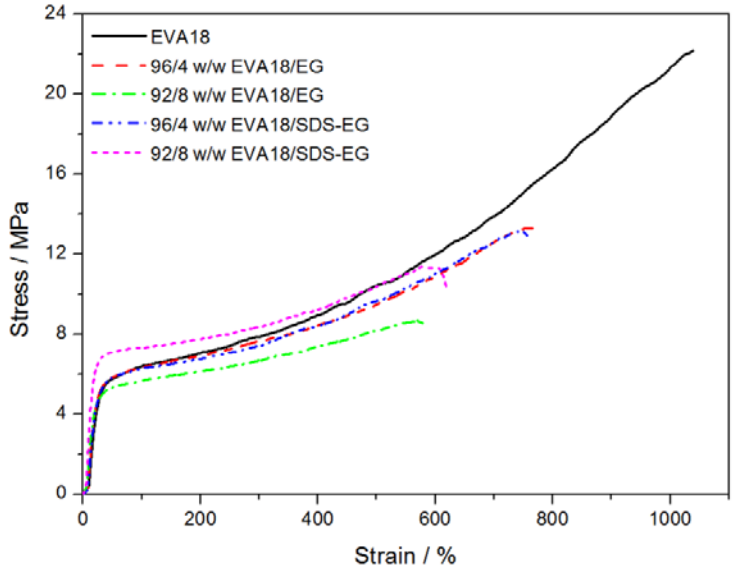

Figure 2.9 Stress-strain curves of the EVA18 filled with EG and SDS modified EG

Figure 2.10 shows the variation of stress at break, elongation at break and tensile modulus for EVA filled with EG and SDS-EG. For both fillers the tensile stress at break decreased significantly (from 22 Mpa for EVA to 8 MPa for EVA with 10 wt.% EG), but the composites containing SDS-EG showed slightly higher stress at break values than the comparable composites with EG. Because of their higher extent of agglomeration, the EG particles in the EVA/EG composites are further from each other and the crazes formed during stretching more

easily develop into cracks that lead to fracture at lower stresses. The EVA/SDS-EG systems have smaller and better dispersed EG particles that are closer to each other. It is therefore more difficult for cracks to develop, because a growing craze which started at one particle may terminate at another particle before it develops into a crack. More strain energy is therefore needed for crack development and growth, so that fracture occurs at higher stress values. In previous investigations a much smaller decrease in stress at break of 39% was observed for a 90/10 w/w EVA14/EG composite [17], and a 36% increase in tensile strength for a 96/4 w/w EVA60/EG composite [18].

The elongation at break values show similar trends as the stress at break, and can be explained in the same way. Krupa *et* al. [17] observed a decrease in elongation at break of 90% for their 90/10 w/w EVA14/EG composite compared to our value of approximately 60% for both systems, while George *et al*. [18] observed a 32% decrease for their 92/8 w/w EVA60/EG composite.

The EVA/SDS-EG composites have modulus values that are about double those of the EVA/EG composites, and the modulus increases with increasing filler content for both types of composites. The modulus for the 90/10 w/w EVA/SDS-EG composite is 225% higher than that of the EVA, compared to 150 and 155% increases previously observed [17,18]. For both types of composites this increase is the result of the presence of the stiff EG platelets. The additional increase in the case of EVA/SDS-EG is due to the better dispersion of the SDS modified EG nanosheets and the better interfacial adhesion between the EG and EVA, leading to a restriction in chain mobility.

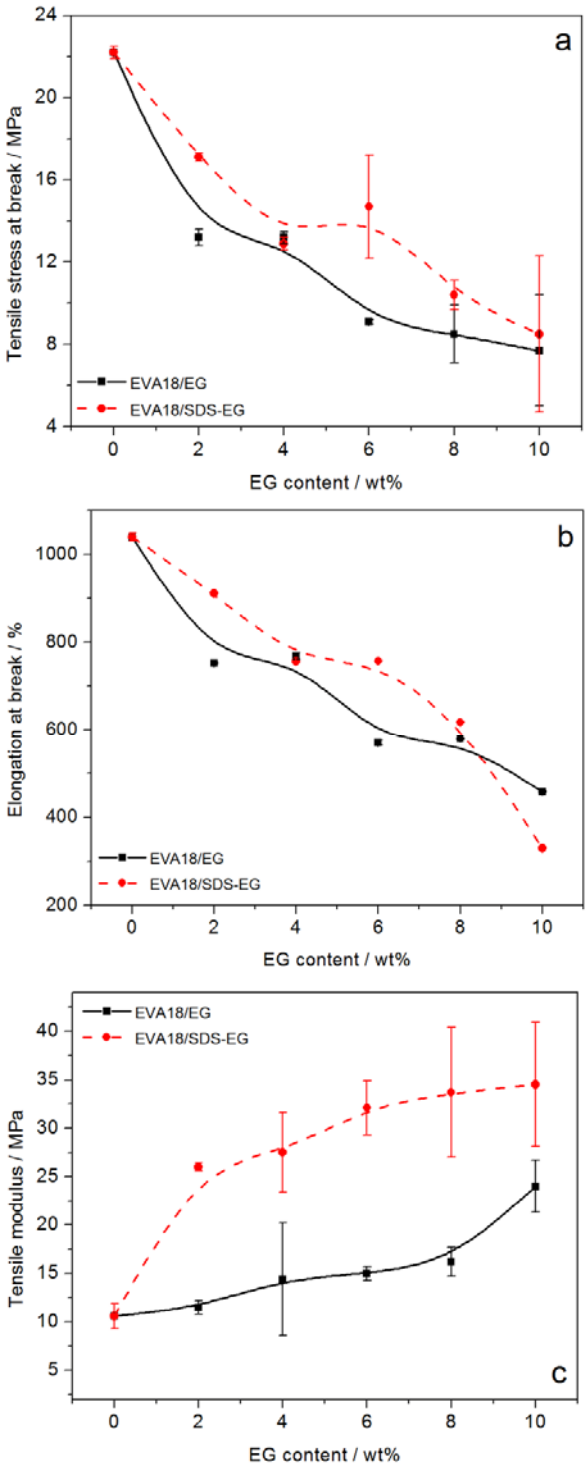

Figure 2.10 Variation of (a) stress at break, (b) elongation at break and (c) tensile modulus of EVA/EG and EVA/SDS-EG samples as a function of filler content

2.4.7 Dynamic mechanical analysis (DMA)

Some of the DMA results of EVA18 and its composites are presented in Figure 2.11. Table 2.3 shows the storage modulus values at -40 and 40 ^{o}C for pure EVA and its composites. The storage modulus generally increases with increasing amount of both EG and SDS-EG in EVA18, which is due to the higher stiffness of the expanded graphite. Unlike our observations for tensile modulus discussed earlier, there were no significant differences in the storage modulus values of the samples containing modified and unmodified EG. There is also a big difference between the storage modulus and tensile modulus values, which shows that because of the dynamic nature of DMA, the amount of filler has a bigger influence on the observed elastic modulus than the interaction between the polymer and the filler. George *et al*. [18] observed a 16% increase in storage modulus at 20 °C of their 92/8 w/w EVA60/EG composite over that of pure EVA60, while we observed an 83% increase for our 92/8 w/w EVA18/EG and 107% for our EVA18/SDS-EG.

Table 2.3 Storage modulus values at -40 and 40 °C for EVA containing untreated and treated EG

Sample	E′ of EVA/EG / Pa		E′ of EVA/SDS-EG / Pa	
	T_{-40} / °C	T_{40} / °C	T_{-40} / °C	T_{40} / °C
Pure EVA	2.89×10^{9}	9.43×10^{7}	2.89×10^{9}	9.43×10^{7}
96/4 w/w EVA/filler	3.07×10^{9}	1.17×10^{8}	2.64×10^{9}	1.11×10^{8}
92/8 w/w EVA/filler	3.92×10^{9}	1.73×10^{8}	4.42×10^{9}	1.95×10^{8}

The loss modulus curve of EVA18 (not included in paper) shows a β-relaxation peak at -17 °C, which is attributed to the glass transition of EVA. There are marginal differences between the peak temperatures of this transition between pure EVA18 and the composites, but since these differences are clearer from the tan δ curves, they will be discussed and explained below. There is little difference between the loss modulus curves for the EVA18/SDS-EG and the comparable EVA/EG composites.

The tan δ curve of EVA18 (Figure 2.11) shows two distinct relaxations, a β-relaxation at -6.2 °C and an α-relaxation at 28 °C. The β-relaxation is attributed to the motion of chain segments of

three or four methylene (–CH_2) groups in the amorphous phase [40,41], and is referred to as the glass transition (T_g). Below T_g the molecular chain segments are frozen in, the damping is low and a small amount of energy is stored for elastic deformations. In the rubbery region, the damping is high compared to the glassy state, because the molecular segments are free to move causing a decrease in stiffness, and excess energy is dissipated as heat. The α-relaxation is related to the motion of amorphous regions within the crystalline phase, which is probably the re-orientation of defect regions between the crystals [41]. The α-transition can also reflect the relaxation of flexible segments of the vinyl acetate (VA) groups present in the EVA copolymer chains. There is a shift in the T_g to higher temperatures with an increase in EG content. This is indicative of reduced chain mobility in the amorphous regions of the polymer due to the interaction between EVA18 and EG, and is in line with previous observations [18,24]. The T_g of the SDS-EG containing composites shows similar increases with increasing filler content (Table 2.4). Therefore any improved interaction between the polymer and the filler had little influence on the glass transition temperature. The intensity of the β-relaxation peak decreased with increasing SDS-EG content, as in the case of the untreated EG, which indicates that the energy dissipation of the system decreased as a result of decreasing polymer chain mobility.

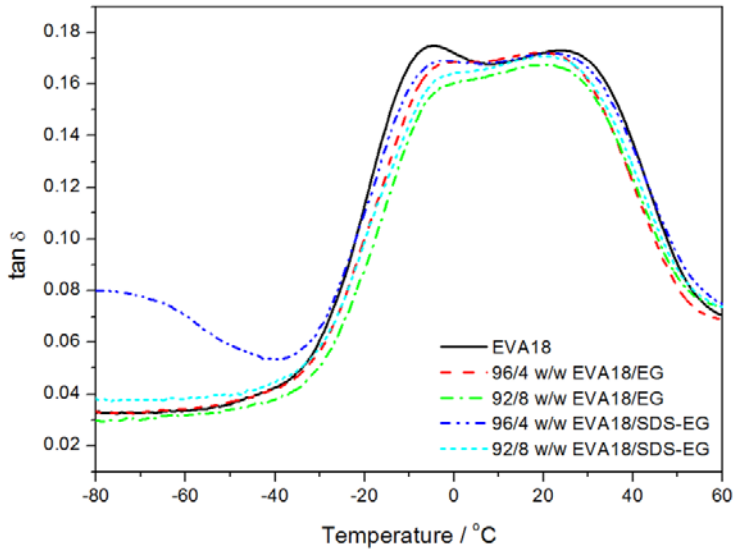

Figure 2.11 Dissipation factor as a function of temperature for pure EVA18 and the EVA18/EG composites in absence and presence of SDS modification

Table 2.4 Relaxation temperatures for the EVA18, EVA18/EG and the EVA18/SDS-EG composites determined from the tan δ curves

Sample	EVA/EG		EVA/SDS-EG	
	β-relaxation temp. / °C	α-relaxation temp. / °C	β-relaxation temp. / °C	α –relaxation temp. / °C
Pure EVA	-6.2	27.8	-	-
96/4 w/w EVA/filler	-5.4	26.9	-5.3	26.5
92/8 w/w EVA/filler	-2.8	26.3	-2.4	25.9

2.5 Conclusions

The effect of the EG and SDS modified-EG content on the structure and thermal stability of EVA18 nanocomposites was investigated. The distribution of EG was more homogeneous and uniform in the case of modified EG. The presence of EG (unmodified or modified) had little influence on the crystalline structure of EVA18, as well as on its melting and crystallization peak temperatures. The degree of crystallinity of EVA with SDS modified-EG was higher than that of EVA with unmodified EG, which is probably due to the smaller EG particles that acted as nucleation sites for EVA. The presence of EG in EVA18 increased its thermal stability, with SDS modification even already at low filler contents. The stress and elongation at break for all the EG containing EVA samples decreased markedly with increasing filler content, but the composites containing SDS treated EG gave better values. The tensile modulus values of EVA/SDS-EG were two times higher than those of the corresponding EVA/EG composites. There was a shift in the T_g to higher temperatures with an increase in both EG and modified EG content in the samples.

2.6 References

1. J. Wang, Z. Shi, Y. Ge, Y. Wang, J. Fan, J. Yin. Solvent exfoliated grapheme for reinforcement of PMMA composites prepared by in situ polymerization. Materials Chemistry and Physics 2012; 136:43-50.
DOI: 10.1016/j.matchemphys.2012.06.017

2. I.M. Afanasov, V.A. Morozov, A.V. Kepman, S.G. Ionov, A.N. Sleeznev, G. Van Tendeloo, V.V. Avdeev. Preparation, electrical and thermal properties of new exfoliate-based composites. Carbon 2009; 47:263-270.
DOI: 10.1016/j.carbon.2008.10.004
3. M. Zhang, D.-J. Li, D.-F. Wu, C.-H. Yan, P. Lu, G.-M. Qiu. Poly(ethylene terephthalate)/expanded graphite conductive composites: Structure, properties, and transport behaviour. Journal of Applied Polymer Science 2008; 108:1482-1489.
DOI: 10.1016/app.27745
4. O.A. Al-Hartomy, F. Al-Salamy, A.A. Al-Ghamdi, A. Attieh Al-Ghamdi, A.M. Abdel Daiem, F. El-Tantawy. New resistive switching and self-regulating heating in foliated graphite/nickel polyvinyl chloride nanocomposites. Journal of Nanomaterials 2011; 2011:1-10.
DOI: 10.1155/2011/694879
5. J.-W. Shen, X.-M. Chen, W.-Y. Huang. Structure and electrical properties of grafted polypropylene/graphite nanocomposites prepared by solution intercalation. Journal of Applied Polymer Science 2003; 88:1864-1869.
DOI: 10.1002/app.11892
6. S. Kim, J. Seo, L.T. Drzal. Improvement of electric conductivity of LLDPE based nanocomposite by paraffin coating on exfoliated graphite nanoplatelets. Composites: Part A 2010; 41:581-587.
DOI: 10.1016/j.compositesa.2009.05.002
7. K. Kalaitzidou, H. Fukushima, L.T. Drzal. A new compounding method for exfoliated graphite-polypropylene nanocomposites with enhanced flexural properties and lower percolation threshold. Composites Science and Technology 2007; 67:2045-2051.
DOI: 10.1016/j.compscitech.2006.11.014
8. T. Rath, Y. Li. Nanocomposites based on polystyrene-b-poly(ethylene-r-butylene)-b-polystyrene and exfoliated graphite nanoplates: Effect of nanoplatelets loading on morphology and mechanical properties. Composites: Part A 2011; 42:1995-2002.
DOI: 10.1016/j.compositesa.2011.09.002
9. K.-C. Tsai, H.-C. Kuan, H.-W. Chou, C.-F. Kuan, C.-H. Chen, C.-L. Chiang. Preparation of expandable graphite using a hydrothermal method and flame-retardant properties of its

halogen-free flame-retardant HDPE composites. Journal of Polymer Research 2011; 18:483-488.
DOI: 10.1007/s10965-010-9440-2

10. A. Yasmin, J.-J. Luo, I.M. Daniel. Processing of expanded graphite reinforced polymer nanocomposites. Composites Science and Technology 2006; 66:1179-1186.
DOI: 10.1016/j.compscitech.2005.10.014
11. S.R. Dhakate, S. Sharma, M. Borah, R.B. Mathur, T.L. Dhami. Expanded graphite-based electrically conductive composites as bipolar plate for PEM fuel cell. International Journal of Hydrogen Energy 2008; 33:7146-7152.
DOI: 10.1016/j.ijhydene.2008.09.004
12. Z. Mo, Y. Sun, H. Chen, P. Zhang, D. Zuo, Y. Li, H. Li. Preparation and characterization of a PMMA/Ce(OH)3, Pr2O3/graphite nanosheet composite. Polymer 2005; 46:12670-12676.
DOI: 10.1016/j.polymer.2005.10.117
13. Q. Chen, C. Wu, W. Weng, D. Wu, W. Yan. Preparation of polystyrene/graphite nanosheet composite. Polymer 2003; 44:1781-1784.
DOI: 10.1016/S0032-386(03)00050-8
14. X.Y. Yuan, L.L. Zou, C.C. Liao, J.W. Dai. Improved properties of chemically modified grapheme/poly(methyl methacrylate) nanocomposites via a facile in-situ polymerization. eXPRESS Polymer Letters 2012; 10:847-858.
DOI: 10.3144/expresspolymlett.2012.90
15. I. Tantis, G.C. Psarras, D. Tasis. Functionalized grapheme-poly(vinyl alcohol) nanocomposites: Physical and dielectric properties. eXPRESS Polymer Letters 2012; 4:283-292.
DOI: 10.3144/expresspolymlett.2012.31
16. G.-H. Chen, D.-J. Wu, W.-G. Weng, B. He, W.-L. Yan. Preparation of polystyrene-graphite conducting nanocomposites via intercalation polymerization. Polymer International 2001; 50:980-985.
DOI: 10.1002/pi.729
17. I. Krupa, V. Cecen, A. Boudenne, Z. Križanová, I. Vávra, R. Srnánek, G. Radnóczi. Mechanical properties and morphology of composites based on the EVA copolymer filled

with expanded graphite. Polymer-Plastics Technology and Engineering 2012; 51:1388-1393.
DOI: 10.1080/03602559.2012.704114

18. J.J. George, A.K. Bhowmick. Ethylene vinyl acetate/expanded graphite nanocomposites by solution intercalation: Preparation, characterization and properties. Journal of Materials Science 2008; 43:702-708.
DOI: 10.1007/s10853-007-2193-6

19. S. Kim, L.T. Drzal. Comparison of exfoliated graphite nanoplatelets (xGnP) and CNTs for reinforcement of EVA nanocomposites fabricated by solution compounding method and three screw rotating systems. Journal of Adhesion Science and Technology 2009; 23:1623-1638.
DOI: 10.1163/156856109X440984

20. I.H. Tavman, A. Turgut, H.M. Da Fonseca, H.R.B. Orlande, R.M. Cotta, M. Magalhaes. Thermal-diffusivity measurements of conductive composites based on EVA copolymer filled with expanded and unexpanded graphite. International Journal of Thermophysics 2013; 34:2297-2306.
DOI: 10.1007/s10765-012-1231-z

21. R. Tlili, A. Boundenne, V. Cecen, L. Ibos, I. Krupa, Y. Candau. Thermophysical and electrical properties of nanocomposites based on ethylene-vinyl acetate copolymer (EVA) filled with expanded and unexpanded graphite. International Journal of Thermophysics 2010; 31:936-948.
DOI: 10.1007/s10765-010-0775-z

22. J.J. George, A. Bandyopadhyay, A.K. Bhowmick. New generation layered nanocomposites derived from ethylene-co-vinyl acetate and naturally occurring graphite. Journal of Applied Polymer Science 2008; 108:1603-1616.
DOI: 10.1002/app.25067

23. J.J. George, A.K. Bhowmick. Influence of matrix polarity on the properties of ethylene vinyl acetate-carbon nanofiller nanocomposites. Nanoscale Research Letters 2009; 4:655-664.
DOI: 10.1007/s11671-009-9296-8

24. J.S. Sefadi, A.S. Luyt. Morphology and properties of EVA/empty fruit bunch composites. Journal of Thermoplastic Composite Materials 2012; 25:895-914.
DOI: 10.1177/0892705711421806
25. J. Jing, S. Chen, J. Zhang. Investigation of UV aging influences on the crystallization of ethylene vinyl acetate copolymer via successive self-nucleation and annealing treatment. Journal of Polymer Research 2010; 17:827-836.
DOI: 10.1007/s10965-009-9374-8
26. S. Chen, J. Zhang, J. Sun. Effect of damp-heat aging on the properties of ethylene-vinyl acetate copolymer and ethylene-acrylic acid copolymer blends. Journal of Applied Polymer Science 2009; 114:3110-3117.
DOI: 10.1002/app.30859
27. S.R. Kim, M. Poostforush, J.H. Kim, S.G. Lee. Thermal diffusivity of in-situ exfoliated graphite intercalated compound/polyamide and graphite/polyamide composites. eXPRESS Polymer Letters 2012; 6:476-484.
DOI: 10.3144/expresspolmlett.2012.50
28. H.M. Seo, J.H. Park, T.D. Dao, H.M. Jeong. Compatibility of functionalized graphene with polyethylene and its copolymers. Journal of Nanomaterials (published online).
DOI: 10.1155/2013/805201
29. H. Quan, B.-Q. Zhang, Q. Zhao, R.K.K. Yuen, R.K.Y. Li. Facile preparation and thermal degradation studies of graphite nanoplatelets (GNPs) filled thermoplastic polyurethane (TPU) nanocomposites. Composites: Part A 2009; 40:1506-1513.
DOI: 10.1016/j.compositesa.2009.06.012
30. D. Liu, J.J. Purewal, J. Yang, A. Sudik, S. Maurer, U. Maurer, U. Mueller, J. Ni, D.J. Siegel. MOF-5 composites exhibiting improved thermal conductivity. International Journal of Hydrogen Energy 2012; 37:6109-6117.
DOI: 10.1016/j.ijhydene.2011.12.129
31. W.-G. Weng, G.-H. Chen, D.-J. Wu, W.-L. Yan. HDPE/expanded graphite electrically conducting composite. Composite Interfaces 2004; 2:131-143.
DOI: 10.1163/156855404322971404

32. V.K. Paruchuri, J. Nalaskowski, D.O. Shah, J.D. Miller. The effect of cosurfactants on sodium dodecyl sulphate micellar structures at a graphite surface. Colloids and Surfaces 2006; 272:157-163.
DOI: 10.1016/j.colsurfa.2005.07.028

33. H.K.F. Cheng, Y. Pan, N.G. Sahoo, K. Chong, L. Li, S.H. Chan, J. Zhao. Improvement in properties of multiwalled carbon nanotube/polypropylene nanocomposites through homogeneous dispersion with the aid of surfactants. Lournal of Applied Polymer Science 2012; 124:1117-1127.
DOI: 10.1002/app.35047

34. L.A. Smith, R.B. Hammond, K.J. Roberts, D. Machin, G. Mcleod. Determination of the structure of anhydrous sodium dodecyl sulphate using a combination of synchrotron radiation powder diffraction and molecular modelling techniques. Journal of Molecular Structure 2000; 554:173-182.
DOI: S0022-2860(00)00666-9

35. S. Cheng, X. Chen, Y. G. Hsuan, C.Y. Li. Reduced grapheme oxide-induced polyethylene crystallization in solution and nanocomposites. Macromolecules 2012; 45:993-1000.
DOI: 10.1021/ma2021453

36. C. Zhang, W.W. Tjiu, W. Fan, S. Huang, T. Liu. A novel approach for transferring water-dispersible grapheme nanosheets into organic media. Journal of Materials Chemistry 2012;22:11748-11754.
DOI: 10.1039/c2jm30955f

37. O. Grigoryva, A. Fainleib, O. Starostenko, A. Tolstov, W. Brostow. Thermoplastic elastomers from rubber and recycled polyethylene: Chemical reactions at interphases for property enhancement. Polymer International 2004; 53:1693-1703.
DOI: 10.1002/pi.1530

38. B. John, K.T. Varughese, Z. Oommen, P. Pötschke, S. Thomas. Dynamic mechanical behaviour of high-density polyethylene/ethylene vinyl acetate copolymer blends: The effects of the blend ratio, reactive compatibilization, and dynamic vulcanization. Journal of Applied Polymer Science 2003; 87:2083-2099.
DOI: 10.1002/app.11458

Chapter 3

Effect of surfactant treatment and electron radiation on the electrical and thermal conductivity, and thermal and mechanical properties of EVA/EG composites

This chapter has been submitted as a publication:
JS Sefadi, AS Luyt, J Pionteck, F Piana and U Gohs. Effect of surfactant treatment and electron radiation on the electrical and thermal conductivity, and thermal and mechanical properties of EVA/EG composites. Journal of Applied Polymer Science.

ABSTRACT

This study presents an investigation of the electrical and thermal conductivities of composites based on an ethylene vinyl acetate copolymer (EVA) matrix and nano-structured expanded graphite (EG). To improve the EG dispersion in EVA, EG sheets were modified by treating them with the anionic surfactant sodium dodecyl sulphate (SDS) in water. The modified SDS-EG platelets, after being filtered and dried, were melt-mixed with EVA to prepare the composites. Finally, both EVA/EG and EVA/SDS-EG composites were subjected to 50 kGy electron beam irradiation. SEM images confirm that the irradiated EVA/EG samples had improved interfacial adhesion, while the irradiated EVA/SDS-EG samples showed even better interfacial adhesion. The gel contents of the irradiated samples without and with SDS treatment increased with increase in EG loading. The EVA/EG composites exhibited a sharp transition from an insulator to a conductor at an electrical percolation threshold of 8 wt%, but with SDS-EG the electrical conductivity was extremely low, showing no percolation up to 10 wt% of filler. The EB irradiation had no influence on electrical conductivity. The thermal conductivity linearly increased with EG content, and this increase was more pronounced in the case of SDS-EG, but decreased after EB irradiation. The thermal properties were little influenced by EB irradiation, while better polymer-filler interaction and better filler dispersion as a result of SDS treatment, and the radiation initiated formation of a crosslinked network, had a positive effect on the tensile properties.

Keywords: EVA; expanded graphite; electron beam irradiation; electrical conductivity; thermal conductivity; mechanical properties

3.1 Introduction

Conventional polymers are materials possessing low thermal and no electrical conductivities, and these primarily depend on the extent of crystallinity. However, there are many industrial applications such as circuit boards, heat exchangers, electromagnetic shielding devices, antistatic plastics, packaging and others that require an improvement in both the thermal and electrical conductivity of polymers [1-9]. One way to improve the thermal and electrical conductivity, as well as the viscoelastic behaviour and mechanical properties, of these materials is to combine polymer matrices with highly conductive fillers. Several types of these fillers (metallic, graphitic, and other inorganic or organic fillers) in numerous shapes are commonly used as electrically and thermally conductive fillers [10,11]. However, metallic fillers have some disadvantages which limit their usage. Most metallic fillers have spherical shapes, which give rise to high percolation thresholds, and thus large filler fractions are necessary in the composite, increasing the price and weight of the material. Nano-structured expanded graphite sheets or platelets are light, anisotropic and conductive [10,12,13]. These properties make EG nano-platelets ideal fillers to achieve light and conductive polymer nanocomposites that can be useful for many industrial applications. The electrical conductivity of the nanocomposites is normally dominated by the interfacial interaction and network pathway contact points. Thus, the conductivity of EG nanocomposites should strongly depend on the surface properties of EG and the polymer-EG interface.

Many polymers reinforced with conductive fillers have been studied, but there are still many unsolved problems with respect to calculations around particle sizes, shapes, concentrations and the properties of each constituent. Some theoretical equations have been proposed to predict the electrical and thermal conductivities of polymeric materials. Only a few studies were dedicated to a comparative analysis of the electrical and/or thermal conductivities of two-phase systems [2,3]. Tlili *et al.* [2] reported on the thermal and electrical conductivities of EVA14 filled with expanded graphite (EG) and unexpanded graphite (UG). Their nanocomposites were prepared by melt mixing. They found that the thermal conductivity increased significantly with increasing EG content. They also found an electrical percolation threshold of about 6 vol% in the EVA/EG composites and 17 vol% in the EVA/UG composites. Tavman *et al.* [3] investigated the thermal diffusivity of conductive composites based on EVA14

filled with EG and UG. They used exactly the same preparation method and their observations were similar to those of Tlili *et al*. [2].

Modification of polymers and their composites by electron beam (EB) radiation can be used for many polymer processing applications including crosslinking, degradation, hardening, surface modification, and coating. According to literature, polymers may simultaneously undergo various reactions such as degradation, crosslinking, grafting and oxidation during electron beam irradiation, depending on the irradiation dose and conditions [14]. The irradiation of polymers with ionizing radiation such as gamma rays, X-rays, accelerated electrons and ion beams are of great importance to many processing applications [15]. The primary advantages of high-energy electron beam radiation are that it is pollution free, and has a high efficiency, low operation cost, room temperature operation and the ability to process large throughputs.

High energy electrons are used for crosslinking of polymeric materials in a wide range of applications such as cable and wire insulations, tubes, foams, heat shrinkable tubes, and shape memory products. High energy electron induced crosslinking is mainly performed at ambient temperature and leads to the formation of three-dimensional networks. Due to these changes in polymer structure an increase in chemical (increased resistance against solvents), mechanical (increased resistance against stress cracking corrosion) and thermal (increased resistance against thermal pressure) properties can be achieved [14-16]. Ethylene copolymers like EVA belong to polymers which can be crosslinked by high energy electrons without any use of additional crosslinking agents. It is generally believed that the crosslinking starts by hydrogen elimination from the terminal methyl groups of the acetate side chain, which then reacts with other activated sites or methylene units of the main chain in a rather complex mechanism, including degradation reactions [17,18].

Although there has been no study on the effect of electron beam irradiation on EVA/EG and/or EVA/SDS-EG composites, the effect of gamma irradiation on EVA-based composites was investigated [19,20]. Sen *et al.* [19] studied the effect of gamma irradiation in nitrogen on EVA13 and EVA13/carbon black composites prepared by a sol-gel method. Their samples were subjected to up to 400 kGy gamma rays at ambient conditions in air atmosphere. They found that oxidation, crosslinking and chain scission resulted from the gamma irradiation in air atmosphere. Khodkar *et al.* [20] investigated the effect of ^{60}Co γ-irradiation in the presence of air and nitrogen on EVA18/hollow fibre composites prepared by melt mixing in a co-extruder. They

showed that this irradiation in nitrogen enhanced the mechanical and thermo-mechanical properties, while irradiation in air caused no changes in these properties. In comparison to EB irradiation, ^{60}Co γ-irradiation in air leads to more degradation of EVA due to lower dose rate and undesired reactions with oxygen.

This study involves a comparative analysis of the electrical and thermal conductivities, as well as thermal and mechanical properties, of non-irradiated and irradiated samples of EVA18 containing EG or SDS-EG. We are not aware of any other reported work on similar systems.

3.2 Experimental

3.2.1 Materials

Expanded graphite, SIGRAFLEX Expandat, was provided by the SGL Technologies GmbH, SGL Group. It has a conductivity of 20 S cm^{-1} (room temperature, 30 MPa, self-made 2-point conductivity tester, coupled with a DMM2000 Electrometer, Keithley Instruments), an apparent volume of ~400 cm^3 g^{-1}, and a specific surface of 39.4 m^2 g^{-1} (77.4 K, N_2 atmosphere, Autosorb-1, Quantachrome). Ethylene vinyl acetate (EVA-460) was manufactured and supplied in granule form by DuPont Packaging & Industrial Polymers. EVA-460 contains 18% by weight of vinyl acetate (VA) with a BHT antioxidant thermal stabilizer. It has a melt flow index (190 °C/2.16 kg) of 2.5 g/10 min (ASTM D1238-ISO 1133), a melting temperature of 88 °C, a Vicat softening point of 64 °C, and a density of 0.941 g cm^{-3}. The sodium lauryl sulphate known as sodium dodecyl sulphate (SDS) was supplied by Sigma-Aldrich and was used without further treatment.

3.2.2 Preparation of nanocomposites

4 g of SDS was dissolved in 5 L deionized water in a glass beaker, and 20 g of the expanded graphite was gradually added to the solution. 500 mL suspensions were sonicated for 30 min, filtered, washed with 100 mL distilled water to remove loosely adsorbed SDS, and dried in a vacuum oven at 50 °C for 72 h. This modified EG, as well as the as received unmodified EG, were respectively mixed with EVA to prepare the nanocomposites. The EVA composites were prepared by melt mixing using a Brabender Plastograph 55 mL internal mixer. The mixing was

done for 15 min at 60 rpm and 100 °C. The samples were melt-pressed at 100 °C and 50 bar for 5 min into 100 mm x 100 mm x 2 mm square sheets by using a hot hydraulic press. For the thermal conductivity test, the samples were compression molded at 100 ºC and 50 bar for 5 min into 5 mm thick cylindrical disks with a diameter of 12 mm. The filler amount in the composites was varied between 0 and 10 wt%.

3.2.3 Electron beam radiation

All the EVA/EG and EVA/SDS-EG samples, packed in polyethylene bags filled with nitrogen in order to avoid oxygen induced degradation, were irradiated with 1.5 MeV electrons using an electron accelerator ELV-2 (Budker Institute of Nuclear Physics, Novosibirsk, Russia) installed in the Leibniz Institute of Polymer Research Dresden [21]. A two-side irradiation was used in order to ensure a good dose uniformity. The absorbed dose amounted to 50 kGy and was applied at room temperature (25 ± 1 ºC) and at a beam current of 4 mA.

3.3 Characterization and analysis

Scanning electron microscopy (SEM) analyses was carried out in a TESCAN VEGA3 Superscan scanning electron microscope (Brno, Czech Republic). The fracture surfaces of the samples were coated with gold to prevent static charges during analysis. Microscope settings of 285.5 nm probe size, 50 mA probe current, and 30 kV AC voltage were used.

The gel content of the samples was determined using Soxhlet solvent extraction. Rectangular test specimens with masses of approximately 0.2 g were wrapped in a 120 fine mesh stainless steel cage and refluxed with xylene at 140 °C for about 12 hours and then dried at 80 °C under vacuum overnight to determine the gel fraction. The gel content values were averaged over at least 2 tests and calculated according to Equation 3.1.

$$\text{Gel content (\%)} = \left(1 - \left[\frac{(m_{BE} - m_{AE})}{(1-F)(m_{BE})}\right]\right) \times 100\ \% \qquad (3.1)$$

where m_{BE} = the sample mass before extraction; m_{AE} = the sample mass after extraction; F = fraction of filler insoluble in xylene in the composites.

The volume resistance measurements of the samples were carried out on a 6157A Keithley Instruments electrometer, connected to an 8009 Keithley Resistivity Test Fixture with two plate electrodes located on both sides of the samples. This method is appropriate for resistance values in the range of 10^7 to 10^{18} Ω at room temperature in accordance with ASTM D257-07. The corresponding conductivity values are in the range of 10^{-19} to 10^{-8} S cm^{-1}, but sensible results can be found in the range of 10^{-19} to 10^{-4} S cm^{-1}.

The thermal conductivity measurements were done using a Hot Disc Thermal Constant Analyser TPS 500 (Sweden) at room temperature (24 °C). The measurement system is based on the transient plane source technique. The sensor is sandwiched between two pieces of sample having cylindrical shapes with 12 mm diameter and 5-6 mm high. The sensor used has a radius of 3.189 mm and the measurement time was 2.5 s with a heating power of 2.048 W. The measurements were done on both surface sides of the non-irradiated system. For the irradiated samples, the sensor was placed between two sample films on top of cylindrical shaped pieces protected with insulator material. The device measures the thermal conductivity (λ), thermal diffusivity (α) and the specific heat capacity (C_p). The material density (ρ_{th}) was determined by the rule of mixtures (Equation 3.2) using a density of 0.941 g cm^{-3} for EVA and 2.25 g cm^{-3} for EG [9], where ρ_{EVA}, ρ_{EG}, and φ are the density of EVA, that of expanded graphite, and the filler volume fraction. By using Equation 3 the theoretical thermal conductivity (λ) can be readily calculated [1-3].

$$\rho_{th} = \rho_{EVA}(1-\varphi) + \rho_{EG}\varphi \quad (3.2)$$

$$\lambda = \alpha.\rho.C_p \quad (3.3)$$

DSC analyses were carried out under nitrogen flow (20 mL min^{-1}) using a Perkin Elmer Pyris-1 differential scanning calorimeter (Waltham, Massachusetts, U.S.A). The instrument was calibrated using the onset temperatures of melting of indium and zinc standards, as well as the melting enthalpy of indium. The sample masses were in the range of 5-10 mg, and they were heated from 25 to 180 °C at a heating rate of 10 °C min^{-1}. The cooling and second heating were performed under the same conditions. For all the samples, the onset and peak temperatures of

melting and crystallization, as well as the melting enthalpies, were determined from the second heating scan. The normalised enthalpies of melting were determined according to Equation 3.4.

$$\Delta H_m^{Norm} = \frac{\Delta H_{m,EVA}}{w_{EVA}} \quad (3.4)$$

where $\Delta H_{m,EVA}$ is the experimentally observed melting enthalpy for the pure EVA, and ΔH_m^{Norm} is the calculated normalised enthalpy of melting for EVA with a weight fraction w_{EVA} in the composite. The degree of crystallinity χ_c was calculated from Equation 3.5.

$$\chi_c = (\Delta H_m^{Norm}/\Delta H_m^o) \times 100\ \% \quad (3.5)$$

where ΔH_m^o is the specific enthalpy of melting for 100% crystalline PE. A value of 288 J g^{-1} was used in the calculations [16,19,20].

Thermogravimetric analysis was done under flowing nitrogen (20 mL min^{-1}) using a Perkin Elmer Pyris-1 thermogravimetric analyser (Waltham, Massachusetts, U.S.A). The samples, weighing ~20 mg each, were heated from 30 to 600 °C at a heating rate of 10 °C min^{-1}.

Tensile testing was performed under ambient conditions on a Hounsfield H5KS universal tester at a cross-head speed of 50 mm min^{-1}. The specimens were dumbbell shaped (gauge length 20 mm, width 2 mm, thickness 2 mm). The tensile modulus as well as stress and elongation at break of the samples were calculated from the stress-strain curves. At least five specimens were tested for each sample and the mean values and standard deviations are reported.

3.4 Results and discussion

3.4.1 Scanning electron microscopy (SEM)

The SEM micrographs of the fracture surface of the irradiated EVA nanocomposites filled with 2 and 10 wt% EG and SDS-EG are shown in Figure 3.1. It can be seen that there are some agglomerates (position B) and cracks (positions A and C) along the interface in the irradiated EVA/EG samples (Figures 3.1a and 3.1c). This indicates that there was interfacial debonding between the EG platelets and EVA. As the filler content increased to 10 wt%, EG clusters are

observed (position D in Figure 3.1c). In our previous work [22] on non-irradiated composites, the SEM images showed big particle agglomerations of the EG present in the materials prepared without any dispersing agent. The explanation was that the EG sheets tend to agglomerate and are more difficult to disperse in the matrix because of insufficient shear force to break down the EG agglomerates.

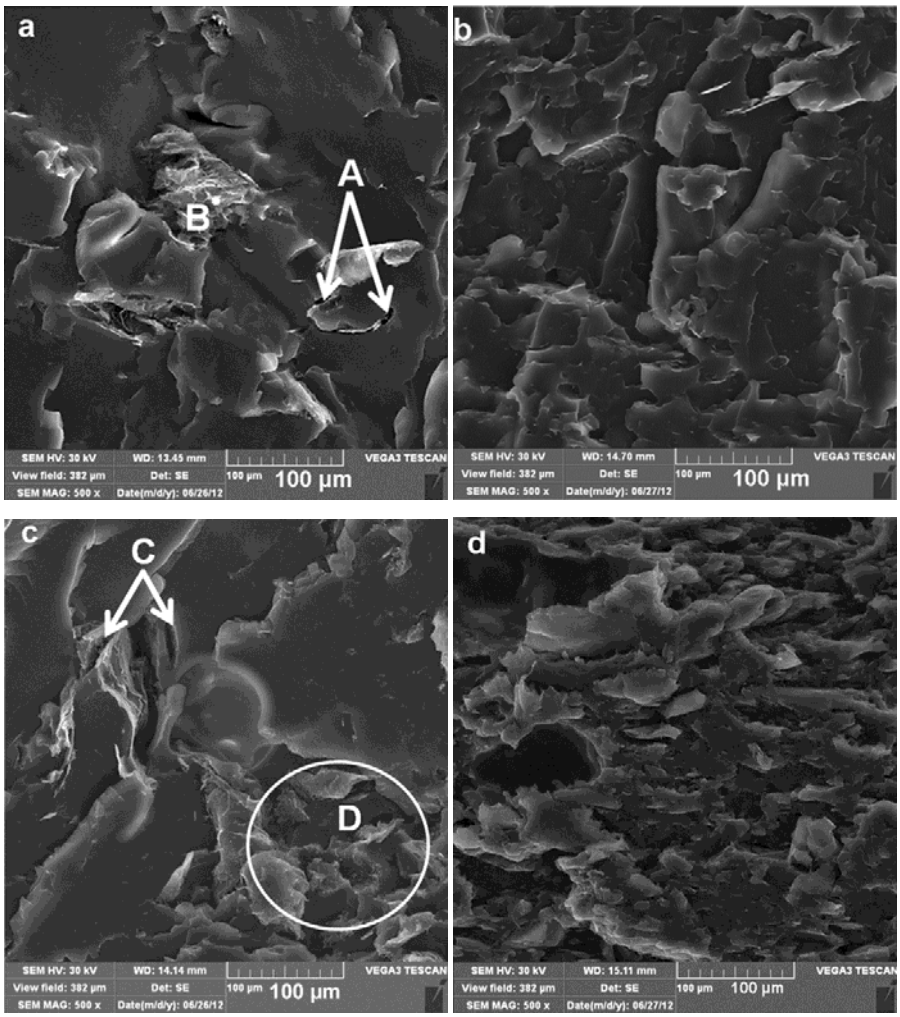

Figure 3.1 SEM micrographs of irradiated EVA/EG composites: (a) 98/2 w/w EVA/EG; (b) 98/2 w/w EVA/SDS-EG; (c) 90/10 w/w EVA/EG; (d) 90/10 w/w EVA/SDS-EG

Figures 3.1b and 3.1d confirm that the SDS-EG sheets were more uniformly dispersed in the matrix of the irradiated composites due to the effect of surfactant treatment in enhancing the interfacial adhesion. There are no obvious voids at the boundaries between the two components, confirming that the pores of the EG are effectively impregnated with EVA. After EB irradiation,

the surface morphology of the samples (Figure 3.1b and d) did not change compared to the non-irradiated EG and SDS-EG composites (see [22]). This indicates that there was no EVA melting at a macroscopic level when the electron beam penetrated the polymer, and the EG or SDS-EG particles could not re-arrange. Similar observations were reported by Dubey *et al*. [23] in their study of radiation processed EVA reinforced with MWCNT prepared *via* melt mixing. They observed homogeneity in all their samples and no agglomerations of MWCNT in the investigated composition range. This was attributed to the better interfacial interactions and good compatibility between the components induced by multifunctional acrylates (antioxidants). These multifunctional acrylates were introduced to the system to overcome the deterioration of mechanical properties of EVA at high radiation dose.

3.4.2 Gel content

The dependence of gel content of the irradiated EVA on the EG and SDS-EG contents is shown in Figure 3.2. The non-irradiated EVA was completely soluble in hot xylene. The gel contents are accepted as a measure of the crosslinking density in EVA. An increase in gel content will cause a decrease in solubility due to the formation of three-dimensional networks in the irradiated polymer [14,15]. Since the radiation induced crosslinking reactions normally occur primarily in the amorphous phase of the polymer [24-29], the EB irradiation will induce crosslinking and some degradation in the amorphous phase, while the crystalline phase should not be affected.

The gel contents of all the samples increased with an increase in EG loading because of increased formation of insoluble macromolecular networks (crosslinks) in the polymer. The EG obviously conducts energy from the EB irradiation and improves the efficiency of free radical formation and crosslinking. The irradiated SDS-EG containing composites have significantly higher gel content values than the irradiated EG samples. This is probably due to the improved interaction and dispersion of the EG platelets in the EVA, which further improved the energy transfer to the EVA chains and the resultant crosslinking efficiency.

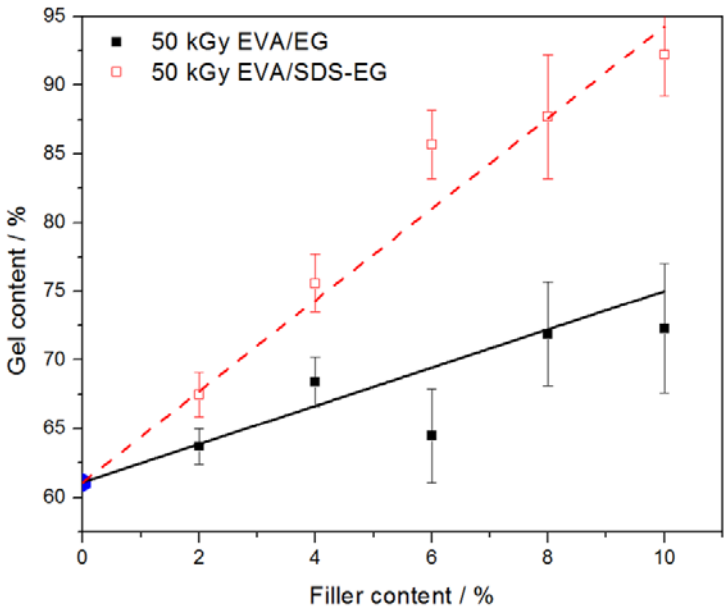

Figure 3.2 Gel content as function of EG content for irradiated samples without and with SDS treatment

3.4.3 Electrical conductivity

Figure 3.3 shows the electrical conductivities of all the investigated samples as a function of EG content. It is evident that the EVA/EG composites with and without radiation had a percolation threshold of about 8 wt%. EB radiation did not have any effect on the electrical conductivities of the composites. In the case of the composites containing SDS-EG there was no conductivity, even at an SDS-EG filling of 10 wt% (9.5% actual EG content), independent of irradiation. Possible reasons for this observation are that (i) the presence of SDS separates the EG platelets so effectively that percolation pathways will only be formed at much higher SDS-EG contents and (ii) the SDS forms an isolating layer around the EG platelets which reduces their effective electrical conductivity.

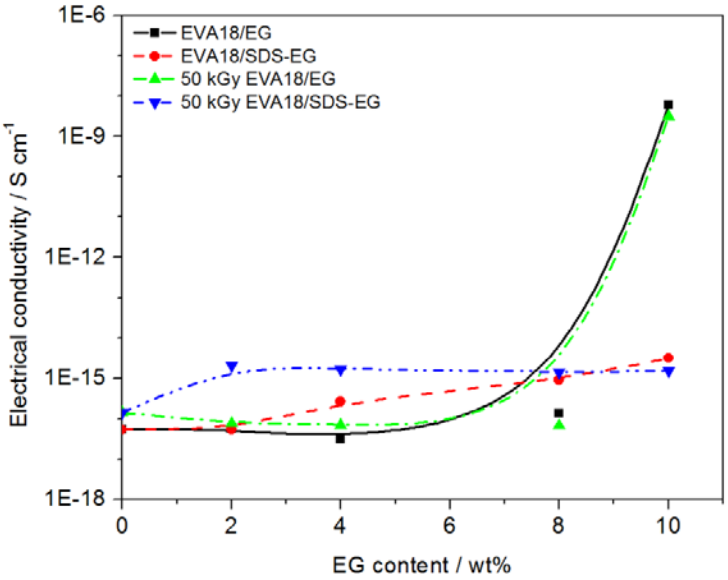

Figure 3.3 Electrical conductivity of EVA composites without and with surfactant modification and electron radiation

3.4.5 Thermal conductivity

The thermal conductivity of EVA and its composites in the absence and presence of SDS, and without or with irradiation treatment, are presented in Figure 3.4 and summarized in Table 3.1. An increase in the thermal conductivity with increasing filler content was observed for all the investigated samples. This is due to the fact that the filler has a much higher thermal conductivity (6.0 W m^{-1} K^{-1}) [28] than EVA (0.35 W m^{-1} K^{-1}). The non-irradiated composites containing EG and SDS-EG have very similar thermal conductivities within experimental error. A number of factors, such as dispersion of EG sheets, matrix crystallinity and crystal structure, degree of interfacial thermal contact between the components, and scattering of phonons contribute to the thermal conductivities of such composites. Scattering of phonons at the EG/polymer interface and at EG/EG contact sites may suppress heat conduction in the composites, and the surfactant itself may have an insulating effect, while the improved dispersion of the EG may increase the thermal conductivity, especially when continuous EG paths are formed. However, a percolation phenomenon is not observed in contrast to the findings on electrical conductivity (compare with Figure 3.3). This difference between the electrical and thermal conductivity is due to a different mechanism of electron transport (allowing electron hopping over a few nm from filler particle to

filler particle) and phonon transport (scattering at interfaces in heterogeneous systems). Since the crystallinities in the EVA/SDS-EG composites are higher than those in the corresponding SDS-free composites [22], which could count for higher thermal conductivities, one can only speculate about the similarity of the thermal conductivities in the two composite systems. The finer morphology of the EVA/SDS-EG composites with higher numbers of interfaces probably counterbalances the effect of higher crystallinity.

The non-irradiated EVA/EG composites have higher thermal conductivity values than the irradiated EVA/EG samples. This is surprising since in the non-irradiated samples the crystallinity decreased with increasing EG content [22], while it increased in the irradiated samples (see Figure 3.6). The crosslinking in the irradiated composites probably induced restricted chain mobility and reduced vibration of phonons, which hampered the heat transfer and led to lower conductivities. The changes in interstitial spaces induced by irradiation also contributed towards fewer vibrational modes which resulted in lower thermal conductivities [28]. The irradiated SDS-EG containing composites also show lower thermal conductivities than the non-irradiated ones, but the difference is not as big as in the case of the EG composites. This is probably the result of the relatively high crystallinity in the irradiated samples ([22] and Figure 3.6), and of the more intimate contact between the EVA and EG in the presence of SDS, even in the absence of irradiation and crosslinking. Both these effects partially balance the negative effect of restricted chain mobility due to crosslinking.

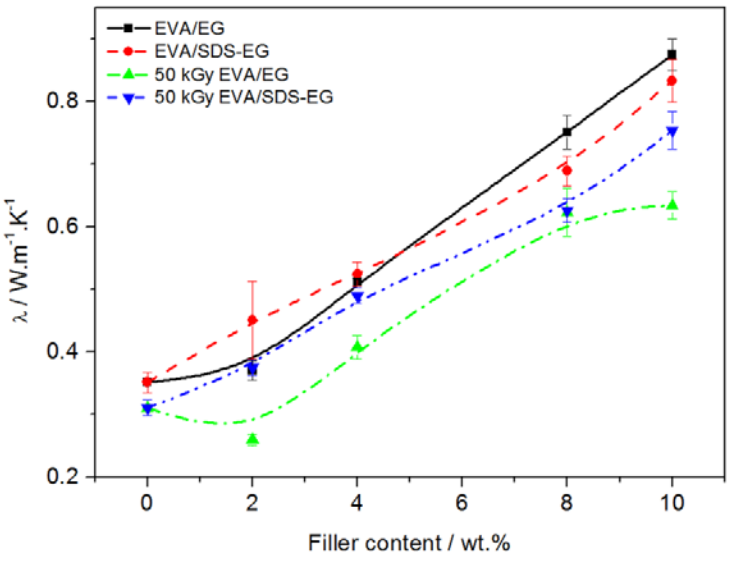

Figure 3.4 Thermal conductivity of EVA/EG composites in the absence and presence of SDS and radiation treatment

Table 3.1 Thermal conductivities of non-irradiated and irradiated EVA samples

	Non-irradiated samples		Irradiated samples	
wt% EG	$\lambda_{EVA/EG}$ / W m^{-1} K^{-1}	$\lambda_{EVA/SDS-EG}$ / W m^{-1} K^{-1}	$\lambda_{50\ kGy\ EVA/EG}$ / W m^{-1} K^{-1}	$\lambda_{50\ kGy\ EVA/SDS-EG}$ / W m^{-1} K^{-1}
0	0.351 ± 0.017	0.351 ± 0.017	0.310 ± 0.013	0.310 ± 0.013
2	0.370 ± 0.015	0.450 ± 0.062	0.259 ± 0.008	0.375 ± 0.012
4	0.511 ± 0.006	0.524 ± 0.019	0.407 ± 0.018	0.489 ± 0.013
6	0.654 ± 0.011	0.657 ± 0.035	0.484 ± 0.009	0.447 ± 0.010
8	0.750 ± 0.027	0.689 ± 0.024	0.623 ± 0.038	0.626 ± 0.019
10	0.877 ± 0.025	0.833 ± 0.035	0.634 ± 0.022	0.753 ± 0.030

$\lambda_{EVA/EG}$; $\lambda_{50kGy\ EVA/EG}$; $\lambda_{EVA/SDS-EG}$ and $\lambda_{50kGy\ EVA/SDS-EG}$ are the thermal conductivities of the EVA/EG, irradiated EVA/EG, EVA/SDS-EG and irradiated EVA/SDS-EG composites respectively

3.4.6 Differential scanning calorimetry (DSC)

The crystallinity of the EVA originates from the polyethylene segments and is directly proportional to the melting enthalpy. The DSC data for the first heating run of all the non-irradiated and irradiated samples are shown in Figure 3.5, and reflect changes in the crystalline structure after EB irradiation. The melting enthalpy values were normalised to the mass content of EVA in the samples (Table 3.2). The crystallinities of the non-irradiated samples increased slightly with increasing EG content up to 6 wt%, after which it slightly decreased. It seems as if at lower EG contents the nucleation effect of the EG particles on the polymer chains was more dominant than the immobilization effect, while the immobilization effect became more dominant at higher EG contents where there was probably more agglomeration. The irradiated samples showed the same trend, but their crystallinities are observably higher than those of the comparable non-irradiated samples. The reason is probably that, because of chain scission and localised melting induced by the electron beam irradiation, some recrystallization occurred and the shorter chain segments rearranged into a more crystalline morphology.

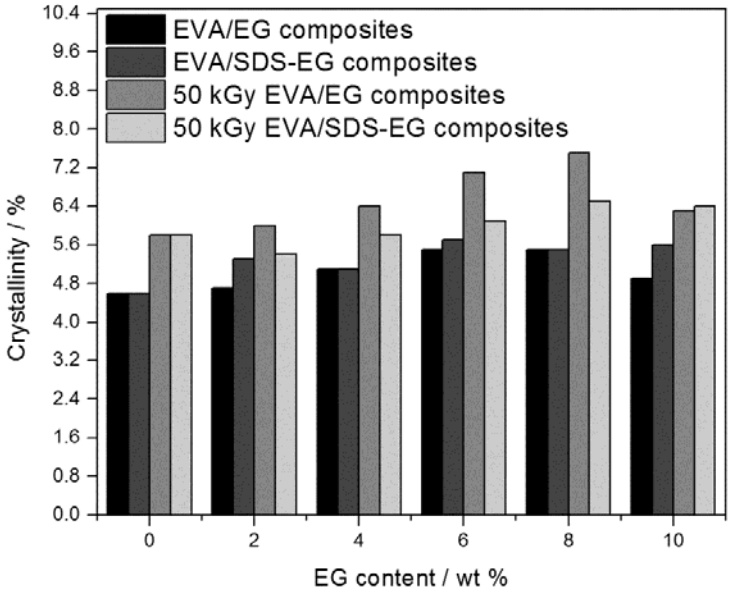

Figure 3.5 Crystallinities of non-irradiated and irradiated EVA18 and its composites with and without SDS as a function of EG content

Table 3.2 Data obtained from the first heating and cooling DSC curves of all the irradiated samples

wt% EG	$T_{p,m}$ / °C	$T_{p,c}$ / °C	ΔH_m / J g^{-1}	ΔH_m^{Norm} / J g^{-1}	χ_c / %
			No modification		
0	84.8 ± 0.8	62.6 ± 0.1	16.7 ± 0.4	16.7	5.8
2	84.4 ± 0.7	62.1 ± 0.2	17.0 ± 0.5	17.3	6.0
4	84.2 ± 0.5	61.8 ± 1.4	17.6 ± 0.7	18.3	6.4
6	84.3 ± 0.1	61.3 ± 0.8	19.3 ± 0.1	20.5	7.1
8	83.4 ± 0.3	61.7 ± 1.3	20.0 ± 3.4	21.7	7.5
10	83.1 ± 0.3	61.5 ± 1.2	16.4 ± 0.1	18.2	6.3
			SDS modification		
2	84.3 ± 0.4	62.3 ± 0.3	15.3 ± 0.1	15.6	5.4
4	84.2 ± 0.4	62.2 ± 0.1	16.1 ± 0.7	16.8	5.8
6	83.6 ± 0.3	62.0 ± 0.2	16.5 ± 0.6	17.6	6.1
8	83.9 ± 0.7	61.7 ± 0.6	17.1 ± 0.1	18.6	6.5
10	83.8 ± 0.2	61.7 ± 1.0	16.6 ± 1.2	18.4	6.4

$T_{p,m}$ is the peak temperature of melting; $T_{p,c}$ is the peak temperature of crystallization; ΔH_m is the measured melting enthalpy; ΔH_m^{Norm} is the normalised melting enthalpy of EVA18 taking into account its mass fraction; χ_c is the EVA18 crystallinity in the samples

The melting and crystallization temperatures of EVA in the irradiated samples did not really change within experimental error in the presence of EG and SDS-EG and with increasing EG content (Table 3.2). These values are, however, slightly lower than those of the non-irradiated samples, where the melting temperatures varied between 85.4 and 84.1 °C and the crystallization temperatures between 65.0 and 66.7 °C. The lower melting temperature is a sign of less perfect or smaller crystallites. This is certainly caused by hindered chain mobility during crystallisation due to the crosslinked structure, which normally causes lower crystallisation temperatures in crosslinked systems.

3.4.7 Thermogravimetric analysis (TGA)

Figure 3.6a shows a comparison of the thermal stabilities of non-irradiated and irradiated EVA/EG and EVA/SDS-EG composites. The TGA curves of the irradiated EVA and its irradiated composites in the absence and presence of SDS treatment are shown in Figure 3.6b. Table 3.3 summarizes the degradation temperatures at 10% mass loss and at the maximum mass loss rate of these samples. It is generally accepted that the first mass loss step between 350 and 400 °C is due to deacetylation with β-elimination of the acetic acid and the formation of carbon-carbon double bonds along the polymer backbone. The results in Figure 3.6 and Table 3.3 show that less acetic is evolved between 350 and 400 ºC for the irradiated samples, probably because of crosslinking taking place in the amorphous phase which consists mainly of VA monomers. This crosslinking restricted the chain mobility and also the mobility of the free radicals formed during thermal degradation. The degradation of the main chain at about 475 ºC was faster for the irradiated samples, which may be due to some degradation of the EVA chains and formation of additional free radicals from tertiary main chain carbons introduced by the EB radiation [17]. The temperature values in Table 3.3 vary within a 10 °C bracket, but there is no trend and the thermal stability of the irradiated composites is comparable to that of the irradiated EVA. Our previous work [22] shows a clear improvement in thermal stability in the presence of EG and SDS-EG, and with increasing filler content.

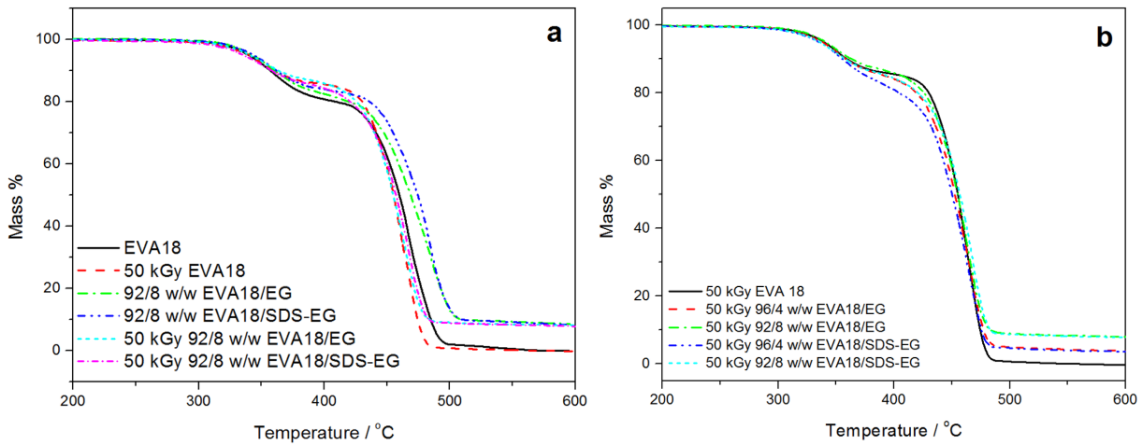

Figure 3.6 TGA curves of non-irradiated and irradiated (a) EVA18/EG and (b) EVA/SDS-EG composites

Table 3.3 TGA results for all the irradiated samples

wt. % EG	$T_{10\%}$ / °C	T_{max} / °C	Weight % residue
No SDS modification			
0	352.7	465.4	0
2	357.7	464.7	1.8
4	351.1	465.1	3.5
6	353.0	466.0	5.2
8	353.7	464.7	7.8
10	350.1	459.1	9.1
SDS modification			
0	352.7	465.4	0
2	359.5	473.5	2.7
4	354.7	462.7	3.5
6	354.2	465.2	6.0
8	352.0	466.0	7.6
10	349.2	468.2	8.1

$T_{10\%}$ and T_{max} are the degradation temperatures at 10% mass loss and maximum mass loss rate

Figure 3.6b shows that the degradation of the main chain started even before the end of the deacetylation step for the EG and SDS-EG samples, and the onset of second step degradation decreases with increasing filler content. The most probable reason for this is the more effective initiation of degradation during irradiation when EG or SDS-EG is present in the samples. As mentioned before, these fillers probably transport heat energy more effectively through the sample, improving the thermal degradation during irradiation. The percentage residues of all the composites correlate well with the EG contents initially mixed into the EVA matrix, indicating good dispersion of the filler in the polymer.

3.4.8 Tensile properties

Composites with good mechanical properties can be obtained when the graphite platelets are well dispersed in the EVA matrix, and when there is good interaction between the polymer and the filler. From previously discussed results we know that the presence of SDS improves the interaction between EVA and EG, and the dispersion of EG in the EVA matrix. The EB irradiation treatment induces crosslinking which should contribute to improving the mechanical properties of the composites, not only because of network formation but also because of trapping the EG platelets in the formed network.

Figure 3.7 shows that the tensile stress at break is generally reduced in the presence of and with increasing EG content. As is generally known and also explained in our previous paper [22], inorganic filler in a polymer normally forms defect centres at which crazes and cracks start forming when stress is applied to the sample. The propagation of the cracks gives rise to sample fracture. For the non-irradiated samples, the results in Figure 3.7 clearly show higher stress at break values for the EVA/SDS-EG composites, and the reason for this has already been explained in our previous paper [22]. The irradiated EVA has a significantly higher value than the non-irradiated EVA, which is to be expected because of the formation of a crosslinked network. It is interesting that the non-irradiated SDS-EG containing samples have about the same stress at break values than the irradiated EG containing samples within experimental error. It seems that the improved interaction and dispersion of the filler particles has the same effect on the stress at break of the composite than the network formation as a result of radiation induced crosslinking of the polymer matrix. However, the improved interaction and dispersion combined

with the radiation induced crosslinking give even better stress at break values, which is important when one wants to improve the thermal properties without sacrificing too much on the tensile properties. Unfortunately the electrical conductivity of the samples treated in this way remains very low up to a filler content of 10 wt%.

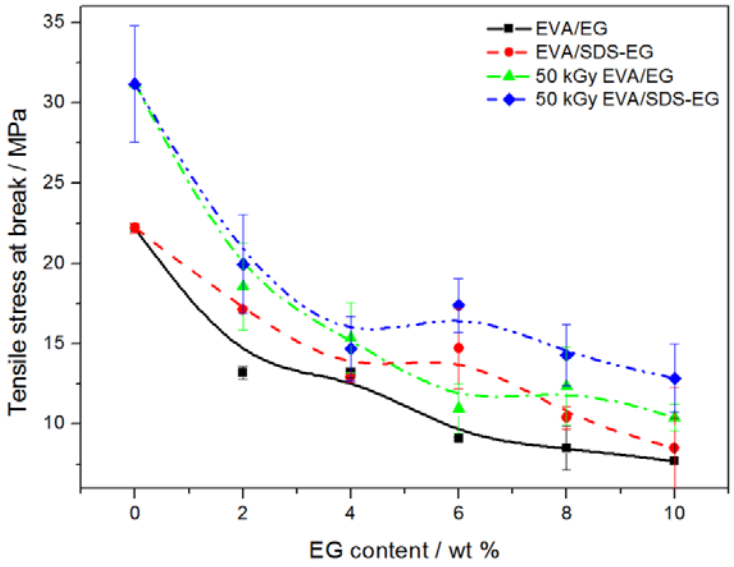

Figure 3.7 Variation of stress at break of non-irradiated and irradiated EVA/EG and EVA/SDS-EG samples as a function of filler content

The elongation at break of the EVA observably increased after EB irradiation (Figure 3.8), which is the result of the crosslinked network formation. The elongation at break values of the composites containing the same amount of EG, however, are very similar within experimental error, independent of surfactant and/or radiation treatment. In these samples there is a complex combination of many factors that contribute to the mechanical stability of the samples, and therefore it is very difficult to explain in exact terms why the elongation at break of the composites was not significantly influenced by improved interaction and dispersion and/or the formation of a crosslinked network. The fracture mechanism of composites is generally independent of crosslinking, but is dominated by the presence of agglomerates; the bigger agglomerates in the SDS free composites probably causes failure at lower stresses than the smaller and more homogeneously dispersed particles, as we have already explained in our previous paper [22]. It is, however, obvious that all the samples exhibited ductile behaviour, also at higher filler loadings.

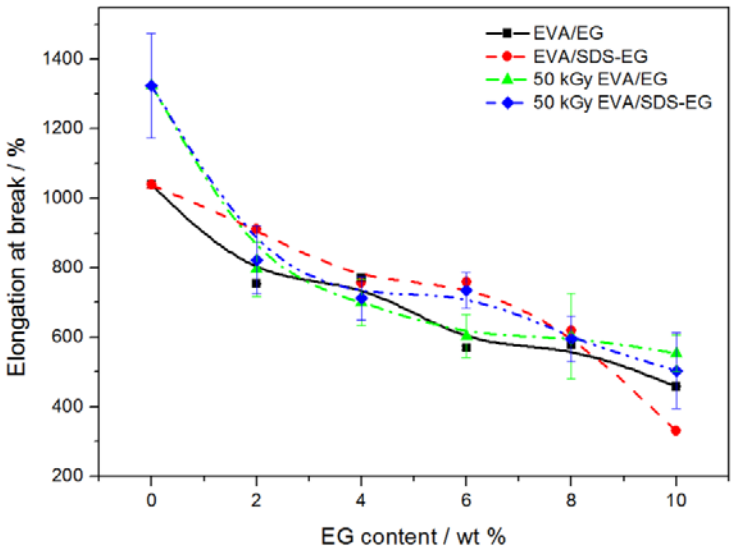

Figure 3.8 Variation of elongation at break of non-irradiated and irradiated EVA/EG and EVA/SDS-EG samples as a function of filler content

The tensile modulus of the composites generally increased with increasing filler content (Figure 3.9), which is to be expected because of the high modulus of the EG filler. Like the stress and elongation at break, the modulus of EVA increased after EB irradiation of the sample because of the radiation induced formation of a crosslinked network. As was observed in the stress at break results, the non-irradiated EVA/SDS-EG samples have modulus values very similar to those of the irradiated EVA-EG samples. The improved interaction and dispersion as a result of SDS treatment result in a similar improvement in composite stiffness than the crosslinking of the polymer matrix. It is further clear from Figure 3.9 that SDS treatment and EB irradiation has an additive effect on the improvement of the tensile modulus, with more than 100% increase in tensile modulus compared to the untreated EVA/EG composites.

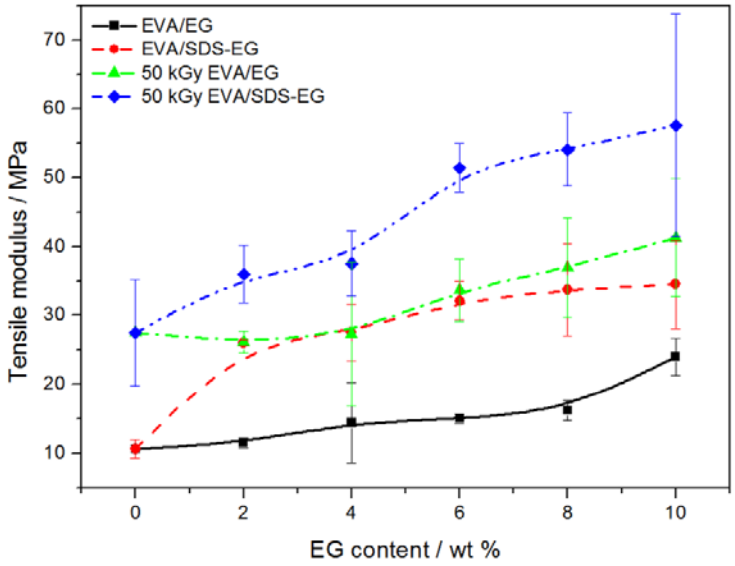

Figure 3.9 Variation of tensile modulus of non-irradiated and irradiated EVA/EG and EVA/SDS-EG samples as a function of filler content

3.5 Conclusions

The effect of the surfactant and radiation treatment on the thermal and mechanical properties, as well as electric and thermal conductivities, of EVA18/EG nanocomposites was investigated. The SDS treatment of EG clearly improved the interaction between EVA and EG and the dispersion of EG in the polymer matrix. EB irradiation initiated crosslinking formed a network in the amorphous part of EVA, and the gel content increased with increasing filler content in EVA. This increase was more significant for the SDS-EG containing samples. However, improved interaction between the filler and the polymer due to irradiation was not found. The improved dispersion of EG due to SDS treatment, the network formation due to EB irradiation, and the combination of these two effects significantly influenced the tensile properties of the composites, improving the modulus and the stress at break of the composites. The thermal properties showed little change as a result of EB irradiation, probably because irradiation mostly affected the amorphous parts of the polymer. The irradiation had very little effect on the electrical conductivities of the composites, while the thermal conductivities of the irradiated composites were generally slightly lower than those of the comparable non-irradiated composites.

3.6 References

1. R. Kochetov, A.V. Korobko, T. Andritsch, P.H.F. Morshuis, S.J. Picken. Modelling of the thermal conductivity in polymer nanocomposites and the impact of the interface between filler and matrix. Journal of Physics D: Applied Physics 2011; 44:1-12.
   DOI:10.1088/0022-3727/44/39/395401
2. R. Tlili, A. Boundenne, V. Cecen, L. Ibos, I. Krupa, Y. Candau. Thermophysical and electrical properties of nanocomposites based on ethylene-vinyl acetate copolymer (EVA) filled with expanded and unexpanded graphite. International Journal of Thermophysics 2010; 31: 936-948.
   DOI: 10.1007/s10765-010-0775-z
3. I.H Tavman, A. Turgut, H.M da Fonseca, H.R.B Orlande, R.M Cotta, M. Magalhaes. Thermal-diffusivity measurements of conductive composites based on EVA copolymer filled with expanded and unexpanded graphite. International Journal of Thermophysics 2013; 34:2297-2306.
   DOI: 10.1007/s10765-012-1231-z
4. G. Carotenuto, S. De Nicola, M. Palomba, D. Pullini, A. Horsewell, T.W. Hansen, L. Nicolais. Mechanical properties of low-density polyethylene filled by graphite nanoplatelets. Nanotechnology 2012; 23:1-8.
   DOI: 10.1088/0957-4484/23/48/485705
5. A. Yasmin, J.-J. Luo, I.M. Daniel. Processing of expanded graphite reinforced polymer nanocomposites. Composites Science and Technology 2006; 66:1179-1186.
   DOI: 10.1016/j.compscitech.2005.10.014
6. S. Bhattacharya, R.P. Tandon, V.K. Sachdev. Electrical conduction of graphite filled high density polyethylene composites; experiment and theory. Journal of Materials Science 2009; 44:2430-2433.
   DOI: 10.1007/s10853-009-3387-x
7. S. Konwer, S.K. Dolui. Synthesis and characterization of polypyrrole/graphite composites and study of their electrical and electrochemical properties. Materials Chemistry and Physics 2010; 124:738-743.
   DOI: 10.1016/j.matchemphys.2010.07.049

8. W.-G. Weng, G.-H. Chen, D.-J. Wu, W.-L. Yan. HDPE/expanded graphite electrically conducting composite. Composite Interfaces 2004; 11:131-143.
DOI: 10.1163/156855404322971404
9. F. Piana, J. Pionteck. Effect of the melt processing conditions on the conductive paths formation in thermoplastic polyurethane/expanded graphite (TPU/EG) composites. Composites Science and Technology 2013; 80:39-46.
DOI: 10.1016/j.compscitech.2013.03.002
10. R.K. Goyal, S.D. Samant, A.K. Thakar, A. Kadam. Electrical properties of polymer/expanded graphite nanocomposites with low percolation. Journal of Physics D: Applied Physics 2010; 43:1-7.
DOI: 10.1088/0022-3727/43/36/365404
11. S. Kim, I. Do, L.T. Drzal. Thermal stability and dynamic mechanical behaviour of exfoliated graphite nanoplatelets-LLDPE nanocomposites. Polymer Composites 2010; 31:755-761.
DOI: 10.1002/pc.20781
12. J.H. Lee, D.W. Shin, V.G. Makotchenko, A.S. Nararov, V.E. Fedorov, J.H. Yoo, S.M. Yu, J.-Y. Choi, J.M. Kim, J.-B. Yoo. The superior dispersion of easily soluble graphite. Small 2010; 6:58-62.
DOI: 10.1002/smll.200901556
13. S. Stankovich, D.A. Dikin, R.D. Piner, K.A. Kohlhaas, A. Kleinhammes, Y. Jia, Y. Wu, S.T. Nguyen, R.S. Ruoff. Synthesis of grapheme-based nanosheets via chemical reduction of exfoliated graphite oxide. Carbon 2007; 45:1558-1565.
DOI: 10.1016/j.carbon.2007.02.034
14. J. Jing, S. Chen, J. Zhang. Investigation of UV aging influences on the crystallization of ethylene vinyl acetate copolymer via successive self-nucleation and annealing treatment. Journal of Polymer Research 2010; 17:827-836.
DOI: 10.1007/s10965-009-9374-8
15. S. Chen, J. Zhang, J. Sun. Effect of damp-heat aging on the properties of ethylene-vinyl acetate copolymer and ethylene-acrylic acid copolymer blends. Journal of Applied Polymer Science 2009; 114:3110-3117.
DOI: 10.1002/app.30859

16. S.R. Kim, M. Poostforush, J.H. Kim, S.G. Lee. Thermal diffusivity of in-situ exfoliated graphite intercalated compound/polyamide and graphite/polyamide composites. eXPRESS Polymer Letters 2012; 6:476-484.
DOI: 10.3144/expresspolmlett.2012.50
17. T. Matsui, M. shimoda, Y. Osajima. Irradiated ethylene-vinyl acetate copolymer (EVA) film (II). Polymer International 1992; 29:91-95.
18. Ch. Hirschl, M. Biebl-Rydlo, M. DeBiasio, W. Mühleisen, L. Neumaier, W. Scherf, G. Oreski, G. Eder, B. Chernev, W. Schwab, M. Kraft. Determining the degree of crosslinking of ethylene vinyl acetate photovoltaic module encapsulants – A comparative study. Solar Energy Materials & Solar Cells 2013; 116:303-218.
http://dx.doi.org/10.1016/j.solmat.2013.04.022
19. M. Şen, M. Copuroğlu. A comparative study of gamma irradiation of poly(ethylene-co-vinyl acetate)/carbon black mixture. Materials Chemistry and Physics 2005; 93:154-158
DOI: 10.1016/j.matchemphys.2005.03.005
20. F. Khodkar, N.G. Ebrahimi. Effect of irradiation on mechanical and structural properties of ethylene vinyl acetate copolymers hollow fibers. Journal of Applied Polymer Science 2011; 119:2085-2092.
DOI: 10.1002/app.32926
21. H. Dorschner, U. Lappan, K. Lunkwitz, Electron beam facility in polymer research: Radiation induced functionalization of polytetrafluoroethylene. Nuclear Instruments and Methods in Physics Research B 1998, 139:495-501.
22. J.S Sefadi, A.S Luyt, J Pionteck. Effect of surfactant on EG dispersion in EVA and thermal and mechanical properties of the system. Journal of Applied Polymer Science 2014; 131: 41352
DOI: 10.1002/app.41352
23. K.A. Dubey, Y.K. Bhardwaj, C.V. Chaudhari, V. Kumar, N.K. Goel, S. Sabharwal. Radiation processed ethylene vinyl acetate-multiple walled carbon nanotube nanocomposites: Effect of MWNT addition on gel content and crosslinking density. eXPRESS Polymer Letters 2009; 3:492-500.
DOI: 10.3144/expresspolymlett.2009.61

24. T.Y. Hwang, S. Lee, P.-H. Kang, K.H. Park, Y. Ahn, J.W. Lee. The effect of electron beam irradiation on the dispersion and properties of poly(ethylene-co-vinyl acetate)/clay nanocomposites. Macromolecular Research 2011; 19:1151-1156.
DOI: 10.1007/s13233-011-1104-5
25. H. Osman, H. Ismail, M. Mariatti. Electron-beam irradiation of recycled newspaper filled polypropylene/natural rubber composites: Effect of crosslink promoters. ICCM-17 conference proceedings, Edinburgh, UK, 27-31 July 2009.
26. S. Dadbin, M. Frounchi, M. Haji-Saeid, F. Gangi. Molecular structure and physical properties of e-beam crosslinked low-density polyethylene for wire and cable insulation applications. Journal of Applied Polymer Science 2002; 86:1959-1969.
DOI: 10.1002/app.11111
27. S. Hassanpour, F. Khoylou, E. Jabbarzadeh. Thermal degradation of electron-beam crosslinked polyethylene and (ethylene-vinylacetate) blends in hot water. Journal of Applied Polymer Science 2003; 89:2346-2352.
DOI: 10.1002/app.12077
28. S. Dadbin, M. Frounchi, M. Sabet. Studies on the properties and structure of electron-beam crosslinked low-density polyethylene/poly(ethylene-co-(vinyl acetate)) blends. Polymer International 2005; 54:686-691.
DOI: 10.1002/pi.1750
29. T.Y. Hwang, S. Lee, P.-H. Kang, K.H. Park, Y. Ahn, J.W. Lee. The effect of electron beam irradiation on the dispersion and properties of poly(ethylene-co-vinyl acetate)/clay nanocomposites. Macromolecular Research 2011; 19:1151-1156.
DOI: 10.1007/s13233-011-1104-5

Chapter 4

Effect of surfactant and radiation treatment on the morphology and properties of PP/EG composites

This chapter will be submitted as a publication:
J S Sefadi, A S Luyt, J Pionteck, F Piana and U Gohs. Effect of surfactant and radiation treatment on the morphology and properties of PP/EG composites. Journal of Materials Science.

Abstract

The effects of surfactant and electron beam (EB) radiation treatment on the morphology and properties of polypropylene (PP)/expanded graphite (EG) composites were investigated. Surfactant treatment and sonication of EG before mixing with PP significantly influenced the morphologies of the composites, and the modification of EG with SDS had a strong negative influence on the electrical conductivities of these composites. The electrical percolation concentration is shifted from 5-6 wt.% filler to above 10 wt.% filler in the presence of SDS. The melting and crystallization temperatures of PP in the composites were not affected by surfactant or EB radiation treatment. There were small differences in PP crystallinity, depending on the type and combination of treatments. The filler particles acted as nucleating agents and the crystallization temperatures shifted to higher temperatures. The thermal stability of PP was significantly higher after irradiation, and improved even further for the samples containing EG, but the presence of EG had little influence on the thermal stabilities of the non-irradiated composites. For both non-irradiated and irradiated composites the maximum tensile stress and elongation at break values are lower than the neat matrix, while the tensile modulus increased significantly.

Keywords: Composites, expanded graphite, polypropylene, morphology, surfactant and radiation treatment

4.1 Introduction

Isotactic polypropylene (PP) is an important and excellent structural commodity to be used as a matrix in polymer composites because of its moderately low price, ease of processing, and excellent properties [1-3]. The physical and mechanical properties of semi-crystalline thermoplastic polymers depend on the degree of crystallinity [4] and on the orientation distribution of the crystalline segments. To improve the properties of PP, much emphasis has been put on the use of carbon nanotubes [5-9] in PP nanocomposites, but little work has been done on PP composites containing unmodified and surfactant modified EG, and no literature could be found on such composites exposed to electron beam radiation.

Graphite possesses a very high modulus along its plane, and has excellent electrical conductivity [10]. These useful properties, and its low cost compared to carbon nanotubes, make it a useful filler for conducting polymer composites for industrial applications. However, the key challenge is still the breaking down of the bundles of EG aggregates to achieve good dispersion in an attempt to optimize the composites' performance. For this reason, several techniques were used to fabricate nanocomposites with uniformly dispersed EG platelets in a PP matrix, such as high shear mixing, and the use of sonication and gamma or electron beam radiation treatments. Sonication is the most common approach, but severe sonication might reduce the lengths of the sheets. Non-covalent functionalization, such as the use of surfactants, has regularly been used to overcome filler entanglements as a result of Van der Waals forces [11-13]. Ion or electron beam irradiation of nanocomposites has been used to modify the morphology and properties of composites [14-17]. During treatment for medical applications, polyolefin matrix has been exposed to a sufficient amount of radiation to induce a significant change in mechanical properties [17].

Nanocomposites can be prepared by different methods such as melt compounding, solution intercalation and *in situ* polymerization [18-23]. The results of the study on the morphological and structural characterization of PP/conductive graphite nanocomposites [24] confirm the presence of some big agglomerates and the change in surface chemistry of the PP/EG composites due to the poor interaction and incompatibility between PP and EG. The study on PP nanocomposites based on non-sonicated and sonicated carbon nanotubes (CNTs) and exfoliated graphene nanoplatelets (xGnPs) [19] in the presence of isopropyl alcohol shows that the samples

prepared after sonication had a lower percolation threshold and higher flexural strength and modulus. In an investigation of maleated polypropylene nanocomposites reinforced with graphite oxide it was found that there was an intercalating effect from octadecylamine (ODA) surfactant where stacks of graphite sheets were partially exfoliated [25]. When investigating the influence of exfoliated graphite and clay platelets on PP it was found that the addition of exfoliated graphite nanoplatelets (xGnP) initiated the crystallization of PP at higher temperatures, confirming that xGnP acted as a nucleating agent [4], and that increasing clay content decreased the melting temperature of the nanocomposites compared to that of pure PP [26] because of the plasticizing effect of the organoclay. Melt mixing is the most industrially compatible and common method used to prepare polymer composites, even if the mixing conditions may have a strong influence on the final properties [27]. In polymer composites, electron beam radiation may induce chain scission and/or crosslinking [14-17], and may change the crystallinity or microstructure.

In the work reported in this paper, we prepared PP/EG composites, without modification and with SDS modification, through melt mixing. Samples from all the composites were exposed to electron beam radiation. The effects of surfactant and radiation on the microstructure and properties of the composites were investigated. The aim of this study was to obtain a better dispersion of EG particles in PP matrix and to improve the interaction between the two components.

4.2 Experimental

4.2.1 Materials

Polypropylene HKR102 was supplied in pellet form by Sasol Polymers, Johannesburg, South Africa. It is a low-flow polypropylene homopolymer. It is formulated with a high processing stabilization package and displays low water carry-over during the extrusion process. It has an MFI (230 °C / 2.16 kg) of 3.5 g/10 min (ASTM D1238-ISO 1133), T_m of 163 °C, Vicat softening point of 154 °C, and density of 0.905 g cm^{-3}. Expanded graphite (EG), SIGRAFLEX Expandat, was provided by the SGL Technologies GmbH, SGL Group. It has a conductivity of 40 S cm^{-1} (room temperature, 30 MPa, self-made 2-point conductivity tester, coupled with a DMM2000

Electrometer, Keithley Instruments), an apparent volume of ~400 cm^3 g^{-1}, and a specific surface area of 39.4 m^2 g^{-1} (77.4 K, N_2 atmosphere, Autosorb-1, Quantachrome). The sodium lauryl sulphate known as sodium dodecyl sulphate (SDS) was supplied by Sigma-Aldrich and was used without further treatment.

4.2.2 Composites preparation

4 g of SDS was dissolved in 5 L deionized water in a glass beaker, and 20 g of the EG was gradually added to the solution. 500 mL suspensions were sonicated for 30 min, filtered, washed with 100 mL distilled water to remove loosely absorbed SDS, and dried in a vacuum oven at 50 °C for 72 h. This modified EG (containing about 5 wt.% SDS), and the as received unmodified EG, were respectively mixed with PP through melt mixing using a Brabender Plastograph 55 mL internal mixer. The mixing was done for 20 min at 60 rpm and 176 °C. The samples were compression molded at 176 °C and 40 bar for 1 min into 1 mm thick sheets by using a LaboPress 200 T. Neat PP, as control sample, was given the same treatment.

The PP, PP/EG and PP/SDS-EG composites were packed in polypropylene bags filled with nitrogen and exposed to electron beam (EB) radiation at room temperature (25 ± 1 ºC). Irradiation was carried out by exposing both surfaces of the samples for uniformity. Details of the conditions and parameters employed during radiation are as follows: energy - 1.5 MeV; current - 4.00 mA; dose - 50 kGy; distance from sample - 20 cm; pulse repetition rate - 75 Hz; operation frequency - 1.2 kHz).

4.2.3 Methods

Scanning electron microscopy (SEM) analyses were carried out in a TESCAN VEGA3 Superscan scanning electron microscope (Brno, Czech Republic). The fracture surfaces of the samples were coated with gold by a Cressington Sputter Coater for 30 seconds. Microscope settings of 285.5 nm probe size, 50 mA probe current, 0.1 nm lateral resolution, and 30 kV AC voltage were used.

The molar mass of the PP in the different samples was determined by gel permeation chromatography (PL-GPC220 of Polymer Laboratories, RI-Detector) using two PL-MIXED-B-

LS columns. The polymer was dissolved in 1,2,4-trichlorobenzene at 150 °C and 1.0 mL min^{-1} flow rate, followed by filtration. The calibrations were done with polypropylene standards.

DSC analyses were carried out under nitrogen flow (20 mL min^{-1}) using a Perkin Elmer Pyris-1 differential scanning calorimeter (Waltham, Massachusetts, USA). The instrument was calibrated using the onset temperatures of melting of indium and zinc standards, as well as the melting enthalpy of indium. The sample masses were in the range of 5-10 mg, and they were heated from 25 to 180 °C at a heating rate of 10 °C min^{-1}. The cooling and second heating were performed under the same conditions. For all the samples, the onset and peak temperatures of melting and crystallization, as well as the melting enthalpies, were determined from the second heating scan. The normalised enthalpies of melting were determined according to Equations 4.1 and 4.2.

$$\Delta H_m^{Norm} = \frac{\Delta H_{m,PP}}{w_{PP}} \qquad (4.1)$$

where $\Delta H_{m,PP}$ is the experimentally observed melting enthalpy for the PP in the composite, and ΔH_m^{Norm} is the calculated normalised enthalpy of melting for the PP weight fraction w_{PP} in the nanocomposite. The degree of crystallinity χ_c was calculated according to

$$\chi_c = (\Delta H_m^{Norm}/\Delta H_m^o) \times 100\% \qquad (4.2)$$

where ΔH_m^o is the specific enthalpy of melting for 100% crystalline PP. A value of 209 J g^{-1} was used in the calculations [28-30].

The structures of PP and its nanocomposites filled with EG and SDS modified EG were determined through XRD. A D8 Advance diffractometer (BRUKER AXS, Germany) with PSD Vantec-1 detectors and Cu-K_α radiation (λ = 1.5406 Å), a tube voltage of 40 kV, a current of 40 mA and a V20 variable slit was used. The samples were scanned in locked coupled mode with 2θ ranging from 0 to 120° at 2θ increments of 0.5 sec $step^{-1}$.

The volume resistance measurements of PP and its composites before and after radiation were carried out on a Keithley Instruments 6157A electrometer, connected to an 8009 Keithley resistivity test fixture with two plate electrodes located on the two sides of the samples. This

method is appropriate for resistance values in the range from 10^7 to 10^{18} Ω at room temperature in accordance with ASTM D257-07. The corresponding conductivity values are in the range from 10^{-19} to 10^{-8} S cm^{-1}, but sensible results can be found in the range from 10^{-19} to 10^{-4} S cm^{-1}.

Thermogravimetric analysis (TGA) was done under flowing nitrogen (20 mL min^{-1}) using a Perkin Elmer TGA7 thermogravimetric analyser (Waltham, Massachusetts, USA). The samples, weighing ±20 mg each, were heated from 30 to 600 °C at a heating rate of 10 °C min^{-1}.

The tensile properties were investigated using a Hounsfield H5KS tensile tester at a cross-head speed of 10 mm min^{-1}. The specimens were dumbbell shaped (gauge length 10 mm, width 1.5 mm, thickness 1 mm). All the reported values from the stress-strain curves are averages of at least five measurements for each composition.

4.3 Results and discussion

4.3.1 Scanning electron microscopy (SEM)

Figure 4.1 shows the SEM micrographs of PP/EG and PP/SDS-EG composites with and without radiation treatment. It can be seen in Figure 4.1 that the dispersion of EG is inhomogeneous and the interfacial adhesion between the PP matrix and the EG sheets is weak, since big agglomerates or voids (Points A and B) are observed. The surfaces of these composites in the presence of EB irradiation seem to be slightly different, showing some cracks or detachments between the PP and the graphite sheets (Points B and D). The SDS-EG particles were fairly well dispersed in the polymer, but some areas show long agglomerated particles (Figure 4.1d) indicating that the SDS treatment and sonication did not completely break up the agglomerates. Therefore, the interparticle attraction was not completely eliminated, although it seems to have been sufficiently reduced to obtain better dispersed EG particles in the PP matrix. It was not expected that the electron beam irradiation would affect the morphology or fracture surface of the samples, since the polymer did not melt during irradiation and therefore there could not have been any re-dispersion of the EG.

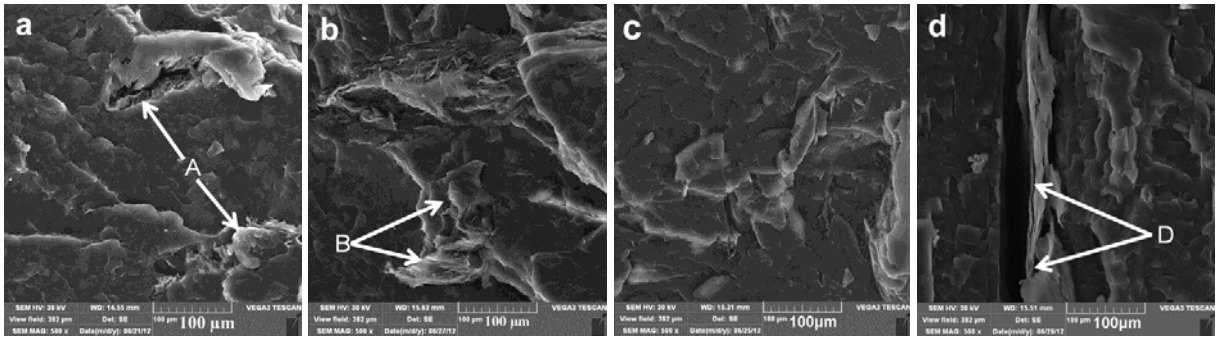

Figure 4.1 SEM micrographs of PP/expanded graphite composites: (a) 98/2 w/w PP/EG; (b) 50 kGy 98/2 w/w PP/EG; (c) 98/2 w/w PP/SDS-EG; (d) 50 kGy 98/2 w/w PP/SDS-EG

4.3.2 Influence of filler and radiation treatment on polymer molar mass

The number weight average molar masses, as well as the dispersity indices, of pure PP and the PP/EG and PP/SDS-EG composites with and without radiation treatment were determined through gel permeation chromatography (GPC), and the results are summarized in Tables 4.1 and 4.2. The molar mass of PP in the irradiated PP/EG and PP/SDS-EG composites was lower than that of PP in the non-irradiated composites. This confirms the degradation effect of the irradiation on the PP, and it seems as if the presence of EG and SDS-EG particles did not inhibit this effect. There was an increase in number-average molar mass with increasing EG content for the irradiated samples (Table 4.2), which indicates the formation of a low level of radiation-induced crosslinks. This was not observed for neat PP, probably because the EG particles assisted in effectively distributing the thermal energy from the radiation. The SDS-EG samples did not show the same increase in molar mass, probably because SDS formed an isolating layer around the EG particles and prevented their effective conduction of thermal energy. The presence of SDS had a similar effect on the electrical conductivity, as can be seen from results discussed later on in this paper. There was a visible colour change in the solvent, and the EG particles were clearly visible. There was no gel after the Soxhlet extraction, confirming that the formation of crosslinked material is a minor process during irradiation.

Table 4.1 Number average and weight average molar masses of the non-irradiated samples

Sample composition	M_n / g mol^{-1}	M_w / g mol^{-1}	DI (M_w/M_n)
PP	41400 ± 140	251500 ± 1410	6.1 ± 0.0
98/2 w/w PP/EG	42000 ± 990	257650 ± 210	6.1 ± 0.1
90/10 w/w PP/EG	35950 ± 1340	173900 ± 570	4.8 ± 0.2
98/2 w/w PP/SDS-EG	42200 ± 1700	257800 ± 4100	6.1 ± 0.4
90/10 w/w PP/SDS-EG	46200 ± 1840	269300 ± 140	5.8 ± 0.2

M_n - number average molar mass; M_w - weight average molar mass; DI - dispersity index

Table 4.2 Number average and weight average molar masses of the irradiated samples

Sample composition	M_n / g mol^{-1}	M_w / g mol^{-1}	DI (M_w/M_n)
PP	33600 ± 0	255900 ± 850	7.6 ± 0.0
98/2 w/w PP/EG	35500 ± 1270	181950 ± 350	5.1 ± 0.2
90/10 w/w PP/EG	43450 ± 500	269300 ± 2550	6.2 ± 0.0
98/2 w/w PP/SDS-EG	35600 ± 280	173200 ± 2830	4.9 ± 0.1
90/10 w/w PP/SDS-EG	34750 ± 640	166950 ± 780	4.8 ± 0.1

M_n - number average molar mass; M_w - weight average molar mass; DI - dispersity index

4.3.3 Differential scanning calorimetry (DSC)

The DSC cooling curves of all the investigated samples are shown in Figures 4.2 and 4.3. The crystallization temperature of PP in all the composites is about 10 °C higher than that of neat PP (Figure 4.2). The expanded graphite clearly acted as a nucleating agent for the crystallization of PP. The crystallization temperatures for the samples containing SDS-EG were the same as those of the EG containing samples within experimental error. From these results alone it seems as if the SDS modification did not significantly change the nucleation effect of the EG platelets, probably because they were not small enough and well enough dispersed despite the SDS and sonication treatment. However, the crystallinity values for the SDS-EG containing samples given in Tables 4.3 and 4.4 show that SDS treatment of EG did cause them to induce higher PP crystallinities. Although the molar masses of the irradiated samples mostly were lower than those

of the non-irradiated samples, this decrease was not significant in influencing the melting temperature (Table 4.4).

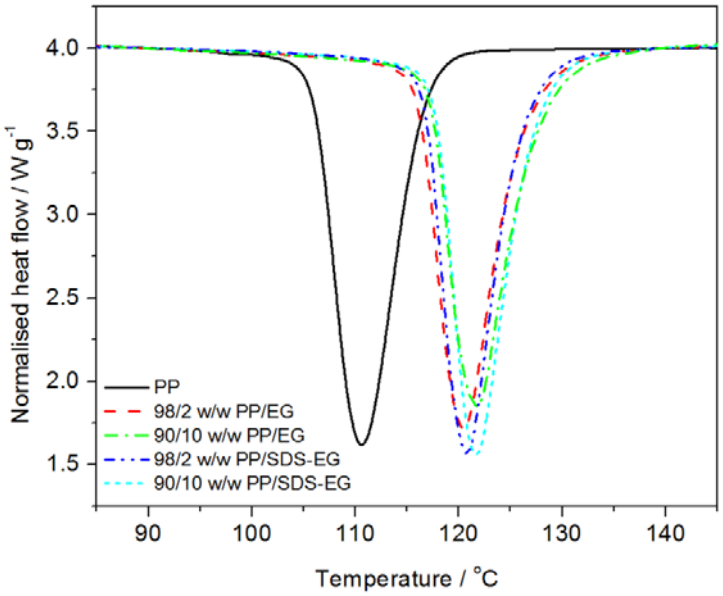

Figure 4.2 DSC cooling curves of non-irradiated PP and its non-irradiated composites

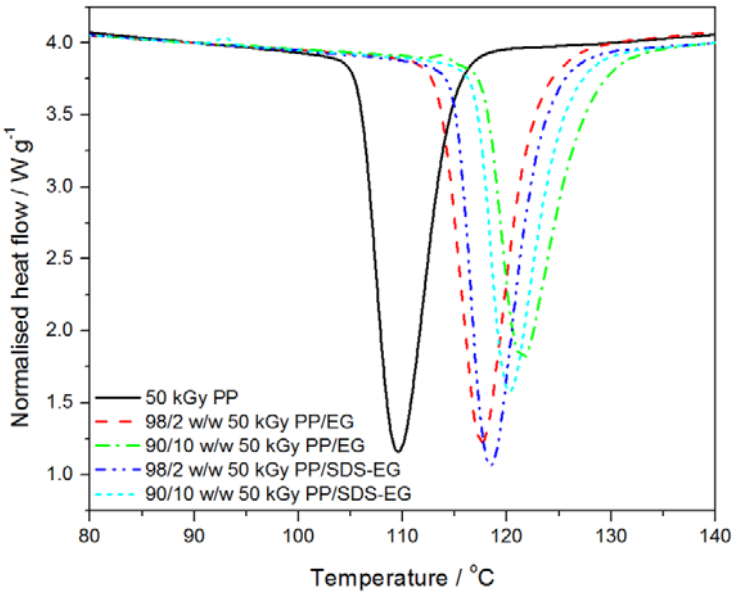

Figure 4.3 DSC cooling curves of irradiated PP and its irradiated composites

Table 4.3 Melting and crystallization temperatures, melting enthalpies and degrees of crystallinity of non-irradiated samples from the first heating and cooling DSC curves

wt.% EG	T_m / °C	T_c / °C	ΔH_m / J g^{-1}	ΔH_m^{Norm} / J g^{-1}	χ_c / %
			Untreated EG		
0	164.0 ± 0.4	110.0 ± 0.1	63.9 ± 5.2	63.9	30.6
2	162.1 ± 0.3	119.9 ± 0.0	71.2 ± 3.6	72.7	34.8
4	162.8 ± 0.3	119.9 ± 0.4	69.7 ± 0.3	72.6	34.7
6	162.8 ± 0.3	119.9 ± 0.2	70.5 ± 1.7	75.0	35.9
8	162.4 ± 0.2	120.9 ± 0.3	67.0 ± 3.1	72.8	34.8
10	160.4 ± 1.8	121.9 ± 0.6	62.4 ± 0.2	69.3	33.2
			SDS treated EG		
2	162.9 ± 0.2	120.9 ± 0.8	77.1 ± 7.0	78.7	37.7
4	162.9 ± 0.5	120.9 ± 0.3	77.3 ± 3.2	80.5	38.5
6	162.4 ± 0.3	121.9 ± 0.0	70.6 ± 0.9	75.1	35.9
8	162.0 ± 0.1	120.9 ± 0.1	71.7 ± 1.8	77.9	37.3
10	162.0 ± 0.2	121.9 ± 0.6	71.3 ± 4.4	79.2	37.9

T_m - melting temperature; T_c - crystallization temperature; ΔH_m - melting enthalpy; ΔH_m^{Norm} - normalised melting enthalpy; χ_c - percentage of crystallinity

Table 4.4 Melting and crystallization temperatures, melting enthalpies and degrees of crystallinity of irradiated samples from the first heating and cooling DSC curves

wt.% EG	T_m / °C	T_c / °C	ΔH_m / J g^{-1}	ΔH_m^{Norm} / J g^{-1}	χ_c / %
			Untreated EG		
0	162.2 ± 3.2	110.0 ± 0.2	72.2 ± 2.1	72.2	34.5
2	161.4 ± 2.1	117.9 ± 0.1	72.8 ± 4.7	74.3	35.6
4	161.0 ± 0.4	119.9 ± 0.0	68.7 ± 1.1	71.6	34.3
6	160.8 ± 0.5	119.9 ± 0.2	68.2 ± 3.2	72.6	34.7
8	160.5 ± 0.2	119.9 ± 0.3	62.4 ± 0.6	67.8	32.4
10	157.0 ± 0.6	120.9 ± 0.3	65.2 ± 6.9	72.4	34.6
			SDS treated EG		
2	161.2 ± 0.2	118.9 ± 0.2	70.7 ± 4.5	72.1	34.5
4	157.6 ± 1.2	119.9 ± 0.1	69.8 ± 3.1	72.7	34.8
6	156.9 ± 0.1	119.9 ± 0.2	72.0 ± 2.4	75.1	35.9
8	156.6 ± 0.3	119.9 ± 0.2	71.8 ± 3.3	78.0	37.3
10	160.9 ± 0.2	119.9 ± 0.3	70.6 ± 5.4	78.4	37.5

T_m - melting temperature; T_c - crystallization temperature; ΔH_m - melting enthalpy; ΔH_m^{Norm} – normalised melting; χ_c - percentage of crystallinity

4.3.4 X-ray diffraction (XRD)

The XRD spectra of neat and irradiated PP, with the corresponding crystallographic planes indicated, are shown in Figure 4.4. It is clear that both the neat and irradiated PP contains mostly α- or monoclinic crystals, as can be seen from the data in Table 4.5. There are, however, also some β- or hexagonal crystals as can be observed from the peaks at 2θ = 16.10° and 21.14°. These β-hexagonal crystal forms are attributed to many factors including (i) the presence of shearing forces during mixing, (ii) β-nucleating agents, and (iii) temperature gradients. In this study the presence of shear forces during mixing seems to be the most probable factor which induced some β-crystals in the polymer melt. The β-peak at about 2θ = 16.10^{o} is much more intense for the irradiated PP than the non-irradiated PP. The relative β-crystal content can be calculated by using Equation 4.3 [31]

$$k_{\beta} = \frac{I_{\beta}(300)}{\left[I_{\alpha}(110) + I_{\alpha}(040) + I_{\alpha}(130) + I_{\beta}(300)\right]} \times 100\% \qquad (4.3)$$

where $I_{\alpha}(110)$, $I_{\alpha}(040)$, $I_{\alpha}(130)$ and $I_{\beta}(300)$ are the diffraction peak intensities of the (110), (040), (130) crystal planes of the α-crystals and the (300) crystal plane of the β-crystals. The relative β-crystal content has been calculated as 15.4% for the non-irradiated PP and 30.6% for the irradiated PP. According to a computer simulation study of the crystal structures of the α- and β-forms of isotactic polypropylene [31], the α-form has alternating rows of right-handed and left-handed helices arranged into a monoclinic crystal structure. This is a meta-stable state which will not readily change into the hexagonal β-form, in which the chains form chiral domains surrounded by boundaries parallel to the (110) and (100) planes. However, it seems as if chain scission induced by EB irradiation created an environment in which the (shorter) chains could more readily rearrange into a hexagonal meta-stable crystal state, probably because of transformations due to localized melting during irradiation.

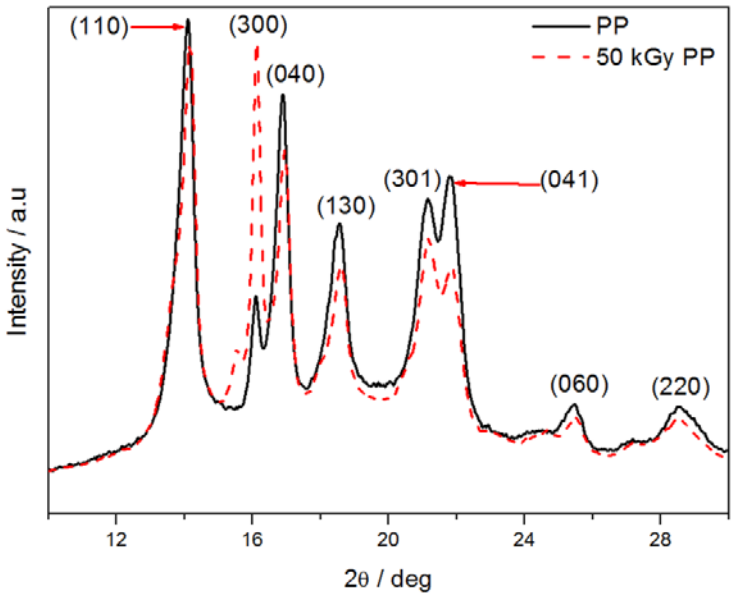

Figure 4.4 XRD spectra of neat PP and irradiated PP

Table 4.5 Typical XRD peaks and intensities of neat PP with corresponding crystallographic planes

2θ	α-form	β-form	Peak intensities for non-irradiated PP	Peak intensities for irradiated PP
14.1	(110)	-	2.0×10^4	1.9×10^4
16.1	-	(300)	8.7×10^3	1.9×10^4
16.9	(040)	-	1.7×10^4	1.4×10^4
18.6	(130)	-	1.1×10^4	9.8×10^3
21.1	-	(301)	1.2×10^4	1.1×10^4
21.9	(041)	-	1.3×10^4	9.7×10^3
25.4	(060)	-	4.3×10^3	3.8×10^3
28.5	(220)	-	4.3×10^3	3.8×10^3

Figure 4.5 shows the XRD spectra of PP and its non-irradiated and irradiated composites filled with EG and SDS-EG. The peaks at $2\theta = 16.1^o$ and 21.1^o become weaker and eventually disappear with the introduction of EG and SDS-EG. This implies that the presence of EG and SDS-EG promoted the formation of α-crystals in PP, with a clear reduction in the amount of β-

crystals. It is, however, interesting that there was formation of some β-crystals during EB irradiation, as can be seen in the re-appearance of the (300) peak at 16.1° for the irradiated samples. The EG and SDS-EG particles clearly inhibit β-crystallization of PP because of the interaction between PP and EG or SDS-EG which reduces the PP-PP interaction responsible for β-crystal formation. The peak at 2θ = 26.6º is clearly related to the EG in the sample. This peak matches the crystallographic (002) plane of expanded graphite (Joint Committee on Powder Diffractions Standards JCPDS database of the International Centre for Diffraction (JCPDS 01-0646, www.icdd.com)). There are, however, significant differences in peak intensity of the EG diffraction peak at 26.6° as a result of SDS modification and electron beam irradiation, but no significant change in the peak position. This is because SDS treatment reduced the EG agglomeration, and improved the crystal perfection. It is also possible that the EB irradiation to some extent separated the EG, maybe through degradation of the polymer and penetration of the shorter chain segments into the EG agglomerates through some localized melting, which should also contribute to making the EG crystal structure more evident.

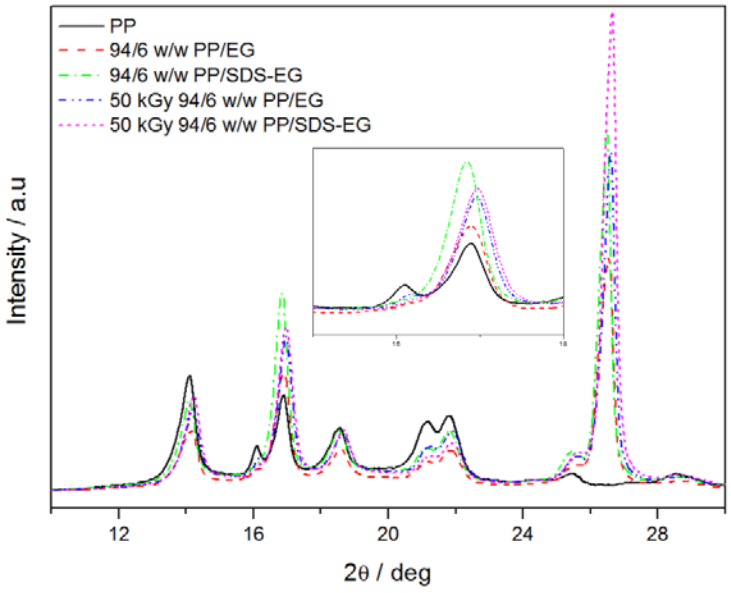

Figure 4.5 XRD spectra of the non-irradiated and irradiated PP/EG and PP/SDS-EG composites

4.3.5 Electrical conductivity

The electrical conductivity of PP is 3.5×10^{-18} S cm^{-1}, confirming that it is an insulator. The non-irradiated and irradiated PP/EG composites exhibit a sharp transition from insulator to conductor with an electrical percolation threshold of ca. 6 and 4 wt.% respectively. The difference in the percolation threshold can be attributed to defects or degradation products induced by the radiation, which created more conductive networks. The electrical conductivity values are about the same for the non-irradiated and irradiated PP/EG composites below and above the percolation threshold. In the SDS-EG containing samples there was little increase in electrical conductivity with increasing filler content, without reaching the percolation concentration up to the filler levels investigated in this project. Possible reasons for this observation are that (i) the presence of SDS separates the EG platelets so effectively that percolation pathways will only be formed at much higher SDS-EG contents, and (ii) the SDS forms an isolating layer around the EG platelets which reduces their effective electrical conductivity.

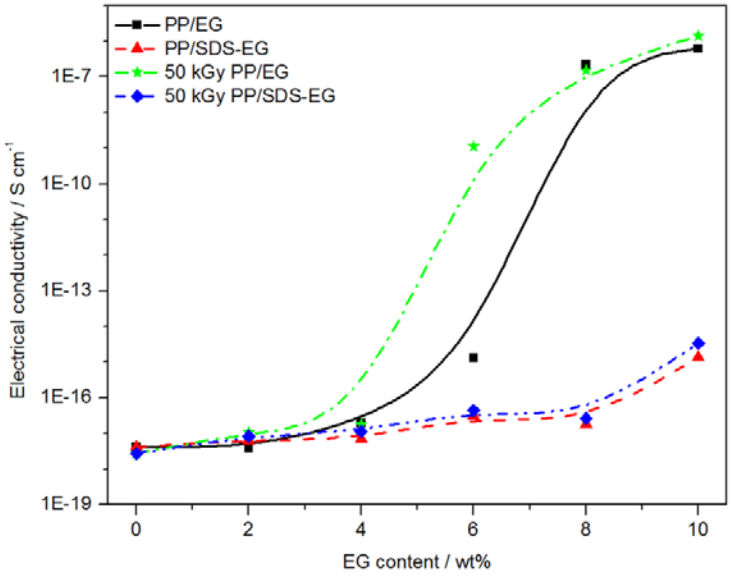

Figure 4.6 Electrical conductivities of all the investigated samples

4.3.6 Thermogravimetric analysis (TGA)

The TGA curves in Figure 4.7 show a single degradation step for PP in all the samples. There is almost no difference between the temperature at 50% mass loss for the non-irradiated samples

containing up to 6 wt.% EG, but this temperature increased quite significantly for the samples with higher EG contents (Table 4.6). There are two possible reasons for this observation: (1) The EG absorbs most of the thermal energy, so that enough energy to initiate degradation is only available at higher temperatures, and/or (2) the more agglomerated EG more effectively interacts with the volatile degradation products, which retards their diffusion out of the sample and gives rise to an observed mass loss only at higher temperatures. The temperatures at 50% mass loss for the irradiated samples in Table 4.6 are very scattered and show no trend with increasing EG and SDS-EG contents. This temperature is much higher for the irradiated PP than for the non-irradiated PP. The irradiation is expected to cause a fair amount of branching or weak crosslinking, and more bonds have to be broken to form volatile degradation products.

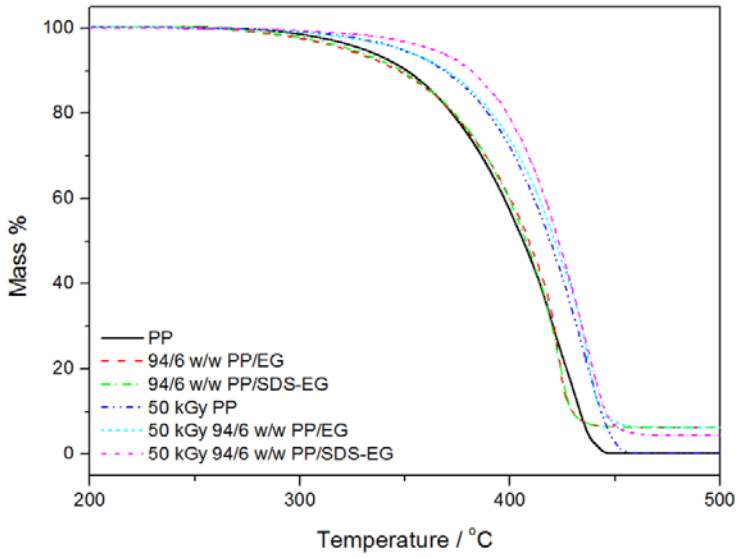

Figure 4.7 TGA curves of the non-irradiated and irradiated samples

Table 4.6 summarizes the degradation temperatures at the 50% mass loss rate of the investigated samples. The PP seems to be more thermally stable after irradiation, and its stability further increases when EG is present in the case of the irradiated samples, but not in the case of non-irradiated samples. The scattered results for the irradiated EG and SDS-EG containing samples could be as a result of crosslinking and degradation taking place in these samples during EB irradiation. These processes probably depend upon the EG particle sizes and dispersion, which may not be consistent from one sample to the other, and therefore the degradation and

mass loss processes do not occur in a consistent manner. There was no residue after the thermal degradation of non-irradiated and irradiated PP. The results in Table 4.6 show that there are generally very good correlations between the % residue and the amount of EG used to prepare the PP/EG samples. However, the values are generally lower for the PP/SDS-EG samples, with the exception of the irradiated sample containing 10 wt.% SDS-EG, because the SDS also degrades/evaporates at temperatures below 500 °C [32].

Table 4.6 Degradation temperatures of all the investigated samples

wt.% EG	$T_{50\%}$ / °C	wt.% residue	$T_{50\%}$ / °C	wt.% residue
	Non-irradiated samples		**Irradiated samples**	
		Untreated EG		
PP	406.8	0	419.0	0
2	406.9	1.3	415.3	1.9
4	407.5	3.6	428.9	3.9
6	408.8	5.4	421.4	5.7
8	422.9	7.4	425.5	7.2
10	427.9	9.6	388.8	7.5
		SDS treated EG		
PP	406.8	0	419.0	0
2	405.7	1.5	407.5	1.0
4	407.1	3.6	415.6	3.2
6	407.4	4.0	423.3	3.8
8	417.3	4.4	416.7	5.7
10	425.7	5.8	410.2	9.9

$T_{50\%}$ is the temperature at 50 % mass loss rate

4.3.7 Tensile properties

The pure PP shows typical ductile deformation behaviour with a clear yield point followed by strain softening. The presence of 6 wt.% filler leads to quasi-brittle fracture during neck formation in the non-irradiated composites, while true brittle fracture was observed for the

irradiated PP and its composites (Figure 4.8) because of crosslinking and chain scission induced by the irradiation.

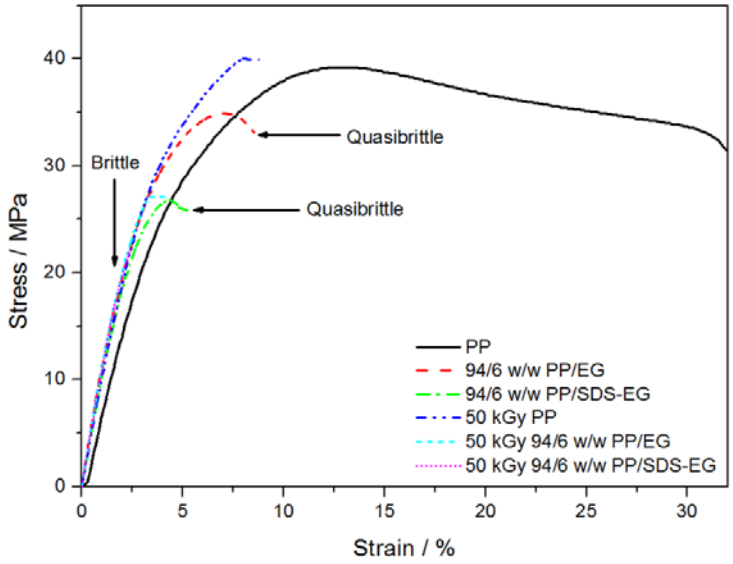

Figure 4.8 Stress-strain curves of some selected samples

The tensile properties of all the investigated samples are summarized in Tables 4.7 and 4.8. The maximum tensile stress of the PP/EG composites generally decreased with increasing EG content. This is the result of poor wettability of the graphite by the PP and poor interfacial adhesion, which reduced the effective stress transfer across the matrix-filler interface. The EG particles then form stress-concentration points at which cracks are initiated leading to stress or catastrophic failure. Although there is a slight improvement in the dispersion of SDS-EG in the PP, the maximum stress values are generally lower than those of the non-irradiated PP/EG composites. This is probably because of the smooth SDS layer around the EG platelets, which reduced the interaction with the PP chains and caused crack formation and propagation to be more effective. EB irradiation did not significantly change the maximum stress values, probably because it gave rise to crosslinking and degradation, and these two effects balanced out each other to such an extent that the irradiated samples show maximum stress values similar to those of the comparable non-irradiated samples.

Table 4.7 Tensile properties of the non-irradiated samples

	Untreated EG			SDS treated EG		
Sample	**$\sigma_m \pm s\sigma_m$ / MPa**	**$\varepsilon_b \pm s\varepsilon_b$ / %**	**E ± sE / MPa**	**$\sigma_m \pm s\sigma_m$ / MPa**	**$\varepsilon_b \pm s\varepsilon_b$ / %**	**E ± sE / MPa**
PP	38.1 ± 0.8	26.4 ± 6.0	52.5 ± 3.5	38.1 ± 0.8	26.4 ± 6.0	52.5 ± 3.5
PP + 2% EG	32.8 ± 0.4	9.2 ± 1.2	261 ± 1	30.7 ± 5.0	9.9 ± 3.7	280 ± 3
PP + 4% EG	31.2 ± 1.9	6.0 ± 0.04	359 ± 2	27.8 ± 8.1	7.5 ± 1.7	260 ± 1
PP + 6% EG	30.4 ± 4.6	6.5 ± 2.8	420 ± 1	23.9 ± 2.2	4.4 ± 0.3	275 ± 1
PP + 8% EG	25.9 ± 1.5	4.2 ± 0.7	500 ± 1	22.8 ± 7.5	4.9 ± 0.1	340 ± 0
PP + 10% EG	22.1 ±10.5	3.9 ± 0.9	560 ± 2	22.1 ± 3.0	5.3 ± 0.4	380 ± 0

σ_m = maximum stress; ε_b = elongation at break; E = tensile modulus and s = standard deviation

Table 4.8 Tensile properties of the irradiated samples

	Untreated EG			SDS treated EG		
Sample	**$\sigma_m \pm s\sigma_m$ / MPa**	**$\varepsilon_b \pm s\varepsilon_b$ / %**	**E ± sE / MPa**	**$\sigma_m \pm s\sigma_m$ / MPa**	**$\varepsilon_b \pm s\varepsilon_b$ / %**	**E ± sE / MPa**
PP	38.7 ± 3.1	9.3 ± 1.9	58.6 ± 7.1	38.7 ± 3.1	9.3 ± 1.9	58.6 ± 7.1
PP + 2% EG	30.1 ± 2.3	2.8 ± 0.4	338 ± 4	28.3 ± 6.2	5.5 ± 0.2	317 ± 3
PP + 4% EG	26.0 ± 0.8	4.2 ± 0.8	366 ± 1	25.9 ± 2.5	5.6 ± 0.6	293 ± 1
PP + 6% EG	26.5 ± 1.0	3.4 ± 1.0	440 ± 1	23.1 ± 1.7	3.0 ± 0.4	444 ± 1
PP + 8% EG	29.1 ± 1.4	3.6 ± 0.5	536 ± 6	21.9 ± 7.1	2.3 ± 0.5	457 ± 5
PP + 10% EG	24.2 ± 0.5	3.3 ± 0.9	603 ± 4	20.2 ± 8.0	3.3 ± 1.4	478 ± 3

σ_m = maximum stress; ε_b = elongation at break; E = tensile modulus and s = standard deviation

The elongation at break decreased significantly with an increase in both EG and SDS-EG contents in the case of the non-irradiated composites. The same explanation used in the previous paragraph is also relevant here. The elongation at break of the irradiated PP/EG and PP/SDS-EG composites are lower than those of the irradiated PP, but the values did not really decrease further with increasing filler content. The lower values are the result of stress concentration at the filler particles, but since the values are already very low, the amount of filler had little influence on these values. When comparing the values in Tables 4.7 and 4.8 it can be seen that the non-

irradiated PP showed significantly higher elongation at break than the irradiated PP. Irradiation initiates both crosslinking and degradation – crosslinking causes a reduction in chain mobility while degradation reduces the number of chain entanglements, both of which will give rise to lower elongation at break values.

The tensile modulus of the non-irradiated composites increased significantly with increasing filler content for both the EG and SDS-EG containing samples. A 970% increase in tensile modulus was observed for the EG-based composites, while the increase was 620% in the case of the SDS-EG based samples. This is the result of the inherent stiffness of the EG platelets, and the interaction between PP and EG which restricted the PP segmental mobility. It is well known that stiff inorganic fillers can significantly increase the modulus of polymer composites [33,34]. The SDS-EG containing samples have lower modulus values than the corresponding EG composites. The reason for this is the smooth SDS layer around the EG platelets, which reduced the interaction between EG and the PP chains, increasing their mobility. The tensile moduli of the irradiated PP/EG and PP/SDS-EG composites are generally higher than those of the comparable non-irradiated PP samples. This is an indication that EB irradiation must have induced crosslinking which will reduce the PP chain mobility and cause the composites to become stiffer.

4.4 Conclusions

The influence of anionic surfactant and EB irradiation treatment on the morphology and properties of PP/EG nanocomposites was investigated in this study. The dispersion of EG was not uniform and the interfacial adhesion between the PP matrix and the EG sheets was poor giving rise to big agglomerates. SDS treatment combined with sonication reduced the interparticle attraction and improved the dispersion of the EG particles in the polymer matrix. There were not any observable changes in the morphologies after EB irradiation. The molecular weights of the irradiated samples were generally lower than those of the non-irradiated samples, confirming that chain scission *inter alia* occurred as a result of irradiation. The presence of EG and SDS-EG in PP did not change the melting temperature of PP, but the filler particles acted as nucleating agents and the crystallization temperatures shift to higher temperatures. This effect was more significant for the samples containing SDS-EG because of the better dispersion of

these particles. The presence of EB irradiation had little influence on the melting temperatures. Pure PP contained both α- and β-crystals, the presence of EG and SDS-EG particles inhibited β-nucleation of the PP. Both non-irradiated and irradiated PP/EG composites without SDS treatment exhibited a sharp transition from insulator to conductor, with a significant lowering of the percolation threshold for the irradiated samples. Both non-irradiated and irradiated PP/SDS-EG showed little increase in electrical conductivity over the investigated EG content range, which was attributed to the SDS forming an isolation layer around the EG particles. The degradation temperatures at 50% mass loss did not significantly change up to 6 wt.% EG content for the non-irradiated samples containing EG and SDS-EG, but they significantly increased for the samples with higher filler contents. No trend could be observed for the irradiated samples, probably because of an inconsistent combination of crosslinking and degradation as a result of the irradiation. Both the addition of filler and irradiation gave rise to brittle samples. Increasing filler content generally gave rise to reduced tensile strength values, while irradiation did not significantly change these values. The tensile modulus values generally increased with increasing filler content, as a result of the higher modulus of the filler particles, and with irradiation, probably as a result of crosslinking.

4.5 References

1. K. Kalaitzidou, H. Fukushima, L.T. Drzal. Mechanical properties and morphological characterization of exfoliated graphite-polypropylene nanocomposites. Composites: Part A 2007; 38:1675-1682.
   DOI: 10.1016/j.compositesa.2007.02.003
2. M. Ranjbar, A. Arefazar, G. Bakhshandeh. Constituting balance between strength and toughness in nanocomposites based on PP/SEBS-g-MA blends. Journal of Thermoplastic Composite Materials 2013; 2:1-8.
   DOI: 10.1177/0892705712475001
3. K. Prashantha, M.F. Lacrampe, P. Krawczak. Processing and characterization of halloysite nanotubes filled polypropylene nanocomposites based on a masterbatch route: Effect of halloysites treatment on structural and mechanical properties. eXPRESS Polymer Letters 2011; 5:295-307

DOI: 10.3144/expresspolymlett.2011.30

4. K. Kalaitzidou, H. Fukushima. P. Askeland, L.T. Drzal. The nucleating effect of exfoliated graphite nanoplatelets and their influence on the crystal structure and electrical conductivity of polypropylene nanocomposites. Journal of Materials Science 2008; 43:2895-2907.
   DOI: 10.1007/s10853-007-1876-3
5. K. Prashantha, J. Soulestin, M. F. Lacrampe, M. Claes, G. Dupin, P. Krawczak. Multi-walled carbon nanotube filled polypropylene nanocomposites based on masterbatch route: Improvement of dispersion and mechanical properties through PP-g-MA addition. eXPRESS Polymer Letters 2008; 2:735-745.
   DOI: 10.3144/expresspolymlett.2008.87
6. T. Kashiwagi, E. Grulke, J. Hilding, K. Groth, R. Harris, K. Butler, J. Shields, S. Kharchenko, J. Douglas. Thermal and flammability properties of polypropylene/carbon nanotube nanocomposites. Polymer 2004; 45:4227-4239.
   DOI: 10.1016/j.polymer.2004.03.088
7. D. Bikiaris. Microstructure and properties of polypropylene/carbon nanotube nanocomposites. Materials 2010; 3:2884-2946.
   DOI: 10.3390/ma3042884
8. A. Huegun, M. Fernández, M.E. Muñoz, A. Santamaría. Rheological properties and electrical conductivity of irradiated MWCNT/PP nanocomposites. Composites Science and Technology 2012; 72:1602-1607.
   DOI: 10.1016/j.compscitech.2012.06.011
9. J. Ma, H. Deng, T. Peijs. Processing of poly(propylene)/carbon nanotubes composites using $scCO_2$-assisted mixing. Macromolecular Materials and Engineering 2010; 295:566-574.
   DOI: 10.1002/mame.200900405
10. I.M. Afanasov, D.V. Savchenko, S.G. Ionov, D.A. Rusakov, A.N. Seleznev, V.V. Avdeev. Thermal conductivity and mechanical properties of expanded graphite. Inorganic Materials 2009; 45:486-490.
    DOI: 10.1134/S0020168509050057

11. D. Ramimoghadam, M.Z.B. Hussein, Y.H. Taufiq-Yap. The effect of sodium dodecyl sulfate (SDS) and cetyltrimethylammonium bromide (CTAB) on the properties of ZnO synthesized by hydrothermal method. International Journal of Molecular Sciences 2012; 13:1327-13293.
DOI: 10.3390/ijms131013275
12. N. Güngör, A. Alemdar, O. Atici, I.O. Ece. The effect of SDS surfactant on the flow and zeta potential of bentonite suspensions. Materials Letters 2001; 51:250-254.
DOI: S0167-577X(01)00299-3
13. M.C. Costache, M. Heidecker, E. Manias, R. Gupta, C. Wilkie. Benzimidazolium surfactants for modification of clays for use with styrenic polymers. Polymer Degradation and Stability 2007; 92:1-23.
DOI: 10.1016/j.polymdegradstab.2007.08.001
14. K.-Y. Lee, K.-Y. Kim. ^{60}Co γ-ray irradiation effect and degradation behaviours of a carbon nanotubes and poly(ethylene-co-vinyl acetate) nanocomposites. Polymer Degradation and Stability 2008; 93:1290-1299.
DOI: 10.1016/j.polymdegrastab.2008.04.007
15. M.J. Martínez-Morlanes, P. Castell, P.J. Alonso, M.T. Martinez, J.A. Puértolas. Multi-walled carbon nanotubes acting as free radical scavengers in gamma-irradiated ultrahigh molecular weight polyethylene composites. Carbon 2012; 50:2442-2452.
DOI: 10.1016/j.carbon.2012.01.066
16. T.Y. Hwang, S. Lee, P.-H. Kang, K.H. Park, Y. Ahn, J.W. Lee. The effect of electron beam irradiation on the dispersion and properties of poly(ethylene-co-vinyl acetate)/clay nanocomposites. Macromolecular Research 2011; 19:1151-1156.
DOI: 10.1007/s13233-011-1104-5
17. F. Khodkar, N.G. Ebrahimi. Effect of irradiation on mechanical and structural properties of ethylene vinyl acetate copolymers hollow fibres. Journal of Applied Polymer Science 2011; 119:2085-2092.
DOI: 10.1002/app.32926
18. K. Kalaitzidon, H. Fukushima, L.T. Drzal. A new compounding method for exfoliated graphite-polypropylene nanocomposites with enhanced flexural properties lower percolation threshold. Composites Science and Technology 2007; 67:2045-2051.

DOI: 10.1016/j.compscitech.2006.11.014

19. K. Kalaitzidon, H. Fukushima, L.T. Drzal. A new compounding method for exfoliated graphite-polypropylene nanocomposites with enhanced flexural properties lower percolation threshold. Composites Science and Technology 2007; 67:2045-2051.
DOI: 10.1016/j.compscitech.2006.11.014
20. H. Quan, B.-Q. Zhang, Q. Zhao, R.K.K. Yuen, R.K.Y. Li. Facile preparation and thermal degradation studies of graphite nanoplatelets (GNPs) filled thermoplastic polyurethane (TPU) nanocomposites. Composites Part A 2009; 40:1506-1513.
DOI: 10.1016/j.compositesa.2009.06.012
21. S. Cheng, X. Chen, Y.G. Hsuan, C.Y. Li. Reduced graphene oxide-induced polyethylene crystallization in solution and nanocomposites. Macromolecules 2012; 45:993-100.
DOI: 10.1021/ma201214531
22. S. Bose, T. Kulia, M.E. Uddin, N.H. Kim, A.K.T. Lau, J.H. Lee. In-situ synthesis and characterization of electrically conductive polypyrrole/graphene nanocomposites. Polymer 2010; 51:5921-5928.
DOI: 10.1016/j.polymer.2010.10.014
23. X.Y. Yuan, L.L. Zou, C.C. Liao, J.W. Dai. Improved properties of chemically modified graphene/poly(methyl methacrylate) nanocomposites via a facile in-situ bulk polymerization. eXPRESS Polymer Letters 2012; 6:847-858.
DOI: 10.3144/expresspolymlett.2012.90
24. V. Causin, C. Marega, A. Marigo, G. Ferrara, A. Ferraro. Morphological and structural characterization of polypropylene/conductive graphite nanocomposites. European Polymer Journal 2006; 42:3153-3161.
DOI: 10.1016/j.europolymj.2006.08.017
25. Y. Wang, H.-B. Tsai. Thermal, dynamic-mechanical and dielectric properties of surfactant intercalated graphite oxide filled maleated polypropylene nanocomposites. Journal of Applied Polymer Science 2012; 123:3154-3163.
DOI: 10.1002/app.34976
26. Y.-Q. Zhang, J.-H. Lee, J.M. Rhee, K.Y. Rhee. Polypropylene-clay nanocomposites prepared by in situ grafting-intercalating in melt. Composites Science and Technology 2004; 64:1383-1389.

DOI: 10.1016/j.compscitech.2003.10.014

27. F. Piana, J. Pionteck. Effect of the melt processing conditions on the conductive paths formation in thermoplastic polyurethane/expanded graphite (TPU/EG). Composites Science and Technology 2013; 80:39-46.
DOI: 10.1016/j.compscitech.2013.03.002
28. B. Wunderlich. Thermal Analysis. Academic Press: New York, 1990.
29. A. Galeski. Polypropylene: An A-Z reference series. Polymer Science and Technology Series Vol. 2, J. Karger-Kocsis (Ed.) (1999).
ISBN: 978-94-011-4421-6
30. S.V.J. Canevarolo (Ed.). Techniques for Polymer Characterization. Ed Artliber: Sáo Paulo, 2003.
31. H. Huo, S. Jiang, L. An. Influence of shear on crystallization behaviour of the β phase in isotactic polypropylene with β-nucleating agent. Macromolecules 2004; 37:2478-2483.
DOI: 10.1021/ma0358531
32. J.S. Sefadi, A.S. Luyt, J. Pionteck. Effect of surfactant on EG dispersion in EVA and thermal and mechanical properties of the system. Journal of Applied Polymer Science 2015; 132:41352.
DOI: 10.1002/app.41352
33. D.R. Paul, L.M. Robeson. Polymer nanotechnology: Nanocomposites. Polymer 2008; 49:3187-3204.
DOI: 10.1016/j.polymer.2008.04.017
34. R. Huang, X. Xu, S. Lee, Y. Zhang, B.-J. Kim, Q. Wu. High density polyethylene composites reinforced with hybrid inorganic fillers: Morphology, mechanical and thermal expansion performance. Materials 2013; 6:4122-4138.
DOI: 10.3390/ma6094122

Chapter 5

Effect of surfactant and electron beam irradiation on rheological and mechanical properties of MAPE /EG composites

This chapter will be submitted as a publication:
JS Sefadi, AS Luyt, J Pionteck, U Gohs. Effect of surfactant and electron beam irradiation on the electrical, rheological and mechanical properties of MAPE /EG composites. Journal to be decided upon.

Abstract

The effect of surfactant and electron beam (EB) irradiation on the electrical, rheological and mechanical properties of maleic anhydride grafted polyethylene (MAPE)/expanded graphite (EG) composites was investigated. SDS treatment of EG during sonication processing and EB irradiation significantly influenced the crosslinking density of MAPE. For both non-irradiated and composites irradiated at different doses, the reinforcement was found to be optimal at an EG content at 4 wt%. The hardness of the composites depended on a combination of the amount of filler, and the extent of irradiation, and whether the filler was treated with a surfactant. The EG containing samples showed lower electrical percolation thresholds than the SDS-EG containing samples, because SDS formed an electrical isolation layer around the EG particles. EB irradiation increased the electrical percolation threshold of the composites. The storage moduli of non-irradiated MAPE samples increased with increasing filler loading and frequencies. The complex viscosities for all the samples increased with increasing filler content, but decreased with increasing frequency. SDS treatment had a more significant effect on both properties at low EG contents, but a similar effect at higher loadings. EB irradiation gave rise to significantly higher storage modulus and complex viscosity values due to radiation induced crosslinking.

Keywords: Composites, expanded graphite, MAPE, electrical conductivity, rheological properties, surfactant and radiation treatment.

5.1 Introduction

The addition of electrically conductive nanofiller to conventional polymers is one way to obtain materials suitable for applications with good mechanical and electrical properties at much lower filler contents than is possible with polymer micro-composites [1-5]. As the nanofiller content increases to a critical value known as the percolation threshold or concentration, the physical properties, such as electrical conductivity, mechanical strength and hardness, and rheological properties can remarkably increase [6]. The main reasons given for these enhanced properties are the high aspect ratios and large surface areas of the nanofiller particles. Natural graphite flakes are abundantly available and highly conductive, with an electrical conductivity of 10^4 S cm^{-1} at room temperature [7,8]. Graphite is an allotrope of carbon whose structure is a single planar sheet of sp^2-bonded carbon atoms that are densely packed in a unique layered crystal structure [8,9]. Commercial expanded graphite (EG) is produced by intercalation [10] or oxidation [11] of graphite followed by thermal expansion at temperatures above 1000 °C [12], which creates the worm-like structure consisting of separated graphite platelets.

The main challenge in producing electrically conductive graphite-containing polymer composites with reasonable properties is to (i) get the graphite to form percolating or conducting paths throughout the polymer, (ii) reduce the agglomerations, due to Van der Waals forces and the incompatibility between the polymer and the graphite, of the graphite-graphite particles. Modification of polyethylene (PE) with maleic anhydride and treating the graphite with surfactant are some of the ways to address the problem. Surfactants or compatibilizing agents are widely used in nanocomposites to reduce the surface tension between the polymer matrix and the filler so that the interfacial adhesion and compatibility can be improved. Surfactants or compatibilizing agents are normally molecules having one hydrophilic end and an organophilic functional group [13,14]. Polymers grafted with maleic anhydride functionalities and subjected to radiation processing are usually effective in improving material properties. It was, for example, found that polyamide 12/maleic anhydride grafted polyethylene/graphite composites exhibited a transition from electrically insulating to conducting at a low percolation threshold of 0.3 vol % due to the formation of an interconnected network [15]. The tensile modulus, strength and elongation at break values of high-density polyethylene (HDPE)/ethylene propylene diene monomer (EPDM) rubber/clay composites subjected to electron beam (EB) irradiation doses of

50 to 200 kGy all noticeably improved [16]. This was attributed to the presence of immobilized polymer chains because of crosslinking-induced reactions.

Crosslinking reactions induced by EB irradiation also improve the rigidity of the polymer matrix [17-19]. EB irradiation treatment has been used recently to introduce crosslinking, degradation, hardening and surface modification in polymers and their composites. Polymers generally undergo simultaneous crosslinking and chain scission reactions during EB irradiation, depending on the irradiation dose and conditions [20]. Crosslinking normally increases with increasing radiation dose and enhance the chemical resistance, as well as the mechanical and rheological properties, of the polymer. Chain scission, degrades the material properties and reduce the crosslinking efficiency [21,22]. Functional groups that may enhance the adhesive properties of the polymer, can however be introduced if the irradiation is done in an oxidizing atmosphere. The irradiation of polymers with ionizing radiation such as gamma rays, X-rays, accelerated electrons and ion beams are important for many industrial applications such as polymer processing, surface curing, sterilization of medical devices, cosmetics, pharmaceuticals and food irradiation [23-25]. High-energy electron beam radiation provides the added unique high-value products for mankind in an environmentally friendly way [26]. The primary advantages of high-energy electron beam radiation are that it is pollution free, has a high efficiency, low operation cost, room temperature operation and the ability to process large throughputs. The crosslinking induced by an electron beam at room temperature is more stable than that induced by conventional curing at elevated temperatures. Crosslinking induced by EB irradiation leads to the formation of three-dimensional networks that improve the resistance to chemicals and abrasion [16,20-27].

In this study, we prepared MAPE/EG composites in the absence and presence of anionic surfactant treatment through melt mixing. The investigated samples were subjected to electron beam irradiation at different doses in a nitrogen atmosphere. The effects of SDS surfactant and EB irradiation treatment on the electrical conductivity, as well as mechanical and rheological properties, of the samples were investigated. No literature was found that reported similar investigations.

5.2 Experimental

5.2.1 Materials

Maleic anhydride grafted polyethylene (MAPE) MODIC® M704E was supplied in pellet form by Mitsubishi Chemical Europe GmbH, Tokyo, Japan. It had a maleic anhydride (MA) content of 3 wt%. It has an MFI (190 °C / 21.2 N) of 3.0 g/10 min (ASTM D-40549), T_m of 120 °C, vicat softening point of 90 °C, yield strength of 9 MPa, elongation at break of > 550%, shore D hardness of 56 and density of 0.92 g cm^{-3}. Expanded graphite, SIGRAFLEX Expandat, was provided by the SGL Technologies GmbH, SGL Group. It has a conductivity of 40 S cm^{-1} (room temperature, 30 MPa, self-made 2-point conductivity tester coupled with a DMM2000 electrometer, Keithley Instruments), an apparent volume of ~400 cm^3 g^{-1}, and a specific surface area of 39.4 m^2 g^{-1} (77.4 K, N_2 atmosphere, Autosorb-1, Quantachrome). Sodium dodecyl sulphate (SDS) was supplied by Sigma-Aldrich and was used without further treatment.

5.2.2 Methods

4 g of SDS was dissolved in 5 L deionized water in a glass beaker, and 20 g of the expanded graphite was gradually added to the solution. 500 mL suspensions were sonicated for 30 min, filtered, washed with 100 mL distilled water to remove loosely absorbed SDS, and dried in a vacuum oven at 50 °C for 72 h. This modified EG, and the as received unmodified EG, were respectively mixed with MAPE through melt mixing using a Brabender Plastograph 55 mL internal mixer. The mixing was done for 20 min at 60 rpm and a temperature of 130 °C. The samples were melt-pressed at 130 °C and 50 bar for 5 min into 2 mm thick sheets by using a hot hydraulic press.

The MAPE/EG and MAPE/SDS-EG composites were packed in polypropylene bags filled with nitrogen and exposed to EB radiation at room temperature (25 ± 1 ºC). Irradiation was carried out by exposing both surfaces of the samples for uniformity. Details of the conditions and parameters employed during radiation are as follows: energy = 1.5 MeV; current = 4.00 mA; dose = 50 kGy; distance from sample = 20 cm; pulse repetition rate = 75 Hz; operation frequency = 1.2 kHz).

The gel content of the samples was determined using Soxhlet solvent extraction. Rectangular test specimens with masses of approximately 0.2 g were wrapped in a 120 fine mesh stainless steel cage and refluxed with xylene at 140 °C for about 12 hours and then dried at 80 °C under vacuum overnight to determine the gel fraction. The gel content values were averaged over at least 2 tests. The percentage extract was calculated with Equation 5.1.

$$\text{Percentage extract (\%)} = \left[\frac{(m_{BE}-m_{AE})}{(1-F)(m_{BE})}\right] \times 100\ \% \qquad (5.1)$$

where m_{BE} = the sample mass before extraction; m_{AE} = the sample mass after extraction; F = fraction of graphite filler. The gel content was calculated using Equation 5.2.

$$\text{Gel content (\%)} = 100 - \text{percentage extract} \qquad (5.2)$$

The tensile properties were investigated using a Hounsfield H5KS tensile tester at a crosshead speed of 10 mm min^{-1} and a gauge length of 20 mm. All the reported values from the stress-strain curves are averages of at least five measurements for each composition.

Hardness was measured on a Zwick 3140 according to DIN EN 868 and the required thickness was 6 mm. The measurement tests were carried out using Zwick 3140 with pneumatic clumps (DIN ISO 868) for a holding time of 15 seconds.

The volume resistance measurements of MAPE and its composites before and after radiation were carried out on a Keithley Instruments 6157A electrometer, connected to an 8009 Keithley resistivity test fixture with two plate electrodes located on the two sides of the samples. This method is appropriate for resistance values in the range from 10^7 to 10^{18} Ω at room temperature in accordance with ASTM D257-07. The corresponding conductivity values are in the range from 10^{-19} to 10^{-8} S cm^{-1}, but sensible results can be found in the range from 10^{-19} to 10^{-4} S cm^{-1}.

The rheological measurements were carried out on 25 mm diameter plates with a 2 mm thickness prepared *via* melt mixing. An ARES G2 rheometer was used employing a parallel plate geometry (diameter 25 mm). The measurements were done at 190 °C under nitrogen atmosphere and the gap between the plates was set at 2 mm. The oscillation frequency sweeps were performed by increasing the frequency from 0.1 to 100 rad s^{-1}, followed by a sweep with

decreasing frequency from 100 to 0.03 rad s^{-1}. The second sweep was considered for the data analysis.

5.3 Results and discussion

5.3.1 Gel content

The gel contents of the irradiated MAPE at different doses of EB irradiation are shown in Figure 5.1 as function of EG and SDS-EG. The non-irradiated MAPE was completely soluble in hot xylene. The crosslinking density of MAPE is directly related to the gel content. The gel contents of all the samples increased with an increase in EG loading up to 4 wt% EG content, which indicates the increased formation of insoluble macromolecular networks (crosslinks) in the polymer. The EG seems to conduct energy from the EB irradiation and enhance the efficiency of free radical formation and crosslinking at these filler contents. However, the gel contents continuously decrease with increasing filler content above 4 wt%, probably because of agglomeration and poorer filler dispersion which reduce the efficiency of the graphite in transporting thermal energy to the polymer chains. The irradiated SDS-EG containing composites have about 4% higher gel content values than the irradiated EG containing samples. This may be due to improved dispersion of the surfactant treated EG platelets in the MAPE, which improved the energy transfer to the MAPE chains and the resultant crosslinking efficiency. There is an observable increase in gel content values when increasing the EB irradiation dose from 50 to 100 kGy, but these values significantly decreased when the dose further increased to 200 kGy. The initial increase is due to radiation induced crosslinking reactions, but at higher doses radiation induced degradation probably dominated so that there was a much lower extent of crosslinking.

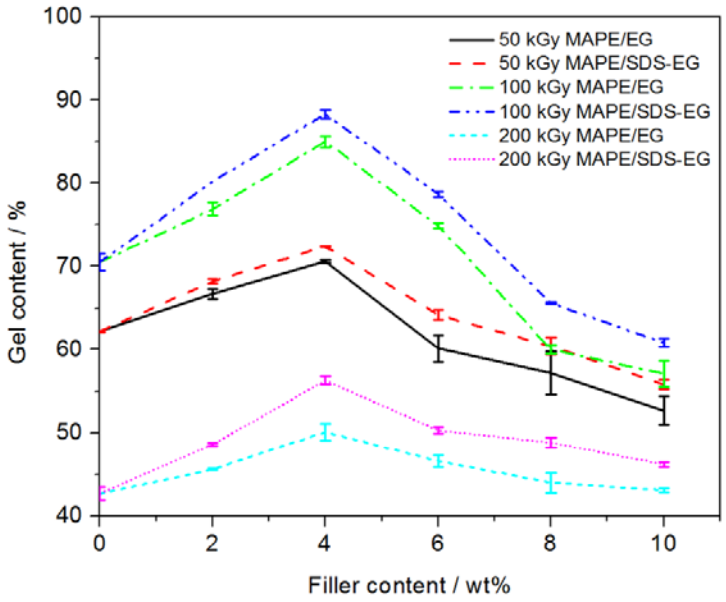

Figure 5.1 Gel content as function of EG content for irradiated samples without and with SDS treatment

5.3.2 Tensile properties

Good mechanical properties in composites can only be achieved if the graphite platelets are well dispersed in the polymer, and if there is good interaction between the polymer and the filler. In our previous work [28,29] we observed that the presence of SDS improved the interaction between EVA and EG, and the dispersion of EG in the polymer. The EB irradiation treatment induced crosslinking which contributed to ensuring improved mechanical properties of the composites, not only because of network formation but also through trapping of the EG platelets in the interconnected network structure. The filler in a polymer usually forms defect centres at which crazes and cracks start forming when stress is applied to the sample. The propagation of the cracks gives rise to sample fracture, but crosslinking will retard this process.

The influence of various EG and SDS-EG contents on the tensile stress and elongation at break values of all the investigated samples is shown in Figures 5.2 and 5.3. Like the already discussed gel contents, the tensile stress and elongation at break for all the samples increased up to 4 wt% graphite content. The main reasons for this is the high extent of crosslinking which also contributed to better interaction between the polymer and EG. This improved interaction may also have been the result of the maleic anhydride groups on MAPE that should have a stronger

affinity for the filler than the polyethylene segments. As discussed above, this will inhibit the formation and propagation of cracks. At higher filler contents there is a noticeable decrease in both stress and elongation at break, which can be related to EG agglomeration that form more effective defect centres for the development and propagation of cracks. SDS treatment of EG had little influence on these properties, because the non-irradiated SDS-EG containing composites showed almost the same values within experimental error than the EG containing composites.

Both stress and elongation at break increased with increasing irradiation dose up to 100 kGy, but there was a significant decrease for the 200 kGy irradiated samples. This is because degradation of the polymer chains was much more pronounced at such a high irradiation dose, which to some extent eliminated the effect of the radiation induced crosslinking. It is interesting that for the irradiated composites, the stress at break values for the composites with higher filler contents were higher in the case of SDS-EG, which could be related to the somewhat better filler dispersion at higher filler contents for SDS-EG.

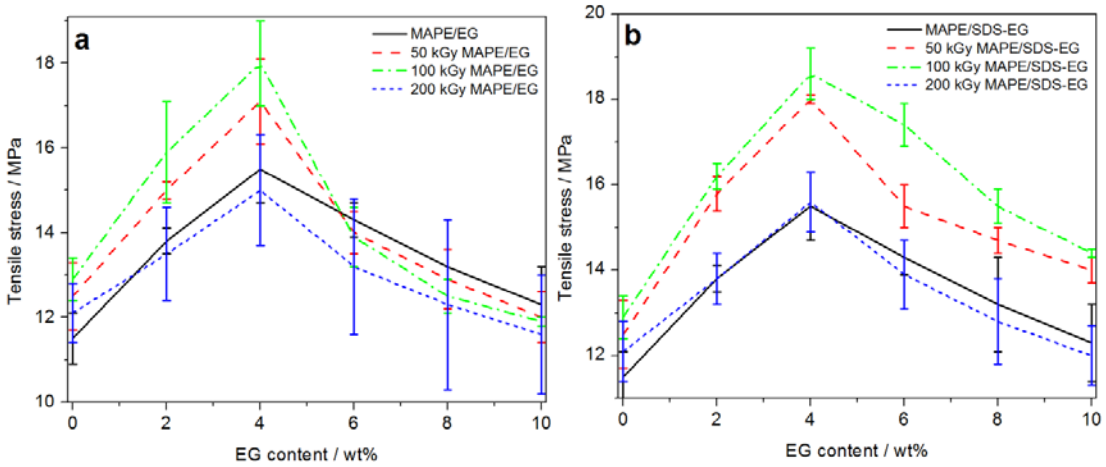

Figure 5.2 Variation of stress at break of non-irradiated and irradiated (a) MAPE/EG and (b) MAPE/SDS-EG samples as a function of filler content

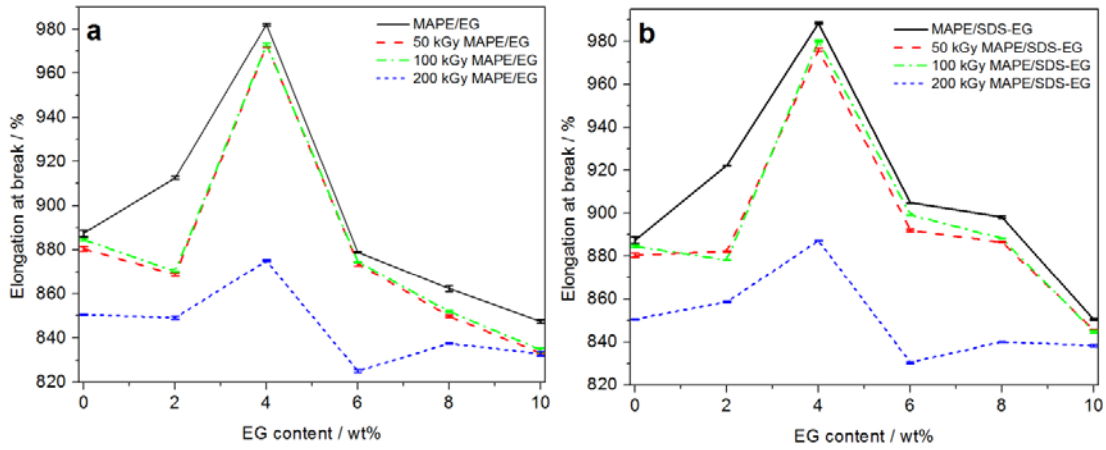

Figure 5.3 Variation of elongation at break of non-irradiated and irradiated (a) MAPE/EG and (b) MAPE/SDS-EG samples as a function of filler content

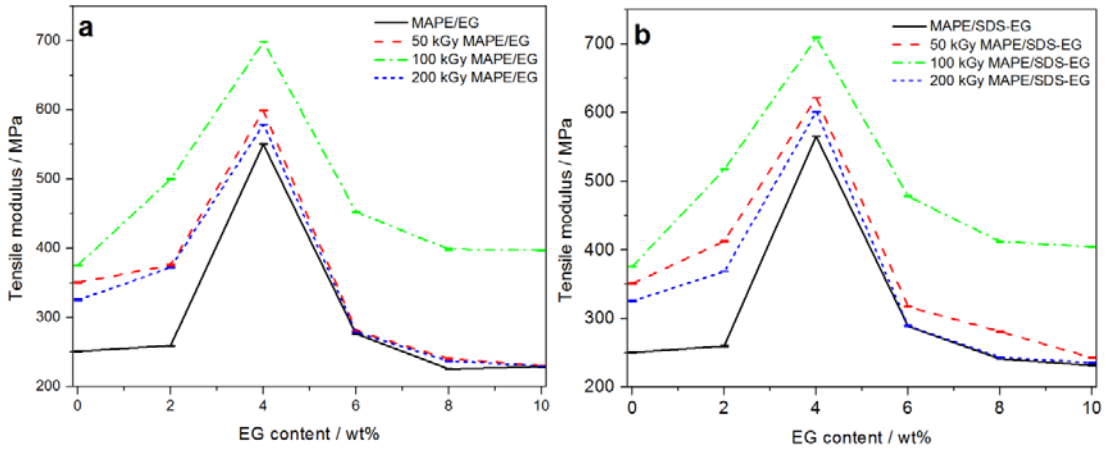

Figure 5.4 Variation of tensile modulus of non-irradiated and irradiated EVA/EG and EVA/SDS-EG samples as a function of filler content

Like the stress and elongation at break, the tensile modulus of the composites increased with increasing filler content up to 4 wt% EG (Figure 5.4), which is expected because of the inherent higher modulus of EG. Crosslinking and the good dispersion of the filler at these contents (Figure 5.4 a and b), which improved the interaction between the polymer and the filler, further contributed to the increased stiffness. As was observed for gel content and stress and elongation at break, 200 kGy radiation significantly decreased the modulus values compared to 100 kGy radiation. As discussed before, this observation is probably related to radiation induced degradation of the polymer becoming more dominant.

5.3.3 Hardness measurements

Hardness is generally termed as the resistance of a material to local deformations. Table 5.1 shows that the hardness values increased with 0-10% increasing EG loading. There is, however, very little difference between the hardness values for the non-irradiated samples and the samples irradiated to different doses. This is the result of increased amount of solid inorganic filler combined with increased levels of agglomeration, which will resist local deformation during the hardness test. Surfactant treatment reduced the particle-particle attraction resulting in a less agglomerated filler structure, while the surfactant itself formed a 'soft' layer around the EG particles. Because of this, the presence of and increased amounts of filler had little effect on the hardness values of the composites.

Table 5.1 Effect of graphite content on the hardness of MAPE/EG and MAPE/SDS-EG at different EB irradiation doses

wt % EG	Shore D hardness			
	Non-irradiated	50 kGy irradiated	100 kGy irradiated	200 kGy irradiated
0	52.8 ± 1.0	53.8 ± 1.2	52.9 ± 0.9	53.5 ± 1.2
2	54.5 ±1.6	54.1 ± 1.8	56.1 ± 2.1	55.5 ± 1.8
4	55.4 ± 0.9	55.8 ± 1.3	56.9 ± 0.6	56.3 ± 2.6
6	55.7 ± 1.5	56.0 ± 0.9	56.8 ± 1.2	57.6 ± 1.1
8	56.1 ± 2.1	57.2 ± 0.4	59.3 ± 1.9	58.2 ± 0.7
10	60.4 ± 0.7	58.4 ± 1.1	59.9 ± 1.7	60.8 ± 0.8
SDS treatment				
2	55.7 ± 2.6	55.6 ± 0.8	56.3 ± 2.0	52.8 ± 2.3
4	56.3 ± 1.9	57.1 ± 1.0	57.3 ± 1.2	57.2 ± 2.1
6	56.1 ± 2.3	53.4 ± 1.7	52.3 ± 1.8	53.8 ± 1.4
8	57.0 ± 2.0	53.9 ± 2.4	52.8 ± 3.2	55.9 ± 1.9
10	58.4 ± 2.3	54.7 ± 0.6	54.3 ± 1.7	53.1 ± 2.2

5.3.4 Electrical conductivity

All the samples show insulating behaviour up to about 5 wt% EG or SDS-EG content (Figure 5.5), but they show electrical percolation thresholds at 5-8 wt% EG or SDS-EG. The EG containing samples, both non-irradiated and irradiated, generally show lower percolation thresholds than the SDS-EG containing samples. The reason for this is probably that the SDS formed an electrical isolation layer around the EG particles which negatively affected their electrical conductivities. Another possible reason for the lower percolation threshold could be attributed to a very high aspect ratio or high specific surface area of EG platelets which seems to be reduced in the presence of SDS treatment. It is further clear from Figure 5.5 that, for both the EG and SDS-EG containing samples, irradiation generally caused an increase in the electrical percolation threshold (φ_c) of the composites. The reason is probably that the radiation induced crosslinking disturbs the formation of electrical percolation networks by causing a more even dispersion of the graphite particles. Srivastava *et al.* [30], however, found a decrease in the electrical percolation threshold for irradiated poly(vinyl chloride) (PVC)/graphite composites, which they explained as being due to the breaking of the filler particles and the production of free radicals during γ-irradiation.

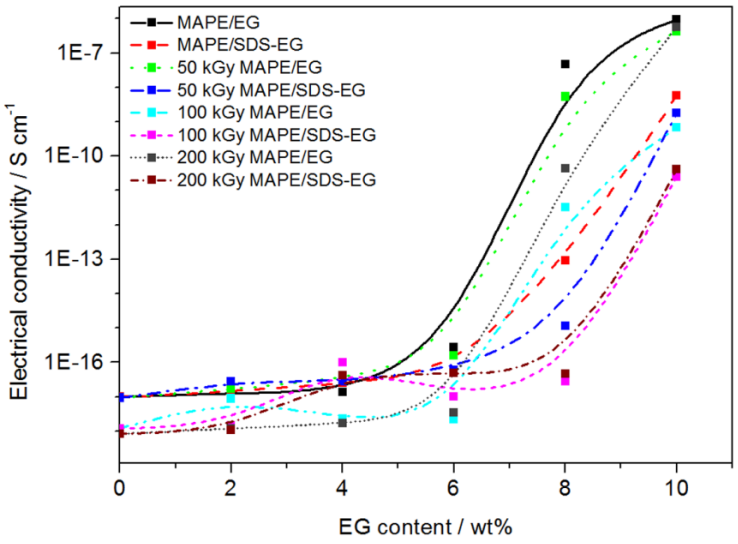

Figure 5.5 Electrical conductivities of all the investigated samples

5.3.5 Melt rheology

The storage modulus (G′) and complex viscosity (η) of the non-irradiated and irradiated MAPE samples (100 kGy and 200 kGy doses) are presented as a function of angular frequency (ω) in Figure 5.6. G′ of the non-irradiated MAPE increases with increasing angular frequency (ω), and exhibits linear viscoelastic behaviour in the low frequency region and a non-linear viscoelastic behaviour in the high frequency region. This indicates that, in the lower frequency region, the polymer matrix is fully relaxed and shows terminal behaviour. EB irradiation and increasing doses result into significantly higher storage modulus values that increase linearly with increasing angular frequency, but the frequency dependence of the storage modulus is much less significant. It is generally known that G' is determined by physical and chemical crosslinking of samples subjected to EB irradiation, and its value normally increases with increasing EB irradiation dose because it gives rise to increased chemical crosslinking in the samples. The lower frequency dependence of the storage modulus for the irradiated samples is due to the increasing molecular weight, long chain branching formation, and crosslinked structures, that are the result of radiation induced formation of free radical chains [24,31]. Network formation normally restricts chain mobility, and reduced chain mobility reduces the frequency dependence of storage modulus.

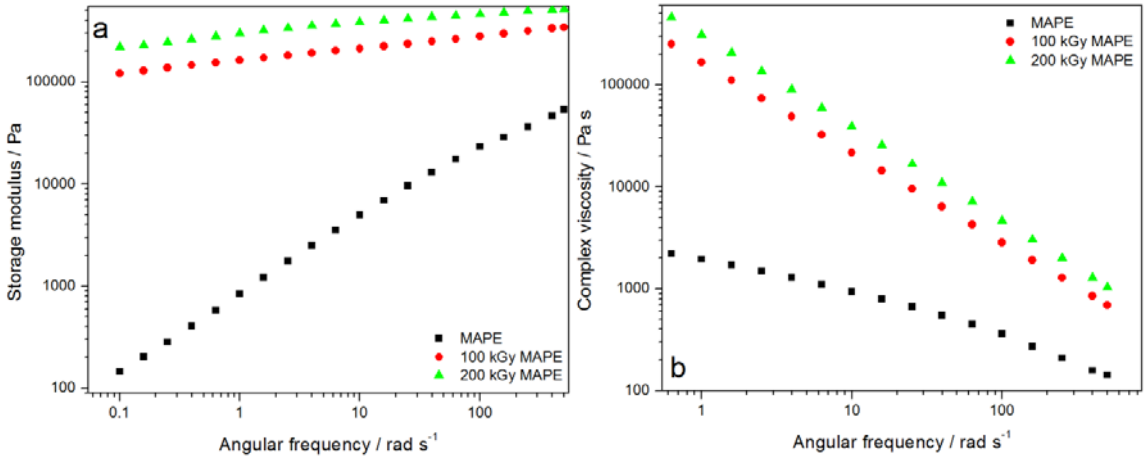

Figure 5.6 (a) Storage modulus and (b) complex viscosity at 190 °C of non-irradiated MAPE and MAPE irradiated with 100 KGy and 200 kGy as a function of frequency

The complex viscosity of the non-irradiated MAPE is more Newtonian-like, which characterizes a liquid-like relaxation at lower frequencies. Pseudoplastic behaviour at frequencies above 1 rad s^{-1} and the gradual decreasing complex viscosity values are observed at higher frequencies, which is indicated by the increase in the rate at which the complex viscosity decreases. The complex viscosities of the irradiated MAPE are higher than those of the comparable non-irradiated MAPE, and increased with increasing irradiation dose, because of the radiation induced crosslinking of the polymer. The same process may have given rise to long-chain branches, especially close to the surfaces of the sample. The viscosities of branched and crosslinked polymers are known to have a stronger frequency dependence, which explains the stronger reduction in complex viscosity with increasing angular frequency observed in Figure 5.6b.

The angular frequency dependence of the storage modulus of the non-irradiated MAPE and its composites with EG and SDS-EG shows that increasing expanded graphite contents increase the storage modulus over the whole frequency range due to the inherent stiffness of the graphite particles (Figure 5.7). There were no obvious changes in the shapes of the curves in Figure 5.7a, which indicates that the graphite sheets reinforced the polymer matrix without influencing the polymer relaxation mechanism. Comparing Figure 5.7a and 5.7b shows that small amounts of SDS-EG have a much more significant effect on the storage modulus of MAPE than the same amount of EG in MAPE, but that higher SDS-EG amounts gave rise to behaviour very similar to that of the composites containing the same amounts of EG. This is attributed to the smaller and better dispersed particles at low SDS-EG contents, while at higher SDS-EG contents the SDS was probably not so efficient in separating the graphite particles, giving rise to agglomeration similar to that in samples containing unmodified EG.

All the investigated samples generally show a decrease in complex viscosity with increasing frequency (Figure 5.8) because of shear thinning. As expected, the complex viscosity increased with increasing EG and SDS-EG contents, which is normal for inorganic filler containing composites [32], and there were no significant differences in the shapes of the curves. At lower contents the SDS-EG particles have a more significant effect on the complex viscosity of MAPE than the same amount of EG, but at higher filler contents MAPE/EG and MAPE/SDS-EG have very similar flow behaviour. As mentioned earlier, at lower SDS-EG contents the particles were smaller and better dispersed, while at higher SDS-EG contents the SDS was not so

efficient in separating the graphite particles, giving rise to agglomeration similar to that in samples containing unmodified EG. All the samples exhibited the shear thinning behaviour, as can be seen from the reduction in the complex viscosity with increasing frequency.

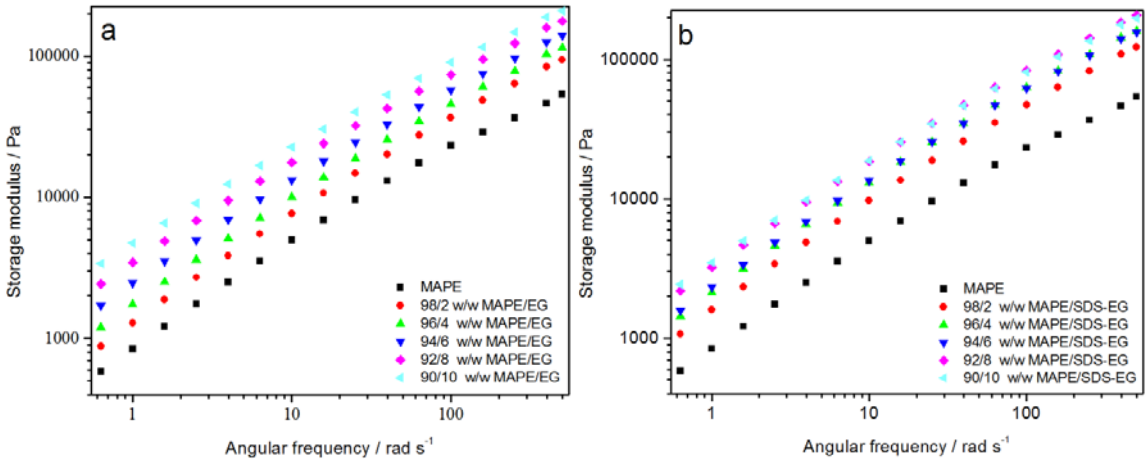

Figure 5.7 Storage modulus at 190 °C of the (a) MAPE/EG samples and (b) MAPE/SDS-EG composites as a function of frequency

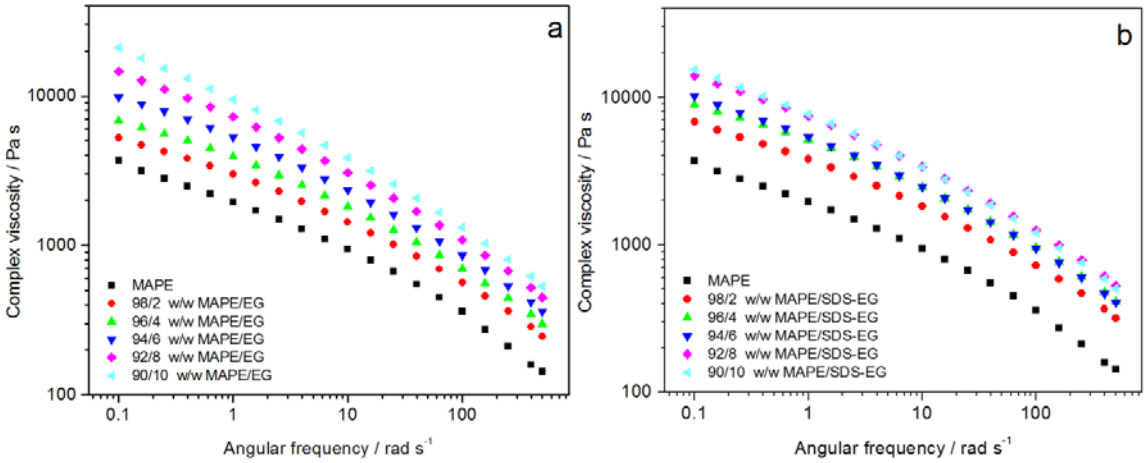

Figure 5.8 Complex viscosities at 190 °C of the (a) MAPE/EG and (b) MAPE/SDS-EG samples as a function of frequency

The storage moduli of the irradiated MAPE/EG and MAPE/SDS-EG composites are higher than those of the non-irradiated composites (Figure 5.9), and these modulus values show a very small change with increasing angular frequency values. Both the presence of filler and increasing

radiation dose increased the storage modulus values. This indicates that the inherent stiffness of the inorganic filler platelets and the additional stiffness as a result of radiation induced crosslinking increased the stiffness of the composites. The storage modulus values of the irradiated samples show a very small frequency dependence, and there are very small differences between these values for the irradiated EG and SDS-EG containing samples. As in the case of neat MAPE, the EB irradiated samples showed a very small frequency dependence of the storage modulus, which is the result of a restriction in chain mobility because of radiation induced crosslinking.

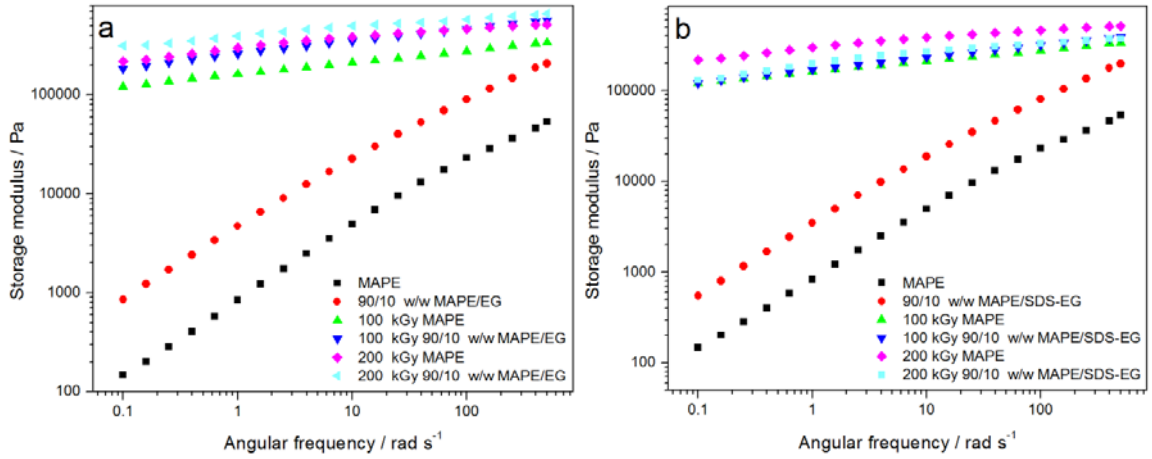

Figure 5.9 Comparison of the storage modulus at 190 °C of non-irradiated and irradiated (a) MAPE/EG and (b) MAPE/SDS-EG samples as a function of frequency

The complex viscosity values for all the samples in Figure 5.10 decrease with increasing frequency because of shear thinning, and are significantly higher for the irradiated samples at low frequencies due to the EB irradiation induced crosslinking of the polymer chains. The irradiated samples also show stronger frequency dependence than the non-irradiated samples because of radiation-induced chain branching and crosslinking which normally increases the frequency-dependence of a polymer's viscosity.

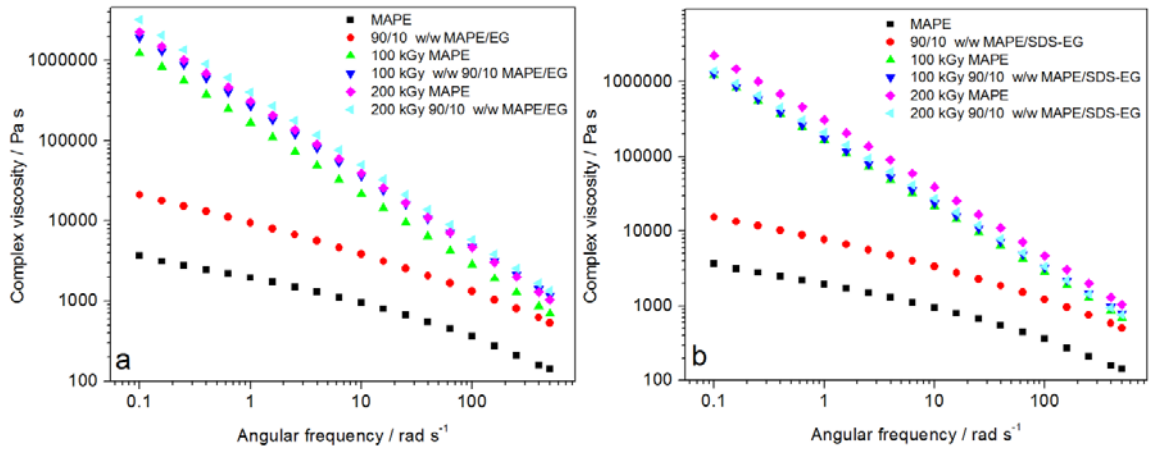

Figure 5.10 Comparison of the complex viscosity at 190 °C of non-irradiated and irradiated (a) MAPE/EG and (b) MAPE/SDS-EG samples as a function of angular frequency

5.4 Conclusions

The effect of anionic surfactant and EB irradiation treatment on the electrical, rheological and mechanical properties of MAPE/EG composites was investigated in this study. The crosslinking density of all the irradiated samples increased and a maximum was observed for samples containing 4 wt.% graphite. The SDS treatment combined with sonication reduced the interparticle attraction and improved the interaction between the EG particles and the polymer matrix, and this contributed to increasing the crosslinking efficiency of the irradiated samples. The addition of EG platelets improved most of the tensile properties up to a maximum of 4 wt% EG, after which they declined, probably because of filler particle agglomeration at higher contents. The EB irradiation up to 100 kGy significantly improved both the tensile strength and tensile modulus as a result of crosslinking, but the higher irradiation dose reduced these properties, probably because of degradation effects. The hardness values depended on a combination of the amount of filler, the irradiation dose, and filler treatment. All the composites showed a sharp transition from insulator to conductor, with irradiation increasing the percolation threshold, while SDS treatment even further increased the percolation threshold. Both the storage modulus and complex viscosity in the melt observably increased with increasing filler content, but the storage modulus values increased and the complex viscosities decreased with increasing

frequency. SDS treatment had a significant effect on both the storage modulus and complex viscosity values at low EG contents, while at high EG loading the effect was similar. This was attributed to the smaller and better dispersed particles at low EG contents, while at higher EG contents the SDS was probably not so efficient in separating the graphite particles, giving rise to agglomeration similar to the EG containing samples. The EB irradiation and increasing doses resulted into significantly higher storage modulus and complex viscosity values due to radiation induced crosslinking of the polymer chains.

5.5 References

1. K. Prashantha, M.F. Lacrampe, P. Krawczak. Processing and characterization of halloysite nanotubes filled polypropylene nanocomposites based on a masterbatch route: Effect of halloysites treatment on structural and mechanical properties. eXPRESS Polymer Letters 2011; 5:295-307.
   DOI: 10.3144/expresspolymlett.2011.30
2. D.R. Paul, L.M. Robeson. Polymer nanotechnology: Nanocomposites. Polymer 2008; 49:3187-3204.
   DOI: 10.1016/j.polymer.2008.04.017
3. M. Moniruzzaman, K.I. Winey. Polymer nanocomposites containing carbon nanotubes. Macromolecules 2006; 39:5194-5205.
   DOI: 10.1021/ma060733p
4. A.K. Geim. Graphene: Status and prospects. Science 2009; 324:1530-1534.
   DOI: 10.1126/science.1158877
5. J.R. Potts, D.R. Dreyer, C.W. Bielawski, R.S. Ruoff. Graphene-based polymer nanocomposites. Polymer 2011; 52:5-25.
   DOI: 10.1016/j.polymer.2010.11.042
6. D.K. Chattopadhyay, K.V.S.N. Raju. Structural engineering of polyurethane coatings for high performance applications. Progress in Polymer Science 2007; 32:352-418.
   DOI: 10.1016/j.progpolymsci.2006.05.003

7. I.M. Afanasov, V.A. Morozov, A.V. Kepman, S.G. Ionov, A.N. Sleeznev, G. Van Tendeloo, V.V. Avdeev. Preparation, electrical and thermal properties of new exfoliate-based composites. Carbon 2009; 47:263-270.
DOI: 10.1016/j.carbon.2008.10.004
8. S.R. Dhakate, S. Sharma, M. Borah, R.B. Mathur, T.L. Dhami. Expanded graphite-based electrically conductive composites as bipolar plate for PEM fuel cell. International Journal of Hydrogen Energy 2008; 33:7146-7152.
DOI: 10.1016/j.ijhydene.2008.09.004
9. Z. Mo, Y. Sun, H. Chen, P. Zhang, D. Zuo, Y. Li, H. Li. Preparation and characterization of a PMMA/$Ce(OH)_3$, Pr_2O_3/graphite nanosheet composite. Polymer 2005; 46:12670-12676.
DOI: 10.1016/j.polymer.2005.10.117
10. B. Tryba, R.J. Kalenczuk, F. Kang, M. Inagaki, A.W. Morawski. Studies of exfoliated graphite (EG) for heavy oil sorption. Molecular Crystals and Liquid Crystals 2000; 340:113-119.
DOI: 10.1080/10587250008025452
11. H. Kim, A.A. Abdala, C.W. Macosko. Graphene/polymer nanocomposites. Macromolecules 2010; 43:6515-6530.
DOI: 10.1021/ma100572e
12. D. Pedrazzoli, F. Tuba, V.M. Khumalo, A. Pegoretti, J. Karger-Kocsis. Mechanical and rheological response of polypropylene/boehmite nanocomposites. Journal of Reinforced Plastics and Composites 2014; 33:252-265.
DOI: 10.1177/0731684413505787
13. Y. Wang, H.-B. Tsai. Thermal, dynamic-mechanical and dielectric properties of surfactant intercalated graphite oxide filled maleated polypropylene nanocomposites. Journal of Applied Polymer Science 2012; 123:3154-3163.
DOI: 10.1002/app.34976
14. W.S. Chow, S.K. Lok. Effect of EPM-g-MAH on the flexural and morphology properties of poly(lactic acid)/organo-montmorillonite nanocomposites. Journal of Thermoplastic Composite Materials 2008; 21:265-277
DOI: 10.1177/0892705708089477

15. D. Yan, H.-B. Zhang, Y. Jia, J. Hu, X.-Y. Qi, Z. Zhang, Z.-Z. Yu. Improved electrical conductivity of polyamide 12/graphene nanocomposites with maleated polyethylene-octene rubber prepared by melt compounding. ACS Applied Materials and Interfaces 2012; 4:4740-4745.
DOI: 10.1021/am301119b
16. N.A. Jamal, H. Anuar, A.R.S. Bahri. Enhancing the mechanical properties of crosslinked rubber-toughened nanocomposites via electron beam irradiation. Journal of Nanotechnology 2011; 769428.
DOI: 10.1155/2011/769428
17. M. Zenkiewicz, J. Dzwonkowski. Effects of electron radiation and compatibilizers on impact strength of composites of recycled polymers. Polymer Testing 2007; 26:903-907.
DOI: 10.1016/j.polymertesting.2007.06.005
18. L. Song, M. Li, Y. Hu, H. Lu. Study on preparation and properties of silane-crosslinked polyethylene/magnesium hydroxide/montmorillonite nanocomposites. Journal of Fire Sciences 2008; 26:493-507.
19. A. Bhattacharya. Radiation and industrial polymers. Progress in Polymer Science 2000; 25:371-401.
DOI: 10.1016/S0079-6700(00)00009-5
20. A.Yoshiga H. Otaguro, D. F. Parra, L.F.C.P. Lima, A.B. Lugao. Controlled degradation and crosslinking of polypropylene induced by gamma radiation and acetylene. Polymer Bulletin 2009; 63:397-409
DOI 10.1007/s00289-009-0102-7
21. S. Park, J. Krotine, S.A.B. Allen, P.A. Kohl. Electron beam hardening of thin films of functionalized polynorbornene copolymer. Journal of Electronic Materials 2006; 35:1112-1121.
22. S. Kim, Y.C. Nho. Effect of radiation on ultra high molecular weight polyethylene (UHMWPE). International Energy Atomic Agency 2009; 1617:92-94
23. H.A. Zen, G. Ribeiro, A.N. Geraldes, C.P. Souza, D.F. Parra, A.B. Lugão. Effect of radiation induced crosslinking and degradation of ETFE films. Radiation Physics and Chemistry 2013; 84:136-139.
DOI: 10.1016/j.radphyschem.2012.06.030

24. Y. Munusamy, H. Ismail, M. Mariatti, C.T. Ratnam. Effect of electron beam irradiation on the properties of ethylene vinyl acetate copolymer/natural rubber/organoclay nanocomposites. Journal of Vinyl and Additive Technology 2009; 15:39-46
DOI: 10.1002/vnl.20174
25. M.M. Hassan, R.O. Aly, J.A. Hasanen, E.-S.F. El Sayed. The effect of gamma irradiation on mechanical, thermal and morphological properties of glass fibre reinforced polyethylene waste/reclaim rubber composites. Journal of Industrial and Engineering Chemistry 2014; 20:947-952
DOI: 10.1016/j.jiec.2013.06.027
26. S. Tagawa, M. Kashiguchi, T. Kamada, M. Sekiguchi, K. Hosobuchi, H. Tominaga, N. Ooka, K. Makuuchi. Economic scale of utilization of radiation (I): Industry comparison between Japan and the U.S.A. Journal of Nuclear Science and Technology 2002; 39:1002-1007.
DOI: 10.1080/18811248.2002.9715287
27. N.A. Jamal, H. Anuar, A.R.S. Bahri. The influence of EB irradiated treatment on enhancing barrier property and crystallization behaviour of rubber toughened nanocomposites. Journal of Nanotechnology 2011; 683725.
DOI: 10.1155/2011/683725
28. J.S. Sefadi, A.S. Luyt, J. Pionteck. Effect of surfactant on EG dispersion in EVA and thermal and mechanical properties of the system. Journal of Applied Polymer Science 2014, 131:41352.
DOI: 10.1002/app.41352
29. J.S. Sefadi, A.S. Luyt, J. Pionteck, F. Piana, U. Gohs. Effect of surfactant and electron treatment on the electrical and thermal conductivity as well as thermal and mechanical properties of EVA/EG composites. Journal of Applied Polymer Science 2014 (submitted).
30. N.K. Srivastava, S. Rattan, R.M. Mehra. Effect of γ-ray irradiation on morphology and electrical properties of poly(vinyl chloride)/graphite composites. Polymer Engineering and Science 2009; 49:1136-1141.
DOI: 10.1002/pen.21366

31. C.-L. Huang, Y.-C. Chen, C. Wang, C.-F. Tu, F.-S. Liao. Structural variations and morphology features of polyethylene/carbon black conductive composites after processing in an internal mixer. Journal of Applied Polymer Science 2013; 130:1038-1046
DOI: 10.1002/app.39251
32. A. Huegun, M. Fernández, M.E. Muñoz, A. Santamaría. Rheological properties and electrical conductivity of irradiated MWCNT/PP nanocomposites. Composites Science and Technology 2012; 72:1602-1607
DOI: 10.1016/j.compscitech.2012.06.011

Chapter 6

Conclusions

The properties of polymer/EG nanocomposites based on EVA, PP and MAPE as polymer matrices were investigated. SDS functionalization of EG was done in water with sonication, and the morphology and properties of composites prepared with non-functionalized and SDS functionalized EG were compared. The influence of various EG contents and EB irradiation on the morphologies and properties of the composites was investigated.

The findings showed the presence of big agglomerated graphite particles for the EG containing composites, while SDS treatment improved EG dispersion in and interactions with the EVA copolymer. In the case of PP, the presence of SDS was not sufficient to completely reduce the graphite interparticle attraction, and thus long agglomerated sheets were observed. In all the investigated samples, the EB irradiation did not influence the morphology of the composites since it could not re-disperse or re-arrange because there was no polymer melting on a macroscopic level.

The incorporation of EG and SDS-EG particles in EVA significantly increased the crosslink density, indicating increased formation of insoluble macromolecular networks in the polymer. The SDS-EG containing samples showed much better crosslinking efficiency due to the better dispersion of EG particles in EVA, and improved interaction and energy transfer between SDS-EG and EVA. There was no gel after the soxhlet extraction for irradiated PP, confirming that crosslinking was a minor process during EB irradiation. The molar masses of the irradiated PP samples were lower than those of the comparable non-irradiated PP samples, confirming that chain scission *inter alia* occurred as a result of irradiation. For MAPE the degree of crosslinking increased to an optimal level at 4% EG content. The increase in crosslink density was due to more efficient free radical formation and crosslinking at lower filler contents, while the decrease was due to agglomeration and poor dispersion at high filler contents, reducing the efficiency of the graphite in transporting thermal energy to the polymer chains. The irradiated SDS-EG containing MAPE composites had a higher degree of crosslinking than the irradiated EG containing samples due to the improved dispersion of EG platelets in the MAPE. Crosslinking

increased with radiation dose up to 100 kGy due to radiation induced crosslinking reactions, but decreased for higher doses because of the domination of radiation induced degradation.

The presence of both EG and SDS-EG had little influence on the crystalline structure of EVA and inhibited the β-nucleation of PP. The presence of EG in the polymers did not change the melting temperatures of the polymers, but the EG particles acted as nucleating agents and increased the crystallization temperatures. The samples containing SDS-EG had slightly better nucleation efficiency and a higher degree of crystallinity because of the better dispersion of these particles. EB irradiation had little influence on the melting temperatures. The thermal properties showed little change after EB irradiation, probably because irradiation mostly affected the amorphous parts of the polymer. The presence of, and increase in the contents of EG and SDS-EG increased the thermal stability of the non-irradiated polymers. No trend was observed for the irradiated samples, probably because of an inconsistent combination of crosslinking and degradation as a result of the irradiation.

The irradiation had very little effect on the electrical conductivities of the composites, while the thermal conductivities of the irradiated polymer composites were generally slightly lower than those of the comparable non-irradiated ones. Both the non-irradiated and irradiated polymer-EG composites showed a sharp transition from insulator to conductor, with a lowering of the percolation threshold for the irradiated samples. For SDS-EG there was little increase in electrical conductivity and no electrical percolation threshold over the investigated EG content range, probably because SDS formed an isolation layer around the EG particles.

There was a shift in the T_g to higher temperatures with an increase in both EG and SDS-EG content in the samples. Both the storage modulus and complex viscosity observably increased with increasing EG content, but the storage modulus values increased and the complex viscosities decreased with increasing frequency. The melt rheological properties of all the EB irradiated MAPE samples showed higher values than the non-irradiated MAPE samples. The stress and elongation at break for all the EG containing samples decreased with increasing filler content, but the tensile modulus values increased. The tensile properties of the composites were significantly influenced by SDS treatment, EB irradiation and a combination of these two treatments. The tensile strength and modulus generally increased with increasing filler content and irradiation dose up to a certain level because of the higher modulus of the filler particles and crosslinking. The stress and elongation at break values increased up to 4 wt% EG content in

MAPE, but decreased at higher EB irradiation doses. The hardness values depended on the combination of amount of filler, irradiation dose, and whether EG or SDS-EG was used.

Future work:

- Investigate the influence of various surfactants (cationic, anionic and neutral) on the properties of polymer-graphite composites.
- Study the combined effects of surface modifiers/effective dispersants on the mechanical and thermal properties of polymer-graphite (nano)composites
- Compare the effect of γ-irradiation, EB irradiation and UV processing on the overall properties of polymer/EG composites.
- Study the behaviour of different antioxidants on the degradation and/ or crosslinking effect of PP-EG composites under radiation processing.
- To study compatibility effect induced by dicarboxylic acid anhydride (DAA) and maleic anhydride (MA) on the electrical and rheological properties of the polymer filled graphite systems